University of Siena – Department of Medical Biotechnologies

Doctorate in Genetics, Oncology and Clinical Medicine (GenOMeC)

XXXIV cycle (2018-2021)

Coordinator: Prof. Francesca Ariani

Characterization and selective isolation of human extracellular vesicle subpopulations from simple and complex biosamples for novel clinical liquid biopsy strategies

Scientific disciplinary sector: BIO/18 – Genetica

Tutor

Prof. Elisa Frullanti

PhD Candidate

Diogo Miguel Lázaro Fortunato

Academic Year 2020/2021

Acknowledgments

Despite not being able to nominate every single one who inspired me and contributed to this journey, or to write exactly the words I would say instead, I feel grateful to everyone I had the chance to get close to throughout my life, who somehow helped shaping who I am today. An especial thanks also to all the people I bonded with after enrolling in university, and after moving from my hometown to Lisbon and abroad, who inevitably nudged me towards where I am today.

Concretely, I would like to acknowledge my colleagues at Exosomics in Siena, where this PhD project was conducted. Thank you, Antonio Chiesi, Davide Zocco, Nataša Zarovni, Barbara Bonucci, Silvia Mancianti, Claudio Corallo, Andrea D'Ambrogio, Francesca Morgera and Clarissa Pozzi. Thanks to my everyday lab partners Mattia Criscuoli, Francesco Carpi, Laura Bianciardi, Giorgia Radano, Erika Maltinti, Ilaria Passalacqua, Filomena Costanza, Giulio Nanni, Elena Bocci and Marta Venturella. I learned a lot from all of you. For warmly welcoming the only foreigner in the building with arms wide open, and for essentially teaching me Italian, I am forever grateful.

I cannot avoid to thank Mattia in particular, for your perseverance and for all your support and discussions inside and outside the lab. For sharing a house with me, for becoming a close friend during the past years and for all the amazing moments and life episodes we lived through together. Similarly, huge thanks Francesco for your friendship, for your usual uplifting mood, for all the experience and wisdom you brought to our workplace, for the discussions and for all the moments we shared both in and outside the lab. RNA and protein queens, respectively Laura and Giorgia, thank you so much for your patience with my requests and questions, for your help, for our discussions and especially for your kindness. Erika, Ilaria and Filomena, more than cool lab partners you also became great friends. Thank you for all the after-hours plans, for your kindness, support and goofiness, which brightened our days even while doing most boring tasks. For the latter I must not forget Giulio!! An especial thanks to Valentina, without whom many experiments would have been delayed or left undone! Thanks for your patience, support, for always finding a solution, for your efficiency, for arranging things when no one else could and for your kindness. A special thanks also to Elena for all her support and courtesy in and outside the lab, and for being my landlord in one of the most cozy and peaceful houses ever.

For their patience and for giving me the opportunity to do this PhD, I would like to thank Antonio, Davide and Nataša. A special thanks to my supervisor Nataša, who always stood by my side and gave me all the freedom to explore how to best tackle our scientific questions. Thank you, Nat for your perseverance, for your support, for our brainstorms, for letting me follow my extravagant ideas and for your kindness.

Thanks to my beautiful and beloved Piaggio Typhoon, for never breaking down during our 3 years together, for taking me around the city and the countryside, for saving me countless hours and the hassle of public transportation and for giving me the joy to ride a scooter across the beautiful Italian city of Siena. I felt like a true Italian, with my Portuguese accent.

I would also like to mention two PhD students from our sister company in Tallinn, who became good colleagues and friends. Thank you, Danilo Mladenović and Francesca Loria, for all the great moments we shared in and outside the lab.

Thanks to Ben Peacock, who introduced us to nanoFCM for single nanoparticle profiling experiments, and provided much support not only with instrument and protocol optimization, but also with maintenance procedures.

I must address my colleagues and friends from the European Liquid Biopsies Academy (ELBA) project – https://elbaproject.eu/, with who we brought life into this PhD journey, making it unique and worth every second, regardless of all the challenges faced. Despite our individual idiosyncrasies and wide age and cultural differences, it is beautiful to look back on how we all bonded together, since the beginning, till the end. Thank you my fellow ELBAnians Silvia D'Ambrosi, Mafalda Ferreira, Julia Elzanowska, Christine Semira, Martyna Filipska, Carlos Pedraz, Yassine Belloum, Lucija Ačkar, Luis Hernandez, Zahra Samarin, Stavros Giannoukakos, Nicolas Potie, Ilias Glogovitis, Jillian Bracht and Beatriz Sebo. Huge thanks also to the ELBA coordinators, Tom Würdinger and Danijela Koppers-Lalic, for building this whole project and creating an environment that led to fulfilling scientific achievements, but more importantly, allowed many meaningful connections to be made.

As part of ELBA, I had the opportunity to conduct four secondments abroad, where I met wonderful people, from who I learned a lot. Firstly, huge thanks to Bruno Costa-Silva and his lab members Joana, Silvia, Ana, Nuno, Julia and Christine for warmly hosting and teaching me. I am particularly grateful to Joana Maia, who kindly and patiently shared all her extensive knowledge and expertise in this field, which essentially guided me to set the foundations of my whole PhD project.

Thanks to Klaus Pantel and Kai Bartkowiak's for hosting me in their labs. Special thanks to the lab members and colleagues Parinaz, Lucija and Yassine, for welcoming me so well, for their guidance in the lab and for the usual madness outside. Moreover, I should mention my Hamburg flat mates, the Eimsbütt-Rudel, who went out of their way to welcome me, even if only for a single month.

Next stop, Barcelona, where I was kindly hosted by all of the Pangaea Oncology team. Thank you so much Miguel Ángel Molina, Ana Gimenez and Cristina Aguado for completely opening the doors to me, for sharing all your knowledge, for all your help, discussions and supervision. Thanks for believing in my ideas, for making them possible and for the fruitful collaborations we set up during this PhD project. Thanks to my colleagues and good friends Carlos, Jill and Martyna, for who I struggle to find words that fully express my gratitude in having met and shared this whole experience with. Huge thanks also to my flat mates Paul and Oddny, who welcomed me as family for over 2 months and made life outside work as fun and as easy as it gets.

Lastly, thank you so much Tom and Danijela for welcoming me Amsterdam. Thanks for believing in my research, for your guidance, for our brainstorms and for our collaborations, which resulted in extremely interesting and novel research projects. Again, I am short of words to address my colleagues and good friends Mafalda and Silvia. I am extremely glad to have had the opportunity to closely work with you, and forever grateful for every moment we shared throughout this project. All the rest stays between us.

A special thanks to Michael Hackenberg and Stavros Giannoukakos, who amongst their pile of accumulated work, still found time and energy to address my requests and collaborate. Stavros, thank you so much for your patience and input, you really helped me pushing my knowledge and becoming more and more interested in data analysis and bioinformatics. Yamas for all we spent together and for whatever is there to come! The rest stays between us as well, agapité mou Stavros.

Cannot avoid to further thank Nat and Dani, this time for agreeing to be this PhD thesis reviewers. Thank you once more for your time, patience and valuable input, which contributed in shaping this whole work.

Fearing that this acknowledgements section is getting long, I must still find room to mention my close friends. Most met before embarking on this PhD journey, but some picked up along the way. No matter we are in the same town, or in antipodal places, I am forever grateful for the experiences we shared and to know we can truly count on each other. Meaningful connections find their way to revisit each other, and I can only look forward with excitement, for what has yet not happened.

Seria um ultraje não mencionar a minha família. Um eterno obrigado não só aos meus avós Francisco, Teresa, Joaquim e Maria do Rosário, como também à minha tia Mariana, que sempre garantiram que nada me faltasse, que me educaram e que me proporcionaram a oportunidade de estudar e fazer o que bem me apetecesse, sempre em boa fé e confiança total no meu juízo. Um eterno obrigado também aos meus pais António e Maria Margarida, aos quais tudo referido acima e mais se aplica. Obrigado a todos pelos valores, estabilidade, amor, carinho e compreensão transmitidos. Obrigado por toda a paciência e pelo exemplo, tudo o que sou hoje a vocês devo. O vosso menino tornou-se um dotôr, seja lá o que for que isso signifique para mim ou para os outros, mas sei que para vocês tem um grande valor. Onde quer que estejam, levo sempre a vossa memória no coração e no pensamento.

Finally, canım benim, I am eternally grateful our paths bumped, and for where this journey as three has brought us so far. We sometimes wonder about meeting at different times in life, and how different would it be. However, despite the limited understanding of this universe, the moments we share make me believe that somehow, a sort of unique affinity between two souls can always unite them at the most fundamental level. No words could ever express how much you mean to me, nor how much I look forward to further building our yeni dünya together. Cannot thank you enough for everything. Hep keyif pezevengi olalım. Seni seviyorum, Aslı.

I am extremely grateful for all the places this whole journey has brought me to. It is evermore clear that any place in the world can become one’s motherland.

Table of contents

List of Abbreviations

EVs = Extracellular Vesicles

MVs = Microvesicles

PFP = Platelet-free Plasma

MVBs = Multivesicular Bodies

MHC = Major Histocompatibility Complex

MIICs = MHC class II-enriched compartments

DC = Dendritic Cell

APC = Antigen-presenting cell

CTLs = Cytotoxic T Lymphocytes

TNFR = Tumor Necrosis Factor Receptor

ESCs = Embryonic Stem Cells

ISEV = International Society for Extracellular Vesicles

JEV = Journal of Extracellular Vesicles

UTRs = Untranslated Regions

DDR = DNA Damage Response

MISEV = Minimal Information for Studies of Extracellular Vesicles

NSCLC = Non-Small Cell Lung Cancer

TME = Tumor microenvironment

VEGF = Vascular Endothelial Growth Factor

CTCs = Circulating Tumor Cells

BMDCs = Bone Marrow-Derived hematopoietic progenitor Cells

PDAC = Pancreatic Ductal Adenocarcinoma

ATP = Adenosine triphosphate

NK = Natural Killer cells

Tregs = Regulatory T Cells

ctDNA = circulating tumor DNA

PET-CT = positron emission tomography-computed tomography

cfDNA = cell-free DNA

UC = Differential ultracentrifugation

DG-UC = Density gradient differential ultracentrifugation

SEC = Size-exclusion chromatography

UF = Ultrafiltration

nFCM = Nano flow cytometry

SSC = Side scatter

CCM = Cell Conditioned Medium

WB = Western Blot

PE = Phycoerythrin

circRNA = circular RNA

TEP = tumour-educated platelet

EPI = ExoDx™ Prostate (IntelliScore)

AUC = area under the curve

SOC = standard-of-care

Summary

All living cells selectively package a wide variety of biomolecules in nanometric entities termed extracellular vesicles (EVs), which actively mediate vital biological events, especially biomolecule recycling and horizontal intercellular communication. To do so, EVs can diffuse through interstitial space, reaching even circulating biofluids to promote long-range paracrine signalling in recipient cells, while sometimes directly functioning as effectors. Despite fundamental knowledge gaps within the field, EVs are frequently dysregulated during disease, often directly sustaining disease hallmarks. Therefore, they are extremely valuable circulating biomarker sources that can provide timed snapshots of individual (patho)physiological status, while carrying cell or tissue-specific cargo, indicative of their origin. Consequently, attention towards EVs has exponentially increased during the last decade, fostered by translational research efforts that have focused on two major EV applications, either as drug delivery vehicles or as analytes in liquid biopsies, which consist in bodily fluid collection for biomarker detection. In contrast to standard tissue biopsies for cancer management, liquid biopsies are heralded as the holy grail of personalized medicine because they are minimally invasive, low-risk, high-throughput and repeated sampling is easy and cheap. These features enable full understanding of tumour heterogeneity, while tumour progression can be tracked longitudinally, as well as resulting alterations in healthy tissues. Liquid biopsies aid clinicians in early disease detection and screening, patient stratification, treatment response monitoring and resistance mechanism identification.

Still, the small size and low amount of cargo in biological nanoparticles limit current state-of-the-art technologies employed for EV profiling. These fail to grasp the full complexity of EV heterogeneity, ultimately straggling the establishment of model EV samples and identification of clinically relevant EV subpopulations. Hence, the first central aim of this thesis, further described in the first chapter of the results section, concerns the identification of EVs among particle noise and characterization of relevant subpopulations, using state-of-the-art, dedicated instruments, optimized for high-resolution single nanoparticle detection. Label-free and fluorescence measurements allowed either indiscriminate or selective detection of EV subpopulations and common contaminants. Analysing the expression of classical surface markers facilitated EV sample characterization. Using thoroughly optimized staining procedures, fluorescently-labelled EVs could be reproducibly generated, and later employed as tracer EV models for accurate measurements in downstream spike-recovery experiments.

Liquid biopsy studies have often selected blood plasma for EV biomarker discovery and detection, as it potentially transports EVs from any cell type, together with other biomarkers. Since blood collection is a well-established routine clinical practice, it is often considered the ideal biofluid for liquid biopsy tests. The majority of these studies purify bulk EVs with co-isolated contaminants from plasma, failing to investigate the specific EV subsets that actually contain relevant biomarkers, which might end up undetected, diluted among many other macromolecules. Thus, in the second chapter of results, the present thesis aimed to further dissect EV heterogeneity in human plasma samples, and to determine whether distinct EV subpopulations can indeed confer differential clinical utility. To this end, several affinity-based EV isolation approaches were optimized and explored for their efficiency and specificity in simple and complex matrices. However, the complexity of biological matrices, especially plasma, drastically hamper affinity interactions. Hence, additional critical gaps in the field regarding sample pre-analytical processing were addressed. Results demonstrated that target EV subpopulations could be efficiently enriched from plasma, but also, that both complex matrix composition and target EV surface phenotypes can dramatically influence the performance of affinity isolation methods. Furthermore, distinct plasma EV subpopulations were indeed captured when targeting different surface moieties. Platelet-derived EVs, but not other EV subsets, evidenced

mRNA expression signatures that could be linked to early-stage lung cancer, proving that distinct EV subpopulations are indeed more relevant than others for liquid biopsy-based biomarker detection.

In conclusion, the original experimental work reported in thesis evidenced that EV labelling protocols should be optimized for each single nanoparticle profiling platform. Moreover, fluorescent dyes, affinity reagents and methodologies employed must be carefully selected and tested, as all contribute to accurate EV measurements in simple matrices, but can also promote confounding particle detection and biased analysis. Also, elimination of dyes in excess is extremely important for precise small EV detection, and protocols used to conduct this step must not affect the original subpopulation composition in EV samples.

On the other hand, the immunoaffinity-based EV isolation protocol devised in this PhD project purified distinct EV subpopulations from plasma. This protocol is compatible with a wide range of downstream procedures and analytical platforms. It is a simple, quick, scalable and automatable pre-analytical workflow, fitting the requirements of routine clinical assays, as to encourage the inclusion of EVs in novel liquid biopsy tests. Importantly, clinically relevant mRNA expression profiles associated to early-stage lung cancer, were obtained upon isolation of platelet-derived EV subpopulations from plasma, using this immunoaffinity protocol. Furthermore, it was evident that pre-analytical variables, sample matrices and EV surface phenotypes are critical parameters to account for when affinity-based methodologies are employed to target specific EV subsets. As result of the research output throughout this PhD project, ongoing multi-centre collaborations have been established, with the goal of integrating EV multianalyte and multi-omics data. Large-scale validation, prospective and explorative studies will be fundamental for robust biomarker detection and inclusion of EVs in novel liquid biopsy-based assays.

General Introduction

Cells selectively secrete portions of their constituting biomolecules in membrane-enclosed particles, named Extracellular Vesicles (EVs). First hints supporting the existence of this subcellular compartment materialized about 80 years ago, although, it is today that the significance of such novel findings is being grasped, as research efforts propelled only during the past 20 to 30 years. Nevertheless, plenty of key mechanisms and biological events remain to be unveiled or better characterized. EVs are round nanoparticles delimited by a double lipidic membrane, ranging from 40-1000nm in diameter. All cells secrete EVs at least for intercellular communication. As such, they can be found in every tissue and bodily fluid.

The introduction of the present thesis begins with a detailed chronological succession of key EV-related discoveries that outlined current central views in EV research. Subsequently, it focuses on the hallmarks of cancer and on the ambiguous roles EVs can play during tumorigenesis. Finally, it addresses the main theme of the work herein reported: early-stage cancer detection through liquid biopsy-based approaches. After briefly summarizing the largest and most impactful studies being conducted towards this goal, which have not yet included EV-specific biomarkers in their workflows, this introduction wraps up by highlighting the diagnostic potential of EVs for early-stage cancer detection and how they could be best leveraged in novel liquid biopsy strategies.

Many different nomenclatures have been adopted in the EV field, which has led to some degree of confusion and lack of consistency across the literature. Generally, the name “exosome” is used when the endocytic origin of vesicles can be proven, whereas the term “microvesicle” refers to vesiculation through direct blebbing from the cell plasma membrane. The diameter of exosomes falls between 40-200nm, while microvesicles (MVs) display a wide size range, from 40-1000nm. Nonetheless, researchers have used these and other terms interchangeably, failing to provide concrete evidence for the subcellular origin of their EV samples. During the introduction, nomenclatures chosen by cited authors will be briefly adopted, while mentioning their literature. However, all original writing, results and discussion herein reported will be addressed adopting the all-encompassing term extracellular vesicle or EV.

Early knowledge on EV functions and biogenesis (1940s to 2000)

During the 1940s, unknowing that these would be the very first direct evidences of EV function, Erwin Chargaff and Randolph West obtained small biological particles from blood, while attempting to isolate clotting factors. They observed that high-speed centrifugation sediments, composed by a “thromboplastic agent” and a small “particulate fraction”, greatly stimulated the clotting process[1,2]. The first reports describing cell-released vesicles date back to the late 1960s, when Harrison Clarke Anderson discovered what he called “matrix vesicles”. He proposed that these vesicles blebbed from the plasma membrane of chondrocytes, and were morphologically associated with mineral deposition during the process of endochondral ossification[3,4]. Some years later, in 1974, Anderson and two co-workers found a strong structural relationship between the membranes of matrix vesicles and cellular membranes, further strengthening the idea that vesicles were indeed originating from the chondrocyte plasma membrane to actively engage in the process of cartilage calcification[5]. Building on the previous observations by Chargaff and West, in 1967 Peter Wolf coined the term “platelet dust” to describe lipid-rich platelet-derived particles, which could be isolated by high-speed

centrifugation from platelet-free plasma (PFP) and serum, retaining pro-coagulant properties[6]. Today, platelet-derived EVs are well documented and known to be abundantly present in blood.

Fast-forwarding to 1981, one study reported that cells displaying ecto-enzyme activity released vesicles which retained the same catalytic properties as the parental cell line. They also concluded that these vesicles originated from the cell plasma membrane, revealing two subpopulations with the average diameters of 40nm and 500-1000nm. Moreover, these researchers coined the term "exosome" to refer to plasma membrane-derived vesicles in general[7].

In 1983, two independent studies simultaneously unveiled the mechanism behind the gradual loss of the transferrin receptor from the cell membrane, which was already at the time considered a hallmark of reticulocyte maturation during erythropoiesis. They demonstrated that transferrin receptors were firstly internalized by endocytosis to then preferentially accumulate at multivesicular bodies (MVBs), which ultimately fused with the plasma membrane to shuttle small vesicles (60-200nm) enriched in transferrin receptors[8,9]. Focused on this mechanistic process, scientists discovered that instead of blebbing from the plasma membrane, small EVs could be generated through another pathway which involved MVB exocytosis, and contribute to recycle or deplete structures no longer useful for cells[10,11]. These two elegant reports were indeed the first to describe an endocytic route for EV generation, but are often erroneously considered the first to discover exosomes or EVs in general. It is important to underline that the previous aforementioned studies mentioned provided substantial evidence for the existence of small cell-derived membranous vesicles, which had a well-defined nano size range and actively engaged in fundamental biological processes.

Nonetheless, at that time many researchers remained sceptical about this novel MVB-mediated secretion pathway, convinced that parts of the cell membrane would simply shed in the form of vesicles[12]. For almost 10 years, there was little interest in EV research. During the beginning of the 1990s, early indications that EVs could be linked to the initiation of immune responses encouraged scientists to unravel a new wave of EV mechanisms and functions. The following discoveries remain today a foundation for many EV-focused studies, which helped to better understand the complex endocytic pathway.

In 1991, it was found that lysosomes can fuse with endosomes to release EVs that either dispose products of lysosome catabolism, or present them via major histocompatibility complex (MHC) class II molecules, at the plasma membrane. As MHC-II is absent in lysosomes, authors proposed that digested peptides meant for antigen presentation were transferred from lysosomes to endosomes, where they could form peptide-MHC-II complexes. Since most antigens require lysosomal hydrolysis, they proposed that MHC class II-enriched compartments (MIICs) would be the primary site for this process to take place. Ultimately, authors stated that immunogenic determinants must be rescued by specific mechanisms for antigen presentation at the plasma membrane[13].

A seminal study by Raposo et al. published in 1996, proved that B cells externalized vesicles enriched with peptide-MHC-II complexes through exocytosis, which triggered specific T cell responses, establishing that EVs play an important role in direct antigen presentation[14]. Their study was inspired by rather early observations, where intact MHC-II molecules could be recovered in 100.000g ultracentrifugation pellets from B cell conditioned medium[15,16]. Soon after, it was postulated that MHC-II molecules were shed in association with plasma membrane lipids, as small membrane-derived vesicles[17]. Raposo et al. showed that instead of shedding, this was a tightly regulated intracellular mechanism, occurring inside multivesicular MIICs, where antigen-MHC-II complexes were formed and loaded in small vesicles for exocytosis. They further hypothesised that exosomes likely functioned as vehicles for the transfer of antigen-MHC-II complexes between immune cells[14].

Still in 1996, a study focused on tetraspanin proteins revealed that CD9, CD63 and CD81 formed organized microdomains between themselves and other proteins, such as the VLA integrins or HLA-DR antigens, at the cell plasma membrane. These interactions were specific, since *de novo* expressed CD9 could associate with pre-existing plasma membrane microdomains. Authors proposed that the association of these surface molecules in close proximity could have specific roles in co-stimulation, antigen presentation and/or cell adhesion[18].

One year after, researchers trying to obtain pure HIV-1 preparations noticed that MVs co-purified with the virus by sucrose density gradient centrifugation. Although not thoroughly assessed, they claimed that these MVs carried a substantial amount of nucleic acids (both DNA and RNA) and also the HLA-DR and β2-M proteins[19].

Another similar report in 1998 showed that dendritic cell (DC)-derived exosomes triggered strong anti-tumoral T cell immune responses *in vivo*. Moreover, the authors found MHC-I, MHC-II and co-stimulatory molecules expressed in DC exosomes, which they saw as a regulated process and postulated that a key physiological role of exosomes would be to act as messengers, markedly facilitating the communication between cells of the immune system. They also proposed that DC-derived exosomes would be a beneficial cell-free alternative for cancer immunotherapy[20].

The first evidence for tetraspanin protein expression at the EV surface was also published in 1998. It was observed that in addition to MHC-II and the immune co-stimulatory molecule CD86, tetraspanins CD63, CD37 or CD82 were highly enriched in B-cell exosomes, while the most enriched one was CD81. This observation was puzzling because tetraspanins did not contain consensus sorting signals in their cytoplasmic tails, hence it was unclear how they were displayed at the exosome surface. Additionally, the roles of tetraspanins were still highly obscure at the time. Regardless, researchers concluded that tetraspanins were likely sorted with different kinetics due to the differences in their relative enrichment. Furthermore, they showed that the proteins involved in MHC-II transport and antigen loading in MIICs were not present in exosomes, indicating that the processing and loading of antigens in the antigen-MHC-II complexes occurred prior to MIIC fusion with the plasma membrane, and consequent exosome release[21].

Additional studies helped solidifying the concept of vesiculation, which did not seem to be restricted to particular cell types. Platelet-derived EVs became of increasing interest to the scientific community[22–26], while novel EV functions kept being proposed, from immune signalling and communication, to membrane and receptor sorting for recycling or elimination[27–34]. The more EVs were identified and implicated in fundamental biological processes, the greater became the need to standardize data reporting and to find generic, EV-specific molecular markers. For that purpose, the characterization of major EV components using DC-derived EVs was conducted in 1999. Hsc73, annexin II, gag and Gi2α were identified as EV lumen proteins. MFG-E8, Mac-1 and CD9 as membrane proteins. The authors also acknowledged the presence of previously reported tetraspanins, such as CD63, CD81, CD82 and the immune regulators MHC-I and MHC-II[35].

By the year 2000, there was a general agreement that MVBs could either fuse with lysosomal compartments for the degradation of biomolecules, which as previously learned, can be recycled for antigen presentation, or directly fuse with the plasma membrane, resulting in the secretion of small EVs to the extracellular milieu. Concrete evidence confirmed the accuracy of these ideas, later in 2009[36].

Ground-breaking EV-related discoveries (2000 to 2011)

With the advent of the 2000s, revolutionary technologies and achievements, such as the completion of the human genome project in April 2003, set in motion an unprecedent pace in the development of biosciences. The EV field did not fall behind this trend, as outstanding breakthrough discoveries were made along the way, setting the foundations of contemporary EV research.

The first extensive protein analysis of an EV population was done on DC-derived exosomes in 2001 by mass spectrometry. This study identified a unique molecular composition of exosomes, which helped to establish them even further as a truly distinct cellular component, with specific biological functions. Moreover, authors reported that DCs constitutively secreted antigen-presenting EVs, responsible for initiating anti-tumoral immune responses[37].

Still in 2001, another study showed that upon the uptake of tumour-derived EVs, mouse DCs triggered a T cell-mediated rejection of autologous tumours and even robust intertumoral cross-protection *in vivo*. This indicated that distinct tumour-derived EV subpopulations carried shared tumour markers, which could be efficiently engulfed and presented by DCs to trigger robust T cell responses. In comparison to tumour-derived EVs, irradiated tumour cells, apoptotic bodies or tumour lysates were poorly immunogenic, suggesting that EVs might display specific receptors or ligands for efficient uptake by antigen-presenting cells (APCs)[38]. Similar claims were made in 2002, where scientists proved that exosomes isolated from malignant effusions could prime cytotoxic T lymphocytes (CTLs) as efficiently as exosomes derived from tumour cell lines, eliciting immune responses that would not naturally occur in patients. This was one of the first reports detecting and isolating EVs from human biofluids[39]. DC-derived EVs could directly activate T cells both *in vitro* and *in vivo*, further linking EVs to antigen presenting roles. Importantly, EVs helped spreading antigen-MHC-II complexes between different DC populations that might have not encountered such antigens before, thus increasing the pool of competent antigen presenting DCs to stimulate naïve T cells and ultimately propagate immune responses[40].

In 2004 and 2005, the first articles characterizing *ex vivo* EVs isolated from urine[41] and blood plasma[42] were published. Researchers noticed that blood plasma EV preps were clearly rich in contaminants from various sources. Still, they were able to detect CD63, CD9 and CD81 on Human leukaemia mast cell-1 (HMC-1) exosomes and on plasma-derived vesicles after CD63 immunoprecipitation (IP). Plasma-derived vesicles contained not only these tetraspanins but also MHC-II, whereas HMC-1 exosomes only carried tetraspanins as this cell line did not express MHC-II. The platelet marker CD41 was also exclusively found in plasma vesicles. These results showed that exosomes circulate through the whole body and potentially mediate long range intercellular communication and/or horizontal transfer of material[42].

From 2006 to 2008, majorly impactful articles demonstrated that EVs carried both mRNA and miRNA. Functional mRNA could be delivered from EVs and translated into protein by target cells. In addition, EVs were increasingly associated with a wide range of regulatory roles and detected across several human biofluids. All these factors combined drew unprecedent attention and interest to the EV field, and the number of EV-related publications grew. In 2006, it was reported that embryonic stem cell (ESC)-derived MVs enhanced the survival and expansion of hematopoietic progenitor cells. MVs were enriched in mRNA coding for several transcription factors, cytokines and surface receptors. MVs also upregulated the expression of early pluripotency transcription factors in receptor cells, such as Oct-4, Nanog, and Rex-1. Finally, the authors validated that at least functional Oct-4 mRNA was delivered to hematopoietic progenitor cells by ESC MVs and actively translated into protein[43].

In 2007, additional EV mass spectrometry experiments compared exosomes isolated from 3 different cell lines. At least 47 proteins were present in all 3 exosome populations. Moreover, RNA was abundantly detected inside exosomes, excluding the possibility of extracellular RNA contamination. Microarray gene expression analysis identified at least 1300 different transcripts and DNA could not be detected. Surprisingly, gene expression profiles were quite different between donor cells and respective exosomes, meaning that they were enriched in distinct mRNAs and suggesting that mRNA was selectively packaged inside EVs. Finally, mRNAs could be translated into proteins, demonstrating that their function was retained[44].

The first study analysing miRNA expression in circulating plasma MVs obtained from healthy donors was published in 2008. Surprisingly, it was found that miRNA signatures were not influenced by gender or age, which was an important finding if these miRNAs were to be used as potential diagnostic biomarkers[45].

A seminal study conducted by Skog et al. in 2008 investigated tumour-derived EVs obtained from human glioblastoma primary cell cultures. RNAse treatment on isolated EVs minorly impacted total RNA recovery, confirming that the majority of RNA was indeed protected inside the EV lumen. Both miRNA and mRNA profiles were characterized using Agilent 44k microarray chips, which were state-of-the-art technology at the time as they covered the entire human genome. Authors found that distinct mRNAs were highly enriched in EVs when compared to donor cells, further supporting the notion of selective transcript sorting. There was a strong correlation between the mRNA profiles of vesicles generated by different donor cells, and between different donor cells themselves, but not between EVs and respective donor cells, once more pointing towards selective transcript enrichment. Tumour-derived EVs transferred functional mRNA molecules to normal neighbour cells, which translated these transcripts, ultimately altering the cellular translational profile. Moreover, glioblastoma EVs induced angiogenesis in brain endothelial cells and stimulated the proliferation of a glioma cell line. Altogether, these results revealed that tumours could exploit EV pathways to manipulate the tissue microenvironment, favouring tumour growth and invasion. Therefore, the authors reinforced that EVs should be isolated from blood to profile clinically actionable nucleic acid markers and introduced the idea that EVs may be used to detect changes in tumour progression, as blood draws can easily be obtained over time. This could potentially apply for any cancer type, and might even allow the localization of tumour foci in patients. The idea to isolate EVs from easily accessible biofluids for diagnostics was not new[46], however Skog et al. elegantly promoted them as the ideal biomarker source for liquid biopsy-based tests, by evidencing the amount of relevant information carried within circulating EVs isolated from a remarkably low sample volume[47]. In fact, during that same year, Skog co-founded ExosomeDx, which was the first company focused on harnessing the potential of circulating EVs for diagnostic or disease detection purposes. In 2016, they launched the world's first FDA-approved exosome-based liquid biopsy diagnostic test.

By 2010, EVs had been isolated from the majority of human biofluids, and the common view was that essentially all cells were capable of actively secreting EVs, as a part of their constitutive metabolic routines[12,48,49]. With the rapid expansion of the EV field, along came the need to reach consensus on important aspects such as nomenclature and methodologies used for EV isolation and analysis. To take on this mission, a group of researchers joined forces and in 2011, the International Society for Extracellular Vesicles (ISEV) was founded, along with the Journal of Extracellular Vesicles (JEV) in 2012.

Gold rush in the EV field and state-of-the-art (2010 to present day)

From the 2010s until the present day there was a dramatic expansion in the number of publications addressing EVs. This phenomenon is quite evident, as depicted in the plot below (Figure 1).

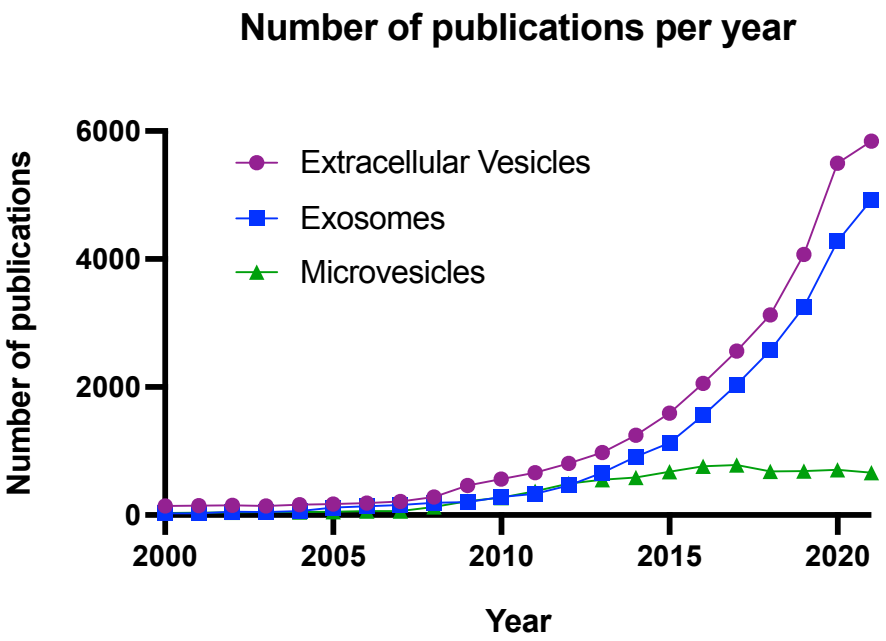

Figure 1. Number of publications per year on PubMed containing the following search queries: Extracellular vesicles (Purple), Exosomes (Blue) and Microvesicles (Green).

Throughout this section I will address the most relevant state-of-the-art concepts in the field, with a heavy focus on cancer biomarker identification and detection, while mentioning potential practical applications of EVs.

The first two studies to perform deep RNA sequencing of EVs were published in 2012 and unveiled that, in addition to miRNA and full-length transcripts, incomplete mRNA fragments were also significantly present. More importantly, these studies showed EVs can carry virtually all RNA species, namely non-coding RNAs, vault RNA, tRNA, Y-RNA, siRNA, snoRNA, scRNA or even retroviral RNA repeats. Since these RNAs were specifically shuttled in EVs, it is possible that they have important regulatory functions, which are still unclear[50,51]. Interestingly, others addressed more in depth the EV mRNA content and found that much of the EV-encapsulated mRNA was fragmented, resulting in an enrichment of the 5' or 3' untranslated regions (UTRs) over full length transcripts[52,53].

Despite the several publications that have provided concrete evidence for the presence of DNA in EVs, this is still a topic of debate in the field as contradictory data has also been published[54–59]. Studies reporting the presence of DNA on EVs were frequently conducted on cancer models. Similar studies performed on healthy controls would be valuable to prove if DNA is indeed physiologically shuttled on EVs, or if this event is restricted to certain contexts, as a result of alterations caused during cancer or other conditions. The latter may actually be a strong hypothesis, as several reports found that DNA was selectively associated with EVs under particular circumstances, for instance during cellular stress or upon activation of the DNA damage response (DDR), which aids in the clearance of cytotoxic cytoplasmic DNA fragments, thereby rescuing cell survival[60–63]. Due to its sensitivity to DNAse treatment, it could be concluded that EV DNA was often externally associated to the EV membrane[63–65]. It is also remotely possible that generally EVs are not released from

parental cells readily carrying DNA on their surface, but rather it can bind as EVs travel through the extracellular milieu. More research on this frontier is required before being able to elaborate clear answers.

It is challenging to pinpoint markers exclusively present in exosomes (endocytic origin) or MVs (plasma membrane). However, there are a handful that have been extensively detected throughout the years, which can be used as faithful markers to support that the starting material for experiments truly contains EVs[55,66,67]:

Table 1. Cellular markers most often found enriched in EV samples.

Surface proteins	CD9, CD81, CD63, CD82, Flotilin-1, Flotilin-2, integrins, lactadherin, ICAM-1, Annexins, RAB GTPases, MHC-I, MHC-II
Membrane lipids	Phosphatidylserine, cholesterol, ceramide, sphingolipids
EV lumen	ALIX, TSG101, HSP70, HSP90, Syntenin, GAPDH, esterases, cytoskeletal proteins

Another critical aspect that has been established throughout time is the wide heterogeneity among EV subpopulations[55,67–73]. Each single cell is capable of secreting quite distinct EV types that differ in their function and phenotype. Moreover, multiple cellular conditions such as activation status, differentiation, ageing or senescence[61,74–76] influence the signatures of EV-packaged molecules and contribute to EV heterogeneity, which can potentially be appreciated at the single-vesicle level. This calls for thorough reporting of methodologies and conditions in EV-related publications as to minimize the amount of irreproducible data and erroneous conclusions.

It is also fundamental to profile EV subpopulations through the identification of conventional EV markers, such as the ones mentioned in the table above, or specific targets of interest. With that in mind and aware of the relentless growth in EV-related studies, ISEV published two position papers, one in 2014[77] and another in 2018[78]. Here, leading experts of the EV field announced that despite the exciting recent discoveries, it was fundamental to maintain rigor due to the complex nature of EVs, which becomes exponentially accentuated when conducting *in vivo* studies. They proposed a series of best practices and minimal experimental requirements as guidelines for future publications. The 2018 update aimed to revise the previous recommendations considering scientific advances made during those 4 years, and to promote their wider acceptance and implementation. Unlike the first edition, the proposed revisions of 2018 were based on the results of a whole ISEV community outreach, where 329 scientists responded to a survey. Upon review by ISEV and JEV members, a comprehensively detailed document (when compared to the 2014 edition) was elaborated, encompassing the views and expertise of scientists directly working in the EV field. The third revision of the Minimal Information for Studies of Extracellular Vesicles (MISEV) guidelines is expected to be published during the current year of 2022.

Current and past research efforts have conceived that EVs hold great promise in many frontiers, some of the most relevant ones being[66,79]:

- Therapeutics (i.e. immunotherapy)
- Diagnostics
- Tracking the progression of pathological states
- Prognosis of tumour progression and metastasis

- Predicting and monitoring therapy response
- Vectors for the modulation of cellular functions *in vivo*
- Bioengineering
- Vaccines (anti-tumour or anti-pathogen)
- Evaluation of the general pathophysiological status of individuals (routine check-ups or screenings)

The central theme of this thesis focuses on exploring the potential of EVs for cancer detection and diagnostics. EVs are important promoters of cancer progression, as will be briefly explained in the subsequent section.

EVs and the Hallmarks of Cancer

Cancer is the most complex disease we have yet encountered. The influential and inspiring publications by Douglas Hanahan and Robert Weinberg remain to this day the most comprehensive outlines on the hallmarks of cancer[80,81]. Despite all the different cancer types and subtypes, encompassing all their complexity and heterogeneity, it was possible to identify 8 hallmark capabilities displayed by all malignant tumours. An accumulating body of evidence reveals that EVs contribute to the initiation, sustainment or exacerbation of most of these pathophysiological traits[82,83]. In the following section, I will list the hallmarks which EVs seem to impact the most, briefly citing supporting literature:

- **Resisting cell death**

Programmed cell death or apoptosis is a process regulated by several sensor and effector proteins, which together are responsible for the elimination of old, damaged or aberrant cells. Therefore, it is an important barrier pre-neoplastic cells must overcome before becoming fully transformed. Only a couple of reports directly identified EV-mediated anti-apoptotic effects in tumour cells *in vivo*[84,85], however, plenty show that EVs actively confer drug resistance, sometimes through the stimulation of anti-apoptotic pathways[86]. Remarkably, cancer cells can selectively pack cytotoxic drugs inside the EV lumen, lowering their effective intracellular concentration to later shuttle them out to extracellular space. Additionally, drug-resistant cancer cells can share their acquired resistance horizontally by exporting drug efflux pumps in EVs that modulate recipient cell metabolism, altering their phenotype for increased resistance or tolerance to therapeutic compounds. EVs can even function as cellular decoys that limit the bioavailability of monoclonal antibody-based drugs, shielding donor cancer cells from the immune system and ultimately reducing the effectiveness of cell-targeted immunotherapies[87–92]. These and many other resistance mechanisms allow cancer cells to escape destruction by therapeutic cytotoxic drugs.

- **Enabling replicative immortality**

Normal cells have a finite number of doubling cycles, which when reached, causes them to enter a state of dormancy termed senescence, resulting in a series of phenotypical changes, where cells remain alive but no longer multiply. However, upon loss of function of both key tumour suppressors p53 and pRb, senescence is lifted and cells restart their division. Due to their compromised viability, this leads to the accumulation of genomic aberrations that ultimately cause vast cell death. Nonetheless, it is possible that from a pool of cells in crisis, an extremely low percentage of them

might survive after massive genomic rearrangements and emerge with the acquired ability to divide indefinitely, becoming immortalized[80,81]. Telomeres are protective caps located at the end of chromosomes, and their length is the main determinant of whether normal cells may further divide, as it grows shorter with each cell doubling. Progressive telomere loss is a physiological process resulting in senescence or extreme genomic instability, both eventually leading to cell death. Therefore, telomere shortening is a central molecular barrier to neoplastic transformation that needs to be overcome by cancer cells[93].

An interesting study by Zomer et al. demonstrated that melanoma cells spread their EVs through the whole body of mice, targeting healthy cells from a variety of organs, which effectively uptake tumour-derived material. The reverse was not as frequently observed[94]. One can conceive such a mechanism for an EV-mediated distribution of cellular immortality. The first cancer cells to achieve this trait might disseminate key factors (i.e. telomerase) to nearby healthy cells, promoting their immortalization and subsequent neoplastic transformation. Despite being a highly plausible possibility, there is not yet concrete evidence reporting the occurrence of such phenomenon.

- **Inducing and sustaining angiogenesis**

The vascular system provides all cells not only a constant supply of nutrients and oxygen, but also means to eliminate unnecessary by-products of metabolism and carbon dioxide. Once vascularized organs are formed, new blood vessels sprout from pre-existing ones through a process termed angiogenesis, which strictly occurs sporadically and transiently. In contrast to normal cells, highly proliferative cancer cells require dedicated vasculature to maintain their turnover and energetic needs. To do so, cancer cells initiate and constitutively sustain angiogenesis, continually expanding the supply of blood vessels in tumour microenvironment (TME), which is a process critically mediated by tumour-derived EVs. Angiogenesis is usually stimulated through the overexpression of the vascular endothelial growth factor (VEGF) and can be induced by a wide variety of EV-mediated cascades of events[95–102].

- **Sustaining proliferative signalling**

The earliest identified and perhaps the most characteristic hallmark of tumour cells is their sustained proliferative capability. Normal cell division requires proliferative stimuli and is tightly regulated by neighbouring cells and tissue microenvironments. This critical homeostatic mechanism maintains a physiological tissue architecture and guarantees that each system in our bodies functions as intended, contributing for the common good of the whole organism. On the other hand, neoplastic cells do not depend on external stimuli, since they constitutively generate their own growth signals, escaping this fundamental homeostatic regulation. As a result, cancer cells stop working for the organism and instead prioritize their own expansion no matter the consequences. Accumulating evidence demonstrates that tumour-derived EVs can hijack normal cells in the TME (i.e. fibroblasts, endothelial or immune cells), forcing them to behave in this way by spreading cancer-enabling characteristics through the activation or overexpression of oncogenes[100,103–105]. The degree of malignant transformation has also been correlated with the number of cell-released EVs, meaning that generally, the more aggressive the phenotype of a tumour cell is, the more EVs we can expect it to secrete[58,82,98,106,107].

- **Activating invasion and metastasis**

During the later stages of cancer progression, some tumour cells acquire the capacity to invade adjacent tissue, escaping the primary tumour mass to eventually colonize distant locations, thus metastasizing. The metastatic process occurs in a rather complex series of events, and accounts for 90% of cancer deaths. Current knowledge on cancer metastasis has essentially expanded during the last two decades, driven by crucial earlier observations. In 1980, Poste and Fidler noticed that despite the presence of circulating tumour cells (CTCs) in the vasculature of multiple organs, tumours consistently metastasized at specific sites[108], indicating that the establishment of metastasis was dependent on a receptive microenvironment[109]. Later on, distant tissue microenvironments were indeed found to be primed before the establishment of metastasis. This process was mediated by bone marrow-derived hematopoietic progenitor cells (BMDCs), which were recruited to the primary tumour site to facilitate primary tumour cell progression, and to increase their metastatic potential by conditioning distant pre-metastatic niches before the arrival of colonizing cancer cells[110].

In 2011[111] and 2012[106], two influential studies showed that EVs are essential in the establishment of pre-metastatic niches. Hood et al. proved that melanoma exosomes induced angiogenesis and an immunosuppressive environment at lymph nodes, priming this pre-metastatic niche to promote recruitment, trapping and growth of melanoma cells, which propagated the settling of secondary tumours at a pre-determined location[111]. Peinado et al. demonstrated that melanoma-derived exosomes stimulate pre-metastatic niche formation through the education of BMDCs by upregulating the oncoprotein MET. Tumour-derived EVs recruited BMDCs to support tumour vascularization, invasion and metastasis through the upregulation of proinflammatory molecules at pre-metastatic sites[106]. In 2015, Costa-Silva et al. further implicated pancreatic ductal adenocarcinoma (PDAC)-derived EVs as critical mediators of pre-metastatic niche formation in the liver. Exosome-carried MIF orchestrated this process, while MIF upregulation could be readily detected in the plasma of stage I PDAC patients, suggesting that this marker could enable early PDAC detection[112]. Additionally, it was shown that malignant melanoma-derived EVs, which carried transcripts promoting cell migration and metastasis, could travel long distances to deliver their cargo to less malignant cells, educating them to increase their migratory behaviour and metastatic potential[94].

Indeed, EVs seem to play a central role in the metastatic process. Elucidating such EV-mediated events is of extreme importance, as metastasis represent the main cause of cancer-related deaths.

- **Deregulating cellular energetics**

During tumorigenesis, cancer cells often reprogram their metabolism, shifting from mitochondrial oxidative phosphorylation to glycolysis, even in the presence of oxygen. This “aerobic glycolysis” metabolism, mostly known as the Warburg effect, generates severely less adenosine triphosphate (ATP) units when compared to cellular respiration, thus forcing an exacerbated glucose uptake. This does not necessarily mean that the oxidative phosphorylation pathway is impaired, however accelerated tumour growth leads to hypoxia. Consequently, the transcription factor HIF-1α is activated, upregulating the expression of glycolytic enzymes and glucose transporters for increased glucose uptake[113]. Thus, aerobic glycolysis not only enables fast expansion of tumour cells, but it also causes TME acidification, which can aid in immune evasion. Additionally, acidic TMEs can increase EV release and uptake, which may favour the cancer-promoting activities of tumour-derived EVs[114]. Moreover, EV-carried biomolecules can induce this metabolic switch in recipient cells, conferring them increased drug-resistance while stimulating their invasive potential, ultimately facilitating cell extravasation and metastasis[115,116].

The content of EVs produced by patient-derived cancer-associated fibroblasts (CAFs) could inhibit mitochondrial oxidative phosphorylation and shift cellular metabolism by facilitating glycolysis[117]. This shows that besides primary cancer cells, once educated, TME cells are exceptionally important in sustaining transformed phenotypes. The involvement of TME EVs in metabolic reprograming and deregulation of cellular energetics during cancer progression is exhaustively covered in a recent review article[118].

- **Avoiding immune-mediated destruction**

Chronic inflammation is by itself a hallmark of cancer that favours tumour progression and therefore, tumours strive to actively maintain it. Immune cells are often educated and exploited locally by cancer cells, through a wide variety of mechanisms. Tumour-derived EVs are certainly one of the main "weapons" for counter-attacking immunocompetent cells, as they generate highly immunosuppressive TMEs. Tumour-derived EVs may display FasL and TRAIL proteins to suppress T lymphocytes or induce their apoptosis, hindering the infiltration of these and other immune cells in the TME, which effectively blocks their anti-tumoral activity[119–121]. TGF-β-expressing EVs could also selectively impair the response of CTLs and natural killer (NK) cells, inhibiting their proliferation in response to IL-2[122–124]. Additionally, tumour-derived EVs stimulate the expansion and suppressor functions of regulatory T cells (Tregs), as well as the differentiation of myeloid cells into immunosuppressive cellular subsets, rather than into immunocompetent DCs[125–127]. Finally, immune checkpoint-loaded tumour-derived EVs, in particular expressing PD-L1 also suppressed T cell proliferation and activation, facilitating cancer progression[128–130].

In a nutshell, cancer is a manifestation of the molecular damage accumulated throughout the life of multicellular organisms. It is the most complex disease known to us because it encompasses the all intricacies of biological systems. Genomic aberrations are the most fundamental and upstream triggers of molecular dysfunction, which may confer increased cellular fitness and cancer enabling characteristics. Consequently, as we learn about the biology of EVs and unveil their essential part in orchestrating homeostasis, the more we inevitably find that they too are ruled by fallible mechanisms and instructions, liable to exploitation. That said, this section did not seek to comprehensively review the relationship between EVs and cancer, but simply aimed to exemplify how EVs may contribute to the establishment and modulation of hallmark capabilities.

The Hallmarks of cancer publications are widely acclaimed and acknowledged on the scientific community. The first was released in 2000[80], followed by a second one in 2011[81], which revisited the past and proposed a next generation of hallmarks. Faithfully, eleven years later yet another update on the hallmarks of cancer was recently published in January 2022[131]. As the pace of scientific knowledge generation does not seem to slow down, this article expands on novel discoveries and current views in an increasing list of hallmarks or cancer enabling characteristics, proposing the inclusion of "unlocking phenotypic plasticity", "nonmutational epigenetic reprogramming", "polymorphic microbiomes" and "senescent cells" as new traits. However, research shows that, despite their individual distinction, cancer hallmarks or enabling characteristics can be perceived from a systems biology perspective as co-dependent, meaning that the relationship between them will also determine cancer pathophysiology. For example, epigenetic reprogramming is one key mediator of cellular plasticity and the predominant oncogenes TP53, KRAS, MYC and NOTCH have been extensively described as drivers of cancer progression, promoting the surge of multiple hallmarks. Cellular senescence is a mechanism complementary to programmed cell death, as both coordinate the inactivation and elimination of unnecessary cells. Nonetheless, recent findings

suggest that senescent cells also contribute to pro-tumorigenic events through biomolecule secretion during senescence-associated secretory phenotype (SASP). SASP-secreted factors can remodel the TME to favor hallmark phenotypes, establishing highly immunosuppressive environments, while supporting local tissue invasion and distant metastasis. Inspired by this collection of publications, several authors followed the same lines to propose molecular hallmarks characterizing other complex biological processes such as ageing[132], which is tightly linked to cancer as both are driven by the accumulation of cellular damage.

Liquid biopsy-based cancer detection and isolation of circulating EVs

Liquid biopsies hold the key for the next generation of non-invasive diagnostic tests. Importantly, they can provide a systemic snapshot of the (patho)physiological state of a particular individual, at any particular time, enabling true precision medicine care. The minimal invasive nature of liquid biopsies allows for frequent sampling, resulting simply in a minor inconvenience but no harm to subjects. It also enables the earliest possible detection of disease onset, even if patients are asymptomatic at the time of testing. In oncology, liquid biopsies can be used for screening, patient stratification, monitoring treatment response and to detect minimal residual disease[133], all from a single blood draw.

Several outstanding studies have demonstrated the validity of liquid biopsies for early cancer detection. The CancerSEEK test examined 1005 non-metastatic cancer patients, against 812 healthy controls, with no history of cancer. The cancer cohort comprised primary tumours from several tissues, namely ovary, liver, stomach, pancreas, esophagus, colorectum, lung, and breast. Researchers queried for driver mutations in 16 genes on circulating tumour DNA (ctDNA) and for the levels of 8 plasma proteins, measured in a single immunoassay platform. Among the 8 cancer types included in the study, the authors achieved a sensitivity and specificity of 70% and >99%, respectively. Tumour location could be pinpointed to two organs with 83% of accuracy, and to one single organ with 63% of accuracy. This was the first large scale, multi-analyte, liquid biopsy-based blood test to report such promising results[134]. The experimental pipeline of the CancerSEEK study was applied to the DETECT-A study in 2020, which enrolled 10 times more patients and was described as an exploratory, prospective and interventional study. DETECT-A was a pioneer and elegant study ahead of its time, which serves as a practical foundation for future liquid biopsy-based cancer screening approaches. It was carefully conceived to test the feasibility of a sequential approach for cancer screening in risk cohorts, without disclosing full details of the study to the subjects enrolled, in order to mitigate anxiety and prevent overdiagnosis. After two rounds of reproducibly abnormal results in blood tests, and after evaluation of each single case by a medical committee, individuals were invited to undergo a full-body positron emission tomography-computed tomography (PET-CT) scan to confirm blood results and localize eventual early-stage tumours, in a minimal invasive fashion[135].

On another frontier, the Circulating Cell-free Genome Atlas is an ongoing large scale study (cancer cohort=10500; healthy cohort=4500), focused on the analysis of methylation patterns on cell-free DNA (cfDNA) from plasma[136,137]. It has also reported extremely promising results, rivalling with the CancerSEEK pipeline. Several other large-scale liquid biopsy-based clinical studies are being conducted, such as STRIVE (~100,000 participants), SUMMIT (~25,000 participants), PATHFINDER (~6,200 participants) and ASCEND (3,000 participants)[138], which underlines the high expectations for the field of liquid biopsies in the present day and near future.

Still, large scale clinical studies specifically regarding EVs as central biomarker sources are lacking. A recently published article demonstrated that the information carried within EVs allowed to cluster

cancer patient samples based on their primary tumour types. Authors compared the EV proteome of 426 different human cancer and non-cancer samples from different sources and identified tumour-associated EV protein signatures of early-stage cancer. These signatures allowed to correctly classify normal and tumour tissues with over 90% of sensitivity and specificity and surprisingly, samples from the same cancer types clustered together after data processing with dimensionality reduction algorithms. Altogether, this study validated the utility of EV protein panels in early cancer detection[139]. Despite such promising results however, not many prospective liquid biopsy-based studies have been conducted, and likely none strongly focused on EVs.

EVs have been widely acknowledged as repositories of cancer biomarkers and are thus highly relevant in clinical diagnostics settings[140–142]. In contrast with cfDNA or ctDNA, which are subject to degradation, thus losing their biomarker quality, EV-carried analytes are shielded inside the EV lumen and sustain their biomarker potential throughout their journey. EVs also have the advantage of encapsulating protein, lipids or nucleic acids, enabling true multi-analyte assays from a single biosource. Such assays, as evidenced by the CancerSEEK study, can more robustly detect disease, provide an ampler overview of its pathophysiology and even pinpoint tissue of origin[133,134].

Because many cell types actively secrete EVs that end up in the bloodstream, circulating plasma EVs not only portray a more complete picture of tumour heterogeneity, but also indicate how healthy cells from various systems have been affected by disease over time, which is simply not possible with cfDNA. Liquid biopsy composition can be greatly affected by a panoply of external factors, usually deemed pre-analytical variables. Essentially, at each step of the procedure, from sample collection until completion of required downstream analyses, it is important to understand the sources of bias that can potentially skew reproducible and trustworthy observations. Acknowledging their inevitability and working to minimize them, or at best systematise them is critical, particularly at the pre-analytical stage, since upstream generated artifacts carry through the whole flow, contributing to the formulation of false conclusions. Many pre-analytical parameters have been previously noted and fairly reviewed, especially with regard to blood-derived EVs[143–150].

The list of practical and technical challenges towards implementing EV-based liquid biopsy tests is long. One of the main roadblocks is the lack of standardized and automatable procedures for sample purification. Moreover, the majority of EV isolation protocols commonly employed in research environments are not adequate or lack the necessary throughput for routine clinical care. Also, circulating EVs are highly heterogeneous, and the overrepresentation of certain subpopulations is often undesirable. In addition to the broad variety of circulating EVs, plasma is a highly complex biological matrix, containing a wide range of possible contaminants, such as lipoproteins and other factors that co-purify with all the conventional EV isolation methods[145,150,151].

These and other aspects hamper the performance of downstream analytical platforms, which fail to discern low abundance subpopulations among particle noise, reflecting similar difficulties encountered during the extraction of extraordinarily low amounts of ctDNA, over total pools of cfDNA[133,143,152]. In fact, it is widely acknowledged that due to their nanoscale, high heterogeneity, paucity of biomarker material, and inconsistent reporting of experimental works, EVs are often insufficiently characterized, revealing that conventionally employed methodologies are not yet suited to fully grasp the complexities of the EV field[153]. Consequently, most studies have prioritized the accumulation of large amounts of bulk EV material, in order to barely reach the limit of detection (LOD) of their instruments, often still lacking the necessary analytical capabilities to appreciate EV heterogeneity. Considering all the challenges listed above, while knowing that patient samples are usually rather limited, that blood is a tremendously rich biofluid and that the composition of samples obtained from different donors broadly fluctuates, resulting in wide inter-donor variations, we can ultimately understand why routine blood-based EV liquid biopsy tests are not yet a reality.

Several EV purification methods have been developed and adapted throughout the years. In fact, this remains one of the most heated debate topics within the scientific community. Since each technique has its advantages and drawbacks, downstream applications of interest should drive the selection of EV isolation approaches. Generally, procedures that rely on physical parameters such as size or density solely permit whole EV isolation – a heterogenous mix of all constituent EV subpopulations of that sample. In contrast, affinity-based isolation strategies can selectively capture and enrich for EVs that display target surface features, namely organ, tissue or disease-specific markers.

In the table below, we compare key characteristics of the most frequently used techniques for EV isolation and purification. No single one is able to circumvent all challenges, therefore they should ideally be orthogonally tested for each specific application before committing[148,150,154,155]. It is not enough to stress that an open and critical scientific mind towards even such preliminary experiments is fundamental, especially in the EV field where analytical challenges pose major concerns. Some of these techniques can often be combined, allowing to cumulatively extract the benefits conferred by each single one. Of note, the protocols chosen to carry out these techniques will also influence final experimental outcomes. Despite several new emerging methodologies having delivered promising results, here we focused on well-established and commonly used ones[148,150,154,155].

Table 2. Comparison between the techniques most frequently employed for EV isolation and purification from simple and complex samples (most often blood)[148,150,154,155].

Technique	EVs recovered	Advantages	Drawbacks	Co-isolated material
Differential ultracentrifugation (UC) or density gradient UC (DG-UC)	Bulk EVs, heterogeneous subpopulations	- Low-cost, - well-established, - wide volume range compatibility, - high purity (DG-UC)	- Largely time-consuming, - laborious, - EV disruption, - EV and protein aggregates, - requires high input material, - difficult to automate, - low yield (DG-UC), - low throughput	- Protein aggregates, - proteins, - lipoproteins, - viral particles, - other nanoparticles
Size-exclusion chromatography (SEC)	Bulk EVs, heterogeneous subpopulations	- Avoids aggregation, - recovers functional EVs, - average to high recovery, - average to high purity, - gentle EV processing, - enables buffer exchange, - wide volume range compatibility, - quick and low-cost, - automatable, - wide variety of different resins (nano pores, ion-exchange, etc.)	- High sample dilution, - might require sample concentration, - quality control of resins, - requires some optimization, - time-consuming setting up and cleaning procedures, - low to average throughput	- large protein aggregates, - lipoproteins, - viral particles, - interacting factors at target EV surface - other nanoparticles
Affinity capture	Targeted EV subpopulations (surface phenotype)	- Select EV subpopulations, - high yield, - high purity, - high throughput, - suited for low volumes, - quick, cheap, scalable, automatable, - direct isolation and *in situ* analysis, - compatible with microfluidics, - enables buffer exchange, - wide variety of affinity reagents, - suited for clinical diagnostics	- Unsuited for high volumes, - difficult elution of functional EVs, - requires thorough optimization, - lack of standardization	- Complex matrix components (non-specific affinity), - interacting factors at target EV surface
Ultrafiltration (UF)	Bulk EVs, heterogeneous subpopulations	- enables sample concentration, - recovers functional EVs, - average to high recovery, - gentle EV processing, - enables buffer exchange, - wide volume range compatibility,	- Requires pre-purification / pre-clearing, - unsuited for complex biological samples, - lack of standardization, - can disrupt EVs,	- Protein aggregates, - proteins, - viral particles, - lipoproteins (on pre-purified samples)

		- quick and potentially low-cost, - low speed centrifugation	- low to average throughput	- interacting factors at target EV surface - other nanoparticles
Precipitation-based polymers	Bulk EVs, heterogeneous subpopulations	- High yield, - cheap, quick, - simple protocol, - easy to implement, - wide volume range compatibility, - low speed centrifugation	- Low purity, - requires pre-purification or pre-clearing, - highly susceptible to contaminants, - often commercial kits, undisclosed composition, - time-consuming, - might alter EV properties	- Protein aggregates, - proteins, - viral particles, - lipoproteins (on pre-purified samples) - other nanoparticles
Microfluidics	Targeted EV subpopulations (surface phenotype and physical properties)	- Suited for low volumes, - compatible with affinity capture, - direct isolation and *in situ* analysis, - quick, automatable, - suited for clinical diagnostics, - designed for target EV detection, - enables size, shape, density and charge selectivity	- Unsuited for high volumes, - difficult elution of functional EVs, - low recovery, - requires thorough optimization, - unsuited for research settings	- Non-specific complex matrix components, - interacting factors at target EV surface, - nanoparticles of similar physical properties

Current barriers to technological advances in the EV field, whether at the analytical or pre-analytical phases, reveal that extracting actionable information from bulk EV material might not actually be as straightforward as previously envisaged. Shotgun approaches, sometimes relying on a “garbage in, gold out” wishful thinking, are not realistically feasible, particularly when aiming to measure minute amounts of biomarker material for the detection of very early disease onsets.

Hence, the need to improve input material quality through the selective enrichment of specific EV subpopulations, becomes not only evident, but also the single foreseeable last resort solution, when technology falls short to provide clarity on the questions being pursued. This idea seems to be gaining popularity among a growing number of researchers and experts in the EV field[153], as targeted isolation and analytical methodologies have the potential to reveal previously undetectable features. The few liquid biopsy-based assays that have made their way into the clinics are highly targeted approaches, which had to undergo arduously long journeys to demonstrate analytical validity, clinical validity and clinical utility. The whole process of complying with numerous strict requisites also requires large sums of money, thus it is not realistically feasible for the large majority of novel clinically-focused liquid biopsy tests[147]. In conclusion, methodologies that allow for better, rapid and selective isolation of EV subpopulations have the potential to improve accurate detection of target features and the performance of downstream analytics, which supports their introduction into routine clinical care.

Aware that implementing real-world liquid biopsy-based clinical assays is a truly herculean task, while reflecting on the conceivable challenges faced along the way, instead of delivering a selective EV isolation solution that would solely fit research and development applications, we broadened our horizons by defining clear milestones, aimed to encompass and comply with the strict requisites that must be met before widespread clinical implementation. As such, we strived to provide optimized approaches that were simple, quick, cost-effective, scalable and automatable, among others.

Certainly, it is impossible to account for all the potential challenges ahead of time. Although, keeping some in mind when tailoring experimental designs, methodologies or protocols, while sustaining a strong focus on the endpoint goal of fitting a realistically feasible clinical flow, might facilitate and expedite the translation of novel procedures into clinically useful approaches.

With that, we introduce the next section, which explains the thesis and motivations of this PhD project.

Motivations and structure of the PhD project

As evidenced in the studies mentioned above, ctDNA or cfDNA is the typical biomarker targeted in contemporary liquid biopsy analysis. In addition, CTCs, platelets and EVs have also proven to be appealing blood-based cancer biomarker sources, which may complement each other to provide ever accurate diagnostic tests. Particularly, platelets and EVs hold a great promise for early-stage cancer detection due to their richness in biomarker material that can potentially provide the earliest possible indication of pathophysiological developments.

With the motivation of expanding current knowledge on liquid biopsies and to deliver novel real-world clinical solutions for cancer diagnostics, the ultimate goal of this PhD project consisted in the analysis of different EV subpopulations, isolated from the blood plasma of early-stage NSCLC patients and healthy donors.

We postulate that the information transported in some, but not all EV subpopulations reflects not only the presence cancer but also the extent of its development, and possibly its location. Identification and selective isolation of such specific EV subsets would allow to assess whether their biomarker content can be robust enough for the establishment of next generation diagnostic and eventually screening tests.

NSCLC is the most common cause of cancer-associated death, as it is mostly diagnosed at advanced stages and tumours display wide heterogeneity. It accounts for 85% of all diagnosed lung cancers, with a 5-year disease-free survival rate of 17,7%[79]. Overall, the same is true for other cancer types, where late-stage detection means dramatically compromised chances of survival. Hence, it becomes clear the need for “early-as-possible” cancer detection strategies, supporting the famous statement that says: early detection is the best protection.

Therefore, we aimed to harness the potential of EVs for early-stage NSCLC detection, by employing liquid biopsy-enabling methodologies in the affinity-based enrichment of tumour-specific signatures, carried within circulating EVs from blood plasma.

The broad scientific objectives of this PhD project were to:

- Obtain comprehensive, clinically relevant information out of individual standardised blood-based biomarker sources;
- Pinpoint diagnostic synergy between biomarker sources or multiple analytes carried within them;
- Identify and validate biomarkers for the detection of stage I-IV NSCLC;
- Identify and validate biomarkers for selection of NSCLC patients for treatment;
- Establish novel bioinformatics tools and protocols for the integrative analysis of multi-source liquid biopsy data;
- Develop blood-based assays and delivering scalable prototypes capable of obtaining regulatory approval.

Concretely, this PhD project was shaped to meet the following central milestones:

1. Testing sample stabilisation and preclearing protocols for maximum, specific and robust recovery of different EV subpopulations from blood;
2. Development of protocols, devices and immunoaffinity reagents for the selection and capture of target EV subpopulations containing NSCLC markers, from complex matrices such as plasma;
3. Identification of relevant EV marker profiles holding potential for early-stage cancer detection;
4. Compilation of analytical solutions for the analysis of multiple co-expressed EV markers.

Considering our broad scientific objectives, an experimental work was devised comprising three sequential phases to achieve the outlined milestones:

1. Characterization of EVs obtained from several different cell lines, using a high-resolution single-particle platform to interrogate classical EV surface markers. Here, we optimized several EV labelling protocols to stain whole EVs indiscriminately, but also to stain specific intraluminal EV components, enabling a precise identification of subpopulations of interest.

2. Demonstration of selective EV recovery and isolation though IP, not only from simple matrices such as saline buffers (PBS-BSA), but also from complex ones (human plasma).

3. In-depth analysis of specific EV subpopulations captured from healthy donor and early-stage NSCLC patient plasma samples. Gene expression profiling was conducted with the nCounter platform, which revealed that different EV subsets from the same samples contain distinct molecular profiles, which might be clinically relevant for novel liquid biopsy approaches.

The results section of this thesis is structured in two parts, each presented by the corresponding original research output in the form of scientific articles or manuscripts. The first one features as it is publicly available, formatted and published according to the respective journal's guidelines. As it is currently under submission, the second article features in the form of manuscript, exactly as it was submitted. Materials and methods are respectively reported in each results section.

Resulting from the success of our proof of principle study (results section, Part 2), additional mRNA profiling experiments were performed on healthy (n=50) and early-stage NSCLC (n=50) plasma samples, for which the clinical information is still being collected since this was a prospective cohort study. Despite already having gene expression data for all samples, it is not possible to conduct its analysis using our dedicated bioinformatics pipeline without complete clinical data. Therefore, this extended cohort study cannot yet be fully presented.

Results

Part 1: Optimization of labelling protocols for model EV characterisation and exploitation as spike-ins

Fortunato, D. *et al.* Opportunities and Pitfalls of Fluorescent Labeling Methodologies for Extracellular Vesicle Profiling on High-Resolution Single-Particle Platforms. *Int. J. Mol. Sci.* **22**, 10510 (2021)

Doi: https://doi.org/10.3390/ijms221910510

International Journal of
Molecular Sciences

MDPI

Article

Opportunities and Pitfalls of Fluorescent Labeling Methodologies for Extracellular Vesicle Profiling on High-Resolution Single-Particle Platforms

Diogo Fortunato [1,†], Danilo Mladenović [2,3,†], Mattia Criscuoli [1,†], Francesca Loria [2], Kadi-Liis Veiman [2], Davide Zocco [1,4], Kairi Koort [3] and Natasa Zarovni [1,2,*]

[1] Exosomics SpA, 53100 Siena, Italy; dfortunato@exosomics.eu (D.F.); mcriscuoli@exosomics.eu (M.C.); dzocco@exosomics.eu (D.Z.)
[2] HansaBioMed Life Sciences Ltd., 12618 Tallinn, Estonia; danilo@hansabiomed.eu (D.M.); francesca@hansabiomed.eu (F.L.); kadi-liis@hansabiomed.eu (K.-L.V.)
[3] School of Natural Sciences and Health, Tallinn University, 10120 Tallinn, Estonia; kairi.koort@tlu.ee
[4] Cell and Gene Therapy Research and Development, Lonza Inc., Rockville, MD 20850, USA
* Correspondence: nzarovni@exosomics.eu
† These authors contributed equally to this work.

Abstract: The relevance of extracellular vesicles (EVs) has grown exponentially, together with innovative basic research branches that feed medical and bioengineering applications. Such attraction has been fostered by the biological roles of EVs, as they carry biomolecules from any cell type to trigger systemic paracrine signaling or to dispose metabolism products. To fulfill their roles, EVs are transported through circulating biofluids, which can be exploited for the administration of therapeutic nanostructures or collected to intercept relevant EV-contained biomarkers. Despite their potential, EVs are ubiquitous and considerably heterogeneous. Therefore, it is fundamental to profile and identify subpopulations of interest. In this study, we optimized EV-labeling protocols on two different high-resolution single-particle platforms, the NanoFCM NanoAnalyzer (nFCM) and Particle Metrix ZetaView Fluorescence Nanoparticle Tracking Analyzer (F-NTA). In addition to the information obtained by particles' scattered light, purified and non-purified EVs from different cell sources were fluorescently stained with combinations of specific dyes and antibodies to facilitate their identification and characterization. Despite the validity and compatibility of EV-labeling strategies, they should be optimized for each platform. Since EVs can be easily confounded with similar-sized nanoparticles, it is imperative to control instrument settings and the specificity of staining protocols in order to conduct a rigorous and informative analysis.

Keywords: extracellular vesicles; exosomes; flow cytometry; nanoparticle tracking analysis; fluorescent dyes; purification; isolation; subpopulations; tetraspanin; antibody

Citation: Fortunato, D.; Mladenović, D.; Criscuoli, M.; Loria, F.; Veiman, K.-L.; Zocco, D.; Koort, K.; Zarovni, N. Opportunities and Pitfalls of Fluorescent Labeling Methodologies for Extracellular Vesicle Profiling on High-Resolution Single-Particle Platforms. *Int. J. Mol. Sci.* **2021**, *22*, 10510. https://doi.org/10.3390/ijms221910510

Academic Editor: Leonora Balaj

Received: 3 September 2021
Accepted: 23 September 2021
Published: 29 September 2021

1. Introduction

For the past two decades, EV research has risen exponentially along with the outstanding discoveries that have revealed numerous biological functions mediated or directly executed by EVs. These membrane-enclosed nanoparticles virtually encapsulate any biomolecule type found in respective donor cells, namely: DNA, RNA, proteins, lipids, or metabolites [1–3]. Nearly all of the cells in the human body actively secrete EVs, which can circulate through all sorts of biological fluids such as plasma, urine, or saliva [1]. Recently, the scientific community realized that EVs were significantly promising non-invasive indicators of an individual's global health status. This sparked the race for the discovery of EV-specific biomarkers, with the goal of improving or enabling the detection of a number of diseases and translating novel non-invasive practices into routine clinical use. Since small EVs (sEVs), typically in a nanoscale range (30–200 nm), are highly heterogeneous and indistinguishable from other biological nanoparticles, the absolute need to

perform true single-vesicle discrimination, analysis, and characterization quickly emerged. For this purpose, high-resolution methodologies, such as nanoparticle tracking analysis (NTA) [4–8], tunable resistive pulse sensing (TRPS) [9,10], Raman spectroscopy [11–13], atomic force microscopy [14,15], super-resolution microscopy [16–19], or nanoflow cytometry [20–24], have been explored [25,26]. Techniques relying on label-free EV analysis can estimate particle size, concentration, and other physical parameters such as zeta potential. Methods focused exclusively on fluorescence measurements help to determine the nature or composition of labelled particles within the samples. Hence, it becomes clear that approaches incorporating both label-free and fluorescence measurements may provide the necessary robustness to discriminate true sEVs in complex samples and to quantitatively characterize relevant subpopulations, often present in extremely low abundance.

In conventional flow cytometers, light scatter measurements alone enable a high-throughput multiparametric analysis of microscopic particles, which can be combined with fluorescent labeling to pinpoint and characterize specific components or biological processes. However, due to the physical properties of particles and light, conventional flow cytometers fail to detect events under 200 nm [27]. Summarily, the intensity of scattered light decreases by orders of magnitude (sixth power), for particles with size smaller than the wavelength of the incident light [28,29]. In order to accurately detect sEVs, dedicated state-of-the-art systems have been developed to increase the sensitivity of nanoparticle profiling in sheathed flow.

NTA has been extensively used for counting and estimating the size of particles based on their Brownian motion in suspension. This platform has a high-resolution capability, detecting biological particles as small as 30 nm; however, measurements of larger particles (>1 µm) tend to be less accurate due to their slower movement [25,30]. Aside from size and concentration, multiple additional parameters can be analyzed, such as zeta potential, volume, surface area, light intensity, and aspect ratio of particles, providing a multifaceted biophysical assessment of polydisperse samples. More recently, NTA platforms developed optimized fluorescence modes (F-NTA), which permit a phenotypic characterization of analyzed particles within a sample [4,31,32]. Fluorophore stability and intensity pose as crucial factors for precise measurement of smaller particles, while the sensitivity required for the reliable capture of such signals renders instruments more susceptible to background noise and contaminants.

All sEVs are structurally similar. They are enclosed by a lipidic membrane, within a well-defined size range and carry different types of biomolecules found in respective donor cells. Cargo loading and release, though not fully elucidated yet, are actively regulated mechanisms that form the unique identity of each sEV and are thus responsible for the wide heterogeneity between vesicle subpopulations [33–37]. Identification and characterization of true sEVs requires a biochemical analysis of their content, often relying on the presence or absence of surface proteins on the lipidic membrane (i.e., classical tetraspanins CD9, CD63, and CD81). Subpopulations containing internal markers of interest can also be identified with specific membrane-permeable dyes.

Recently, several strategies for EV labeling have been proposed. These often consist of adapting staining protocols of fluorescent dyes intended to be applied in cells [20]. Dyes used for EV labeling were selected based on their specificity for different EV components such as proteins, lipids, or nucleic acids. Moreover, we applied fluorescently labeled antibodies to probe for specific outer membrane molecules. sEVs were characterized on nFCM, a dedicated high-resolution nanoflow cytometry platform that combines single-particle fluorescence detection with respective scattered light, suitable for biological particles down to 40 nm. To understand whether optimized staining protocols for purified EVs or cell-conditioned media (CCM) could be transversally applied between different platforms, we further tested them in F-NTA. Finally, we underline some of the main hurdles to single sEV discrimination, which are often related to potential co-isolated contaminants, such as large protein complexes, soluble proteins, or cell culture media components.

2. Results

2.1. EV Labeling with Membrane and Cytoplasmic Dyes

Different staining approaches were evaluated in this study. One consisted of staining the lipidic membrane constituents of EVs using amphipathic molecules, such as the CellMask™ (CM) Plasma Membrane Stains, CMG and CMR, which emit green and red fluorescence, respectively. Secondly, we exploited the properties of CellTrace™ cell proliferation dyes, in this case, carboxyfluorescein succinimidyl ester (CFSE) and CellTrace™ Red (CTR). These dyes differ only in the wavelength of emitted fluorescence (CFSE: green; CTR: Red), but their mechanism of action is identical. Briefly, dye molecules easily penetrate the lipidic bilayer of EVs, becoming activated by an enzymatic cleavage and covalently bound to proteins present in the EV lumen. This process effectively traps dye molecules inside every single EV, generating a stable fluorescent signal [38,39]. Over 90% of the particles in the HT29 sEV samples were stained by CMG, CMR, CFSE and CTR and detected on nFCM (Figure 1A). Larger sEVs displayed notably higher fluorescence intensities on dot plots, which was likely elicited by the incorporation of more dye molecules (Figure 1B). Staining protocols were also tested on F-NTA, with the scope of validating them on a state-of-the-art orthogonal platform. Staining performance with CFSE was ~88% on F-NTA, comparable to the one detected on nFCM (Figure 1A), although a higher concentration of dye was required to reach a staining plateau (50 μM in F-NTA, with respect to 10 μM used in nFCM measurements). On the other hand, CMG displayed a consistently lower staining efficiency, with a maximum of ~32% obtained at the concentration of 20× CMG (Figure 1A). Particle size distribution (PSD) histograms demonstrated a prevalent detection of larger particles on F-NTA, as they harbored more dye (Figure 1C—CMG). Bulk fluorescence signal-to-background ratios measured on a microplate reader varied linearly with the number of stained particles for all dyes, although the highest sensitivity was obtained with both green dyes, CFSE and CMG (Figure 1D).

To control dye specificity, besides the compulsory use of blanks and unstained controls (Supplementary Figure S1), a protein called thyroglobulin was included in this study. Due to its large size, single events could be picked up in the side scatter channel. Hardly any thyroglobulin particles were stained by CMG, however, after CFSE staining the number of detected fluorescent events in F-NTA surpassed the scattered ones by orders of magnitude, even after 300 kDa ultrafiltration (UF) washing (Supplementary Figure S5). In nFCM, CFSE-labelled thyroglobulin particles were also detected (data not shown). A comparable degree of dye activation was observed in F-NTA with CFSE-stained BSA controls, while UF successfully removed all fluorescent events (Supplementary Figure S5).

2.2. Characterization of sEV Subpopulations Using Single Fluorophore Tetraspanin Labeling Strategies

To identify the fluorophores conferring maximum sensitivity for sEV detection on nFCM, we compared the staining of HT29-derived sEVs obtained with anti-CD9 primary antibodies conjugated to PE, AF488, AF647, and APC. Maximal CD9 staining was achieved with PE and AF488, as both allowed detection of similar percentages of the CD9 subpopulation (close to 50%). The red fluorophores, AF647 and APC, did not stain CD9+ sEVs to a comparable degree (Figure 2A). Henceforth, in nFCM experiments we opted for PE and AF488-conjugated antibodies, having PE as reference fluorophore due to its higher brightness. Despite its extreme brightness, the high photobleaching rate of PE renders it unsuitable for the F-NTA platform, where precise measurements rely on signal acquisition for longer time periods. Therefore, AF488 was chosen for sEV phenotyping on F-NTA, since it is a more stable fluorophore.

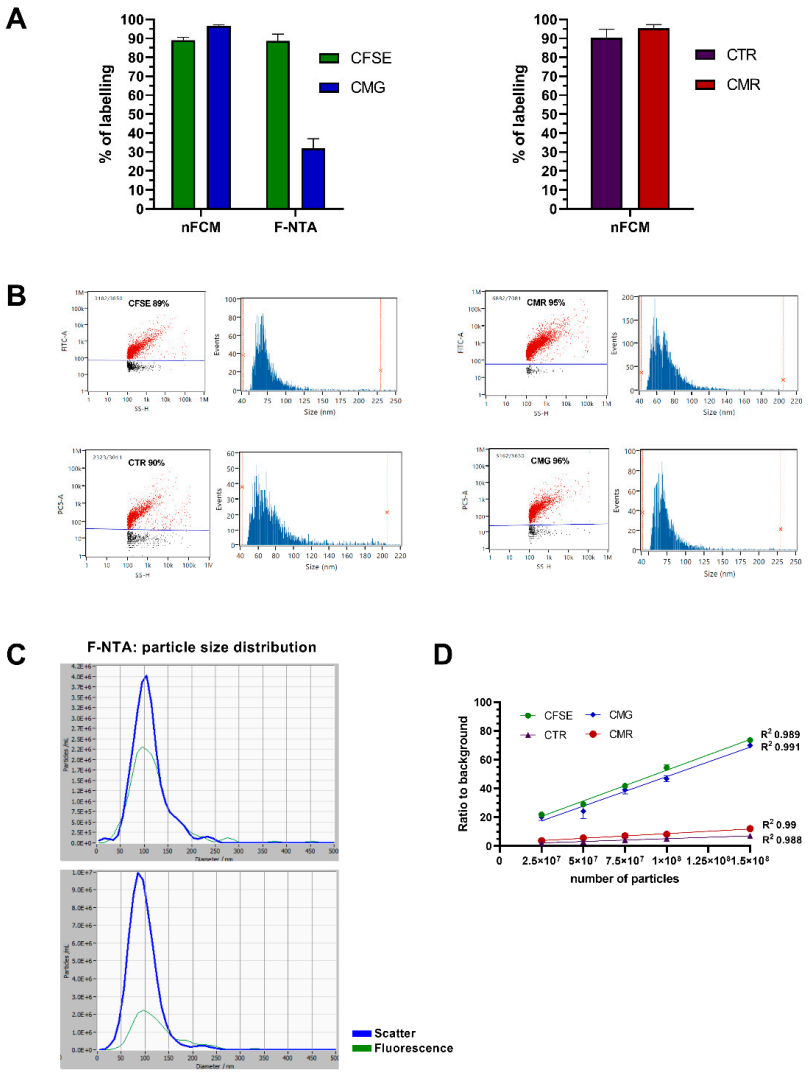

Figure 1. Fluorescence measurements on nFCM, F-NTA and plate reader after sEV staining with membrane and cytoplasmic dyes. (**A**) HT29 sEVs were stained with membrane-specific (CMG or CMR) or cytoplasmic dyes (CFSE or CTR) and analyzed on nFCM and F-NTA to evaluate labeling %. Data is presented as mean ± SEM of at least three independent experiments (except for nFCM-CMG and CMR, and F-NTA-CFSE, which were repeated twice). (**B**) Representative nFCM dot-plots and PSD histograms, and (**C**) histograms obtained after analyzing EVs by F-NTA in scatter and fluorescence mode. (**D**) Bulk fluorescence intensity of a dilution series of stained HT29 EVs was measured by plate reader. Signal over background (PBS) ratios are represented and trendlines drawn for the assessment of correlations. Additional data from procedural controls is provided in Supplementary Figure S1.

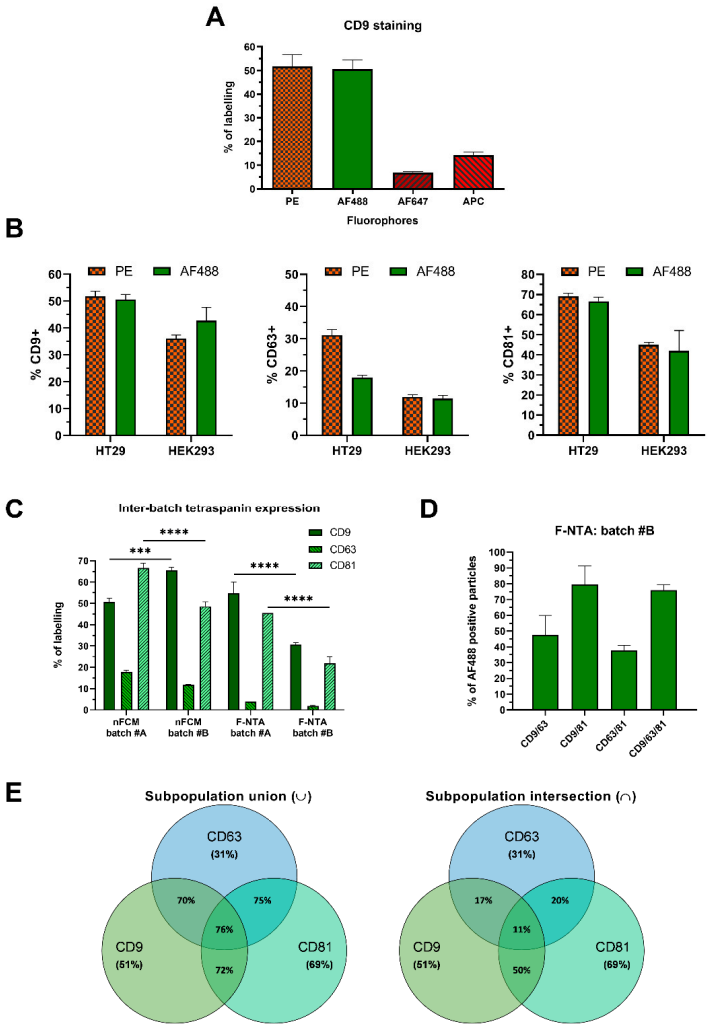

Figure 2. Characterization of purified sEV subpopulations based on their surface markers. (**A**) Antibody staining efficiency was evaluated by nFCM using anti-CD9 antibodies conjugated with different fluorophores. (**B**) HT29 and HEK293 sEVs were stained with anti-tetraspanin (CD9, CD63, and CD81) antibodies, conjugated with either PE or AF488, and analyzed on nFCM ($n \geq 3$; mean ± SEM). (**C**) Cross-platform and inter-batch variability was assessed by single-staining HT29 sEV (batches #A and #B) with anti-tetraspanin AF488 antibodies ($n = 3$; mean ± SEM). Differences in tetraspanin expression between nFCM and F-NTA, and batches #A and #B, were assessed using two-way ANOVA with Tukey's test for multiple comparisons (alpha = 0.05, $p = 0.1234$ (ns), 0.0002 (***), <0.0001 (****)). Detailed results of the statistical analysis are provided as supplementary material. (**D**) To evaluate single, as well as co-expressing, events, HT29 sEVs were stained with a mix of 2 and 3 different anti-tetraspanin AF488 antibodies and analyzed on F-NTA ($n = 3$; mean ± SEM), or on (**E**) nFCM using PE-conjugated antibodies ($n = 3$; mean ± SEM). HT29 sEV subpopulations expressing either 1, 2, or 3 markers are represented in the Venn diagram on the left. The Venn diagram on the right refers to the same HT29 sEVs, however it depicts subpopulations co-expressing both 2 or 3 markers simultaneously. Additional data from procedural controls, as well as the F-NTA PSD histograms, are provided in Supplementary Figure S1.

To evaluate whether the chosen fluorophores indeed performed equally well, HT29 and HEK293 sEVs were stained with PE or AF488-conjugated anti-CD9, -CD81 and -CD63 primary antibodies, followed by nFCM analysis (Figure 2B). In HT29 sEVs, CD9 was detected at 51% (PE)/50% (AF488), CD63 at 31% (PE)/18% (AF488) and CD81 at 69% (PE)/66% (AF488). For HEK293 sEVs, detected CD9 events accounted for 36% (PE)/42% (AF488), CD63 for 12% (PE)/11% (AF488) and CD81 for 45% (PE)/42% (AF488) (Figure 2B). Both fluorophores generally allowed for the detection of similar proportions of EV subpopulations, with a major discrepancy observed only for CD63 detection in HT29 sEVs. The latter may be due to the fact that different anti-CD63 antibody clones labeled with two fluorophores were available and used in this study. To assess antibody specificity, in addition to the blank reactions, where sEVs were absent (Supplementary Figure S1), thyroglobulin was also stained as a negative control, since it is a protein particle and does not carry tetraspanin epitopes. All anti-tetraspanin antibodies caused negligible labeling, especially PE-tagged ones. CD63-AF488 revealed the highest degree of unspecific staining (Supplementary Figure S5).

Tetraspanin expression in EVs is known to vary across cell types, as well as across EV batches. When two independently harvested and purified batches of HT29 sEVs (batch #A and batch #B) were compared on both nFCM and F-NTA, we identified variations in tetraspanin expression (Figure 2C). Purified sEVs, from two different batches of HT29 CCM were stained with AF488-labelled antibodies and showed a significantly different expression level of CD9 (50.6% vs. 65.7%) and CD81 (66.6% vs. 48.7%) in nFCM, while for CD63 (17.9% vs. 11.9%) difference was not statistically significant (two-way ANOVA, Tukey's multiple comparisons test, alpha = 0.05). Staining and analysis of batch #B sEVs in F-NTA resulted in 30.7%, 22% and 1.9% for CD9, CD81 and CD63, respectively, substantially lower percentages compared to batch #A (CD9 = 54.9%, CD81 = 45.5%; CD63 = 3.9%). Although the expression of each single tetraspanin significantly differed between batches (particularly CD9 and CD81), in F-NTA their relative trend of expression was maintained: CD9 >> CD81 >> CD63 (F-NTA batch #A and batch #B—Figure 2C). Instead, in nFCM the relative expression of tetraspanins slightly differed between the batches (batch #A CD81 >> CD9; batch #B CD9 >> CD81). From the perspective of inter-platform comparison, tetraspanin expression was significantly different across the two platforms, except for CD9 in batch #A (two-way ANOVA, Tukey's multiple comparisons test, alpha = 0.05; detailed statistical analysis in supplementary material). A consistent trend of relative expression between platforms was obtained only in batch #B (CD9 >> CD81 >> CD63).

To analyze the single and concomitant expression of these tetraspanins, HT29 sEVs were stained with double (CD9 + CD63; CD9 + CD81; CD81 + CD63) and triple (CD9 + CD81 + CD63) antibody combinations, conjugated with PE for nFCM and AF488 for F-NTA. Nearly 76% of all particles observed on nFCM contained either CD9, CD81, CD63, or a combination of each, thereof (Figure 2E, left). The percentage of events detected upon double or triple antibody staining were not purely cumulative, which is consistent with the expectation that each sEV may express one, two, or even three tetraspanins, concomitantly. The overall portion of sEVs positive for all tetraspanins could be reproduced on F-NTA, with 76% of the particles stained by a triple antibody mix (Figure 2D). The proportion of double-positive sEVs detected on F-NTA, showed a more prominent increase when compared to previously measured single staining events, with 47.6% of particles stained with a mix of anti-CD9/anti-CD63, 79.4% with anti-CD9/anti-CD81, and 37.8% with anti-CD63/anti-CD81. Even though the signal was much higher than the sum of individually stained reactions (e.g., CD9/63 > CD9 + CD63), the patterns of expression maintained the trend expected from individual tetraspanin expression—CD9/81 >> CD9/63 >> CD63/81.

After double and triple antibody staining and understanding the expression of each single tetraspanin, sEV subpopulations co-expressing these markers could be calculated through a Venn diagram intersection analysis. Since on nFCM 70% of events co-stained with anti-CD9/anti-CD63, 72% with anti-CD9/anti-CD81 and 75% with anti-CD63/anti-CD81, we could estimate that 17% of all HT29 sEVs co-expressed CD9 and CD63, 50%

co-expressed CD9 and CD81, around 20% co-expressed CD63 and CD81, and only 11% expressed all three tetraspanins simultaneously (Figure 2E). Interestingly, we noticed that CD9+ accounted for 51% and that CD9 + CD81+ for 50% of total events, which meant that all CD9+ events expressed also CD81, in our HT29 sEV samples (Figure 2E, right).

2.3. SEC Purification and Ultrafiltration Do Not Change the Overall Composition of sEV Subpopulations

Optimized sEV staining protocols included a filtering step for buffer exchange, which was able to retain sEVs and to remove dyes and antibodies in excess. After testing several filtration devices, Nanosep 300 kDa ultra-filters and SEC were chosen for this purpose. One major concern was that background fluorescence could mask the mild fluorescent signal derived from fluorescently labeled nanoparticles and impede the acquisition of true positive events, resulting in skewed measurements. Indeed, free dye and antibodies impinged on sEV analysis, as clearly demonstrated on F-NTA where the fluorescence background led to overestimations of labeling efficiency (Figure 3A). PSDs of fluorescently labeled sEVs were also affected, as the size distributions shifted to the left, revealing a peak below 50 nm (Supplementary Figure S2). Similarly, on nFCM the excess of free fluorophores in solution led to increased thresholds in fluorescence channels. Therefore, filtering proved to be a critical step for the reliable detection of labeled vesicles, as even traces of free dyes and/or antibodies generated artifacts and overwhelming fluorescence noise on both instruments.

Nonetheless, we questioned whether these buffer exchange methods could inadvertently select specific sEV subpopulations and thus result in biased analysis. To this end, HEK293 sEVs (10^8 particles/µL) were stained with PE-conjugated anti-CD9, -CD63, or -CD81 and detected subpopulations compared after sample over-dilution, SEC and UF at nFCM. Sample over-dilution consisted of diluting a complete staining reaction in PBS until the concentration of the unbound fluorescent antibody was low enough to avoid background fluorescence, while sEV concentration was maintained at the optimal range for measurement. Since the over-dilution approach is inherently unbiased, it functioned as reference staining. Regardless of the method applied, we observed no significant difference between tetraspanin expression levels (Figure 3B), suggesting that neither SEC nor UF alters the composition of sEV subpopulations. This was also supported by the mean and median values of sample PSDs (Figure 3C,D).

2.4. Identification and Quantification of sEV Populations upon RNA Staining

Aiming to further characterize HT29 sEV subpopulations, we evaluated their nucleic acid content with membrane-permeable dyes, specific for RNA-SYTO™ RNASelect™ and Quant-iT™ RiboGreen™. Since both dyes only exhibit their full brightness upon binding to RNA, the background signal generated by unbound dye molecules should be drastically reduced compared to PE or AF488. Such reasoning prompted us to explore the suitability of the sample over-dilution approach in this context. After staining reaction over-dilution, fluorescent subpopulations detected by nFCM averaged around 10.2% and 10.6% for Syto and RiboGreen, respectively (Figure 4A). However, UF washing caused a consistent drop in fluorescent events for both dyes, with respect to the sample over-dilution reference. Loss of fluorescent events after UF also reflected on PSDs, as a noticeable reduction in particles with smaller diameters was observed (Figure 4B).

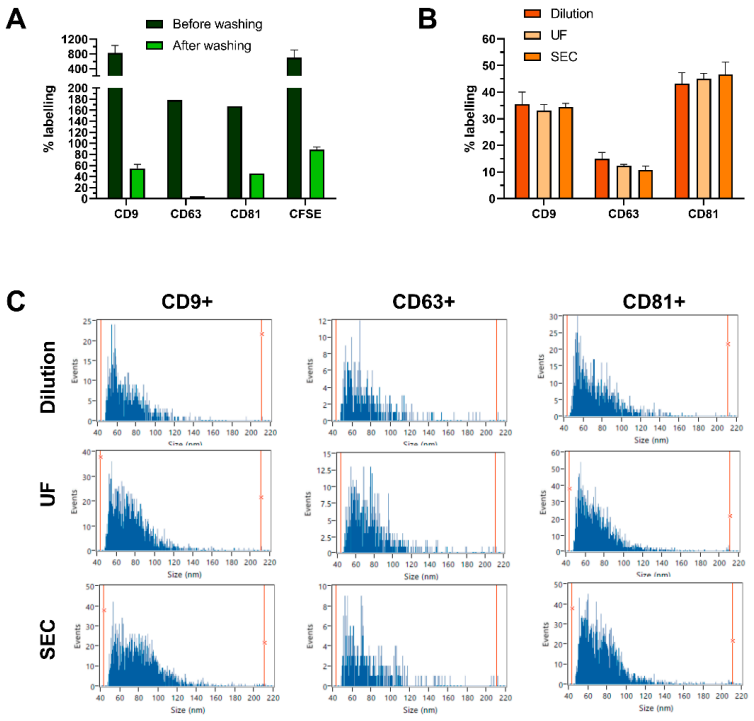

D

CD9+	% labelling		Median nm		Mean nm	
	Average	SEM	Average	SEM	Average	SEM
Dilution	35.47	4.53	65.92	0.67	70.26	1.63
UF	33.03	2.37	71.92	0.33	76.32	0.55
SEC	34.47	1.30	72.08	2.59	75.56	4.20

CD63+	% labelling		Median nm		Mean nm	
	Average	SEM	Average	SEM	Average	SEM
Dilution	14.97	2.39	68.75	0.29	75.20	1.89
UF	12.33	0.55	72.58	1.33	78.72	2.09
SEC	10.80	1.48	73.25	1.60	81.71	3.41

CD9+	% labelling		Median nm		Mean nm	
	Average	SEM	Average	SEM	Average	SEM
Dilution	43.20	4.06	71.25	0.76	74.73	0.78
UF	45.00	2.13	68.92	0.17	73.62	0.44
SEC	46.63	4.67	70.92	0.93	75.08	0.93

Figure 3. Suitability of SEC and UF as methods for clearing dyes in excess after sEV fluorescent labeling and their effect on subpopulation ratios. (**A**) Comparison of labeling % for stained HT29 sEVs before and after the removal of excess dye. 1×10^9 or 5.5×10^9 sEVs were incubated with antibodies (aCD9 1:12.5; aCD63 1:12.5; aCD81 1:25) or CFSE (50 µM), respectively, and measured by F-NTA. To remove the excess dye, UF washing strategy was applied, followed by F-NTA detection. (**B**) To compare different strategies for the removal of fluorescent antibodies in excess, labeling %, (**C**) PSD histograms, and (**D**) median and mean particle diameter were assessed for CD9+, CD63+ and CD81+ HEK293 sEVs, on nFCM. 2×10^9 sEVs, at a concentration of 10^8 particles/µL, were incubated with PE-labelled antibodies (aCD9 1:500; aCD63 1:25; aCD81 1:500) and unbound antibodies were removed by SEC or UF. Sample dilution (500–1000-fold) served as staining reference. Data is presented as mean ± SEM of at least three independent experiments. F-NTA PSD histograms of samples analyzed before and after washing are provided in Supplementary Figure S2.

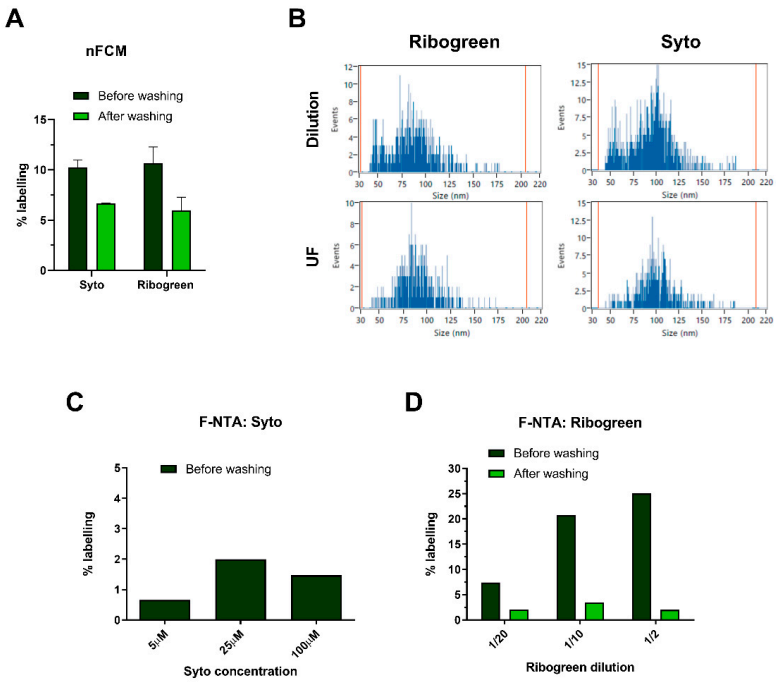

Figure 4. Identification and quantification of sEV populations based on their RNA content. (**A**) HT29 sEVs were stained with the RNA dyes Syto (25 µM) and RiboGreen (1:50). After incubation, staining reactions were washed by UF and fluorescent particles subsequently measured, with respective (**B**) PSDs analyzed on nFCM. (**C**) HT29 sEVs were incubated with Syto at increasing concentrations and the % of positive events was read on F-NTA, without applying further washing steps. (**D**) The impact of UF washing was evaluated on labeled HT29 sEVs, at increasing concentrations of RiboGreen. Fluorescent subpopulations were detected using F-NTA. Staining for nFCM was performed in three independent experiments (n = 3; mean ± SEM), while for F-NTA, representative results of titration experiments are shown for both dyes. Additional data from procedural controls, as well as the F-NTA PSD histograms of analyzed samples, are provided in Supplementary Figure S3.

Similar observations were made after analyzing Syto and RiboGreen-stained HT29 sEVs on F-NTA. No significant fluorescence signal was detected with Syto (<2%), even at the highest concentration of dye used (100 µM) (Figure 4C). Conversely, sEVs stained with different concentrations of RiboGreen reached up to 25% of labeling efficiency (Figure 4D). Notably, detected fluorescent particles showed a tendency towards larger PSDs (Supplementary Figure S3). Nevertheless, after washing the samples with UF, the fluorescent signal was completely lost (Figure 4D). Blank controls (without sEVs) showed a negligible number of fluorescent events on both instruments, indicating that free dye alone did not generate false-positive counts, either before or after washing (Supplementary Figure S3).

2.5. Identification and Quantification of sEVs Directly in Cell-Conditioned Media

Purified EVs are ideal for a single-particle characterization. However, purification can be lengthy, labor-intensive, and biased if the process enriches certain EV subpopulations. To evaluate the possibility of avoiding sEV purification from CCM, while still accurately detecting sEV subpopulations, previously optimized staining protocols were directly applied in HT29 CCM and particles were measured by nFCM and F-NTA. As shown in Figure 5A, CFSE and CMG labeled ~90% of events when analyzed on nFCM, well recapitulating the results obtained with purified HT29 sEVs (Figure 1A). On the contrary,

CFSE and CMG staining on HT29 CCM resulted in only 33% and 27% of labeling on F-NTA, respectively (Figure 5A). Peak and overall PSD of fluorescent subpopulations leaned towards higher values, as opposed to total particles measured in a scatter mode (Supplementary Figure S4).

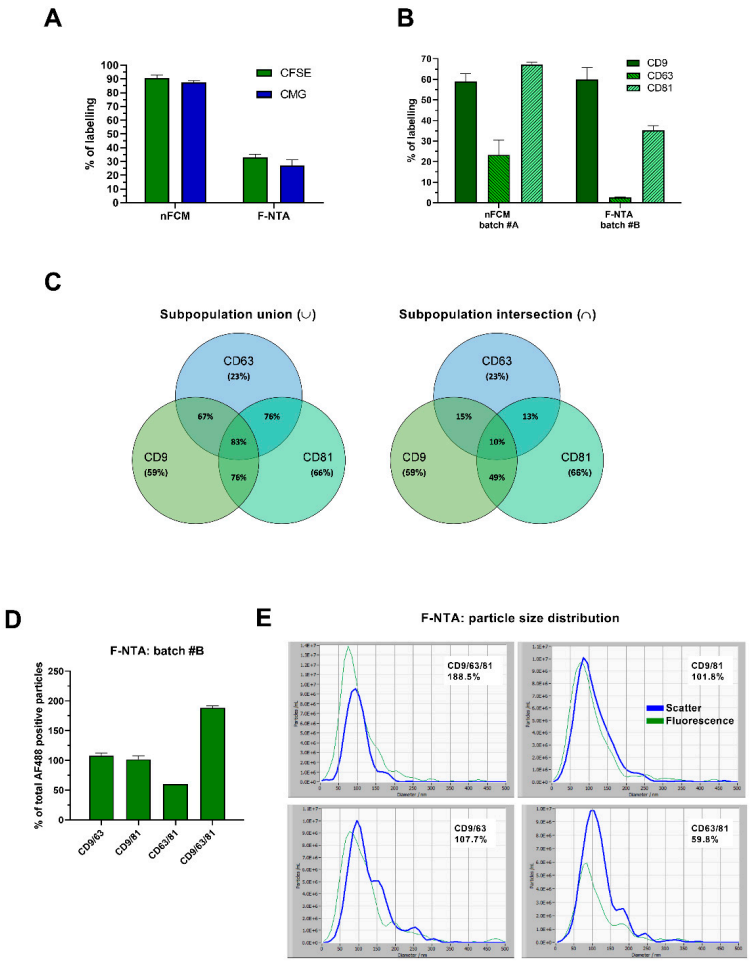

Figure 5. Characterization and quantification of sEVs directly from non-purified cell-conditioned media. HT29 CCM particles were stained and analyzed following the optimized protocols for sEV labeling with CMG, CFSE or fluorescently labeled anti-tetraspanin antibodies. (**A**) Staining efficiencies of CMG-, CFSE-, and (**B**) single antibody-labeling were assessed on both platforms. (**C**) Co-expressing markers were also evaluated on HT29 CCM by applying a mix of 2 and 3 anti-tetraspanin, PE-conjugated antibodies for nFCM measurements. The Venn diagram on the left depicts subpopulations that carried 1, 2, or 3 tetraspanins, while the one on the right represents sEV subpopulations which expressed 2 or 3 markers simultaneously. (**D**) HT29 CCM staining employing mixes of 2 and 3 AF488-labelled anti-tetraspanin antibodies was carried out for F-NTA, and staining efficiencies, as well as the (**E**) PSDs in scatter and fluorescence modes were assessed. Data represents triplicate experimental points (n = 3; mean ± SEM), except for (**C**) which was performed in two independent experiments (n = 2; mean ± SEM). F-NTA PSD histograms of CCM samples after CFSE-, CMG- and single antibody-labelling, are provided in Supplementary Figure S4.

Direct incubation of anti-tetraspanin antibodies in HT29 CCM and subsequent nFCM analysis revealed slight variations in the tetraspanin expression profiles, with respect to those reported for purified HT29 sEVs. Percentages of positive events were 59% for CD9, 67% for CD81 and 23% for CD63 (Figure 5B). On F-NTA, percentages of staining with AF488 antibodies were 59.8% for CD9, 35.3% for CD81, and 2.6% for CD63 (Figure 5B), higher than in purified HT29 sEVs from the corresponding batch (Figure 2C, F-NTA). Nevertheless, the same trend of expression was maintained between HT29 CCM and HT29 purified sEVs (CD9 >> CD81 >> CD63). Detailed statistical analysis by two-way ANOVA, comparing variability in tetraspanin expression levels between purified (sEVs) and non-purified (CCM) samples, is provided in the supplementary material.

In line with the purified sEV experiments reported above, we evaluated the concomitant expression of the three tetraspanins in HT29 CCM, applying combinations of CD9, CD81, and CD63 antibodies, PE-conjugated for nFCM and AF488-conjugated for F-NTA. Nearly 83% of the detected particles on nFCM displayed either CD9, CD81, or CD63, slightly more than the 76% previously determined for purified sEVs from the same CCM batch (Figure 5C). Regarding tetraspanin co-expression on nFCM, 15% of events carried both CD9 and CD63, almost 50% displayed both CD9 and CD81 and 13% were positive for both CD63 and CD81, while 10% resulted positive for all the three markers. The profile of tetraspanin expression was identical to the one obtained in purified sEVs, evidencing a maximum fluctuation of only 7% (Figures 2E and 5C).

AF488-conjugated antibody combinations did not reproduce the same values on CCM, as observed for purified EVs on F-NTA. Double and triple staining reactions evidenced unrealistic fluorescent event numbers, yielding over 100% of events detected in scatter mode. The combination of multiple antibodies in a complex, non-purified biofluid likely resulted in poor removal of unbound antibodies in excess (Figure 5D). Background fluorescence hampered correct analysis, as shown by the shift in PSD histograms between scatter and fluorescence mode (Figure 5E).

2.6. Characterization of sEV Subpopulations Using Multicolor Fluorescence Labeling Strategies

Depending on the complexity of biological samples, a wide range of contaminants can co-purify with sEVs, adding up to the already high heterogeneity of subpopulations. Consequently, it is crucial to pinpoint and discriminate true sEVs from confounding particles, whilst extracting additional information about their nature and/or contents. This prompted us to attempt multiple labeling strategies, combining different dyes and antibodies. Firstly, purified HT29 sEVs were stained with CD9-AF488 and CD81-PE alone, to individually determine the expression of each marker. Then, both antibodies were combined, and the staining efficiency was compared. CD9-AF488 alone stained 50% of particles and in combination with CD81-PE, this number slightly increased to 55%. The labeling efficiency obtained with CD81-PE was 70% in single staining and 68% after incubation together with CD9-AF499 (Figure 6A). As for the double-positive CD9+/CD81+ subpopulation, 48% of the particles displayed a double fluorescent signal, which perfectly matched the co-expression level of CD9 and CD81, previously identified in HT29 sEVs using a combination of strictly PE antibodies (Figures 2E and 6A). In line with the goal of further distinguish the nature of antibody-labeled particles, we attempted to optimize a double staining protocol applying CTR and CD81-AF488. The labeling obtained for each individual dye matched well with single stain controls. It was observed that the entire CD81+ subpopulation could be simultaneously stained with CTR, thereby supporting the presence of true sEVs (Figure 6B). Surprisingly, HT29 sEVs expressed nearly 40% of CD81 in this experiment, whereas in previous ones it was detected at 65–70% (Figure 2B).

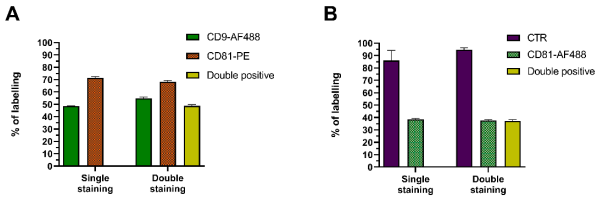

Figure 6. Multiplex fluorescence analysis for enhanced sEV identification and characterization. (**A**) Purified HT29 sEVs were labeled with anti-CD9-AF488 and anti-CD81-PE either individually (single staining) or in combination (double staining). (**B**) HT29 sEVs were stained with CTR and anti-CD81-AF488 either individually or in combination. Results are shown as % of labeled particles detected on nFCM, in two fluorescence channels (n = 3; mean ± SEM).

3. Discussion

In the present study, we compared single nanovesicle profiling platforms, aided by fluorescent labeling with different dyes and antibodies. To this end, we evaluated the capabilities of two platforms, the recent nFCM and the more established NTA, which has been recently upgraded for compatibility with fluorescence measurements—F-NTA. Although both instruments perform single-particle analysis, there are crucial differences in their hardware components and mode of operation. nFCM gathers scattered light to estimate particle size, while F-NTA calculates their hydrodynamic diameter by tracking particle diffusion motion.

The accuracy of nFCM particle size estimations relies on calibrating the instrument using silica beads with refractive properties similar to those of sEVs. The resulting calibration curves are in accordance with the Rayleigh scattering theory as they fit the expected model for the light scattering of particles smaller than the wavelength of incident light [28]. However, the refractive index (RI) of silica beads (1.46) does not exactly match the RI of EVs (1.36–1.4), and given the heterogeneity of EV sizes and biomolecular scaffolding, even greater differences in refractive properties between subpopulations of particles could arise [40,41]. To account for these limitations, size estimation in nFCM has implemented Mie scattering theory calculations, which adjust calibration curves to minimize any potential errors stemming from differences between size standards and EVs [42–44].

On the other hand, NTA requires a longer acquisition time window to determine particle size and the analysis of polydisperse samples imposes protocol readjustments to encompass a wider range of sizes [30]. Additionally, accurate size estimation based on Brownian motion becomes challenging with larger particles due to their slower diffusion, which could be affected by the EV surface composition, medium viscosity, and temperature [5,45–47]. The strength of NTA lies in the fact that it is a well-established method and does not rely on RI, which provides great flexibility for measuring nanoparticles of different compositions without the need for reference material in each analysis. However, when it comes to fluorescent labeling and detection, NTA poses certain limitations (bright and stable fluorophores; longer signal acquisition time) and requires further development and optimization. Furthermore, avalanche photodiodes (APD) in nFCM might allow for higher resolving power and better signal detection, especially in fluorescence mode, when compared to CMOS camera sensors [48].

In this study, F-NTA measurements required more washing cycles to completely eliminate background fluorescence, than nFCM. Stronger laser power (15 mW in nFCM vs. 40 mW in F-NTA), the fact that F-NTA acquires fluorescent signal from a stationary liquid in a cell for a longer fraction of time, compared to a fast detection in continuous flow on nFCM, and that nFCM applies SSC-triggered measurements of fluorescence, might be some of the reasons for a higher susceptibility to background noise on F-NTA. This was especially the case when analyzing more complex biofluids, such as CCM, drawing attention towards limited EV analysis in non-purified matrices.

Despite the need for more washing cycles, the analysis of purified sEVs could be carried out on both instruments. Cytoplasmic dyes, particularly CFSE, performed comparably well on both instruments, representing an optimal balance between fluorescence intensity and photostability. CFSE and cell-trace dyes theoretically require enzymatic cleavage by esterases to covalently bind to intraluminal proteins and become fluorescent. Several studies employing various nanoparticle profiling platforms have applied CFSE as a way to selectively stain EVs [20–24,49,50]. Nonetheless, CFSE and cell-trace dyes should be used with caution, since in our hands they became activated independently of intraluminal esterases. The presence of non-vesicular proteins and potential contamination with soluble esterases may cause CFSE activation—as evidenced by the staining of thyroglobulin particles and by the significant number of fluorescent artifacts in BSA controls reported in this work. Cell membrane dyes (CMG, CMR) did not exert the same extent of background fluorescence; however, their staining efficiency was sub-optimally detected in F-NTA experiments.

For ideal single nanoparticle profiling, it was important to choose widely available, photostable, and high brightness fluorophores. On nFCM, AF488 and PE performed equally well and surprisingly, allowed for increased sEV staining efficiencies over the red fluorophores AF647 and APC, even though AF488 theoretically should have the lowest brightness (extinction coefficient x quantum yield) out of them all (see the Supplementary Table S1). Generally, red fluorophores may also be more prone to self-quenching, consequently diminishing their quantum yield [51]; therefore, it would be relevant to address the properties of such dyes within the scope of single nanoparticle analysis. For F-NTA, AF488 provided the optimal balance between stability and brightness. Despite being one of the brightest commercially available dyes, PE was omitted from F-NTA measurements due to its fast bleaching, which could result in the underestimation of truly stained particles.

The fact that total particle counts (scatter mode) on F-NTA were nearly 4–5 times higher than they were on nFCM might be explained by differences in laser power, as the strength of incident light sources and the composition of illuminated particles directly correlate with the intensity of scattered light and ultimately, with the number of detectable nanoparticles. On the other hand, CMOS sensors might not be as sensitive as APDs, which could lead to poorer detection of faintly expressed epitopes on the surface of sEVs, limiting the number of fluorophores associated per fluorescent event. This could help to explain the significantly lower labeling percentages detected with F-NTA during antibody staining experiments. Such reasoning is further corroborated by double and triple antibody staining experiments, where the number of fluorescent events was higher than the sum obtained after each single staining (Figure 2C,D). EVs displaying few CD9, CD63 or CD81 epitopes on their surface would remain undetectable on F-NTA until multiple tetraspanins are labeled (Supplementary Figure S6). Nevertheless, F-NTA still provided consistent results between batches, revealing a trend in tetraspanin expression that was comparable in the case of single (CD9 >> CD81 >> CD63) as well as multiple antibody reactions (CD9/CD81 >> CD9/CD63 >> CD63/CD81).

These limitations did not seem to occur in nFCM, however, CD63-PE and CD63-AF488 resulted in 31% and 18% of staining on HT29 sEVs, respectively (Figure 2B). The fact that suppliers and clones were different between PE and AF488 antibodies could explain this discrepancy, though it was noticed only for CD63 and on HT29 samples; CD63 staining efficiencies using PE or AF488-conjugated antibodies were equal on HEK293. Notably, CD63 protein is reported to have different isoforms deriving from different splicing variants or post-translational modifications that may have functional or morphological implications and affect their partnering with other membrane molecules [52]. Therefore, the potential specificity of certain Ab clones for cell types or conditions must be better understood. Another possibility aligns with the phenomenon described just above, since CD63 was the least abundant tetraspanin in this study, AF488 staining may miss events carrying very few epitopes. Generally, nFCM was able to better discern fluorescently labeled EVs and also enabled the characterization of multiple surface markers through a single-color fluorescent

analysis, which is extremely valuable, especially in dedicated high-resolution platforms that are limited to a few channels for fluorescence detection. Therefore, we can argue that nFCM is more sensitive and consistent for fluorescent measurements.

For applications where sEV purification is not feasible, or minimal sample processing is a concern, we questioned whether our protocols for sEV fluorescent labeling could be applied directly in more complex biological samples such as CCM. Results between purified sEVs and CCM sEVs were surprisingly similar on nFCM. On the other hand, F-NTA was more promiscuous—lower fluorescent signal with CFSE in CCM could mean the presence of many non-EV particles, however, antibody staining gained percentages that were significantly higher than those obtained with purified sEVs. Behind this contradiction may be a reduced antibody washing efficiency, attributed to the richness of CCM. Double and triple antibody staining experiments further supported this hypothesis, where fluorescence background was even higher, leading to the conclusion that for background-free F-NTA measurements, purified material is preferred, or alternative washing procedures should be used instead of UF. It should be noted that the efficiency of UF washing was reduced when presented with CCM samples and multiple-antibody staining reactions.

We also assessed the feasibility of a sample over-dilution approach as an alternative staining protocol that avoids further processing for dye removal. Staining reactions had been previously optimized, maintaining a fixed range of sEVs (10^8–10^9), while titrating both dyes and antibodies to determine their optimal concentrations (at which a staining plateau was reached). For dyes, the dilution approach was not feasible for either of the instruments, as at the optimal dilution for the sample measurement, background fluorescence levels were still massive. On F-NTA, this problem also persisted when the over-dilution was applied to anti-tetraspanin antibody staining, confirming the need for a washing step after optimized staining reactions. Conversely, this protocol could be applied in nFCM, though it required an elevated concentration of purified sEV input (up to 10^8 per microliter). This allowed for staining reactions in lower volumes, minimizing the amount of antibody while maintaining optimized concentrations. Samples could be directly analyzed after a 500–1000-fold dilution, without any loss in sEV staining efficiency, with respect to UF or SEC.

The sample dilution-based protocol also featured as a reference method to evaluate possible biases introduced by UF or SEC, employed in this study for sEV buffer exchange and as a benchmark separation method for EV isolation. We confirmed that regardless of the dye removal method, there were no significant differences between CD9, CD81, or CD63 subpopulations. In this way, we demonstrated that neither SEC nor UF alters the composition of sEV subpopulations (Figure 3B). Similar mean and median size values also supported this claim (Figure 3C,D). Throughout the study, we favored the use of 300 kDa UF devices, as it is a more practical method than SEC and also confers higher sample processing throughput.

Overall comparison of washed and unwashed sEV samples proved to be useful in the early assessment of the efficacy and specificity of sEV staining protocols, including nucleic acid-specific dyes. The use of RNA-specific dyes for EV characterization has been reported in earlier works [53–55]. In this study, both SYTO™ RNASelect™ and Quant-iT™ RiboGreen™ revealed a low abundance of RNA-containing HT29 sEVs. As the activation of these dyes is dependent on nucleic acid binding, interference caused by background fluorescence signal seemed unlikely, hence the sample over-dilution approach was successfully applied. The low percentage of stained events questions not only the overall amount and accessibility of EV RNA but also the brightness of hereby employed dyes.

Following the MIFlowCyt-EV guidelines [56], procedural and assay controls, as well as washing steps, were included in all the experiments. Similarly, staining reactions with RNA dyes were also subjected to UF. This reduced the percentage of fluorescent events, leading to the conclusion that RNA staining may not be as specific or stable as with other dyes and antibodies. Such a decrease in fluorescent events after UF washing raises concerns

on the possible artifacts generated by dyes, as well as on the nature and strength of nucleic acid association to EVs. Given that RNA dyes can minimally bind to DNA molecules, the overall weak fluorescent signal could be justified by a low affinity binding to extravesicular DNA, which would then be lost upon UF washing. The presence and topology of nucleic acids on EVs have been the topic of discussion in previous publications [35,36,57–59], which might pose more critical approaches to assess the true EV nucleic acid content, location, and their usefulness as biomarkers. It is also possible that fluorescent events are not sEVs, but rather large individual ribonucleoprotein complexes [35,54,60,61]. This could be addressed through co-staining experiments with RNA-specific dyes and anti-tetraspanin antibodies. Although their blank controls show a low presence of fluorescent events, we cannot exclude the possibility that SYTO and RiboGreen may nonspecifically adsorb to EVs.

Since nFCM is equipped with two fluorescence channels, it allows for colocalization analysis. Dual fluorophore labeling proved to be a viable strategy for sEV subpopulation assessment, using either a combination of two antibodies or one antibody with another dye, as long as their emission spectra are sufficiently far apart to avoid fluorescence bleed-through between channels. The downside of this approach lies in its prolonged incubation time, which may have resulted in lower staining efficiency—HT29 sEVs expressed nearly 40% of CD81 after double-staining, whereas after single-staining CD81 was detected at 65–70% (Figures 2B and 6B). In conclusion, after careful optimization of staining protocols, it is possible to combine multiple fluorophores efficiently, to enable multiparametric sEV characterization.

4. Materials and Methods

4.1. Cell Culture and sEV Isolation

Cell lines HT29 (ATCC® HTB-38™, Manassas, VA, USA) and HEK293 (ATCC) were expanded in McCoy's and DMEM growth media (Euroclone, Pero, Italy), respectively, supplemented with 10% FBS (Euroclone) and 1% pen/strep (Sigma, St. Louis, MO, USA). Cells were grown in T75 or T150 Flasks and maintained in a humid atmosphere of 5% CO_2 and at 37 °C. Once expanded to the desired confluence (80%), cells were washed 2 times with 1× PBS and conditioned in a serum-free medium (to avoid serum-derived confounding particles) for 48–72 h. CCM was harvested and clarified by differential centrifugation at (1) 300× *g* for 10 min, (2) 1200× *g* for 20 min, and (3) 10,000× *g* for 30 min at 4 °C. Pre-cleared CCM was directly used for experiments, further processed for EV purification and isolation, or stored at −80 °C.

For sEV isolation, CCM was concentrated using an Amicon Stirred Cell ultrafiltration unit (Ultracel 100 kDa Ultrafiltration Discs, Merck Millipore, Burlington, MA, USA). A maximum volume of 500 mL of CCM was concentrated down to 10 mL for each isolation. Concentrated CCM was fractionated in size-exclusion chromatography (SEC) columns (Sepharose CL-4B bed volume 70 mL, GE Healthcare, Chicago, IL, USA), pre-equilibrated with 1 × 0.22 µm filtered PBS. Fractions of 1 mL were collected and EV-containing fractions 16 to 40 were pooled (total volume ≈ 25 mL). SEC-purified sEVs were concentrated down to 0.5–1 mL by 100 kDa ultrafiltration (Amicon® Ultra-15 Centrifugal Filter Unit, Merck Millipore).

4.2. Staining Protocols

4.2.1. Staining with Cytoplasmic, Membrane, or RNA-Specific Dyes

To ensure the optimal working concentrations of dye for our platforms, incremental concentrations were tested on a fixed number of particles (2×10^9). Dye concentrations at which the percentage of stained events reached a plateau were henceforth applied. After determining particle concentration (10^7 to 10^8 particles/µL), between 5×10^8 to 2×10^9 particles (purified sEVs or CCM) were loaded in each staining reaction with CellTrace™ CFSE (CFSE; 10 µM; Thermo Fisher Scientific, Waltham, MA, USA), CellTrace™ Far Red (CTR; 15 µM; Thermo Fisher Scientific), CellMask Green (CMG 20×; Thermo

Fisher Scientific) and CellMask Red (CMR 20×; Thermo Fisher Scientific), in filtered PBS. Reactions were incubated for 1.5 h at 37 °C under shaking, protected from light. After incubation, reaction volumes were brought up to 500 µL with filtered PBS and loaded into SEC columns (Sepharose CL-4B bed volume 10 mL, GE Healthcare) for the removal of unbound dye in excess. Fractions of 500 µL were collected and the EV-containing fractions (7, 8 and 9) were pooled, resulting in a total of 1.5 mL of stained sEV samples, which were immediately analyzed. SYTO™ RNASelect™ (Syto; Thermo Fisher Scientific) and Quant-iT™ RiboGreen® (RiboGreen; Thermo Fisher Scientific) were added at 25 µM and diluted 1:50, respectively. For Syto and RiboGreen, samples were incubated for 1.5 h and 30 min, respectively, both at 37 °C under shaking, protected from light. Afterward, they were washed 3–4 times with PBS using ultrafiltration centrifugal devices (Nanosep® 300 K, Pall Corporation, Port Washington, NY, USA; hereinafter referred to as UF) and analyzed.

As the ZetaView PMX-120 NTA instrument (Particle Metrix, Inning am Ammersee, Germany; in this text referred to as F-NTA) has only one laser (488 nm), red dyes were not used on this platform due to their longer excitation wavelengths. Furthermore, F-NTA detected 4–5.5 times more total particles than the Flow NanoAnalyzer (model U30, nanoFCM Inc., Xiamen, China; in this text referred to as nFCM), hence the particle amount and dye concentration for staining reactions were additionally optimized on this platform. For F-NTA analysis, 1×10^9–5.5×10^9 of particles (purified sEVs or CCM) were incubated with CFSE (50 µM) and CMG (20× concentrated) for 1.5 h at 37 °C. Afterward, the excess dye was removed by repeated washing (6–8 times) with 500 µL PBS and UF. Washed samples were measured in both scatter and fluorescence mode. Titration was also conducted for Syto (5, 25, and 100 µM per reaction) and RiboGreen (1/20, 1/10, and 1/2 dilution per reaction), samples were incubated for 1.5 h and 30 min at 37 °C, respectively, after which only RiboGreen stained samples were washed 8 times with PBS using UF. Samples were then analyzed in both scatter and fluorescence mode.

In both platforms, unstained samples and blanks (PBS and dye) were used as procedural and assay controls. The number of thyroglobulin (Merck/Sigma-Aldrich) particles was equivalent to the number of sEVs per staining reaction and the same protocols applied. Additionally, 20 µg of purified bovine serum albumin (BSA) standards (Thermo Fisher Scientific) were used in a control reaction of CFSE specificity.

4.2.2. Single Fluorophore Antibody Staining

Optimal working dilutions for antibodies were determined following the same approach described above. For each staining reaction in nFCM, 2×10^8–2×10^9 particles (purified sEVs or CCM) were incubated with fluorescent primary antibodies for 1 h at 37 °C under shaking, protected from light. Next, PBS was added up to 500 µL, unbound antibodies were removed by 3 to 4 rounds of UF or SEC and stained samples were characterized. The following fluorescently-labeled primary antibodies were used: Phycoerythrin (PE)-conjugated mouse anti-human CD9, CD63 and CD81 (dilution 1:10 for all; Exbio, Vestec, Czech Republic), Alexa Fluor® 488 (AF488)-conjugated mouse anti-human CD9, CD63 and CD81 (1:500, 1:25 and 1:500, respectively; R&D Systems, Minneapolis, MN, USA), allophycocyanin (APC)-conjugated mouse anti-human CD9 (1:10; Exbio), Alexa Fluor® 647 (AF647)-conjugated mouse anti-human CD9 (1:10; Exbio). Since PE is quite susceptible to photobleaching and APC and AF647 require a 600–640 nm excitation wavelength, only AF488-conjugated anti-human CD9, CD63 and CD81 were used in F-NTA, diluted 1:12.5, 1:12.5, and 1:25, respectively. 1×10^9 particles (purified sEVs or CCM) were used for the staining reaction at 37 °C, for 1.5 h. Unbound antibodies were removed by repeated washing (6–8 times) with 500 µL PBS and UF, prior to analysis.

4.2.3. Multicolor Fluorescence sEV Staining

It is important to avoid the overlap between the emission spectra of dyes to be used in combination, which results in the detection of false-positive events. With that in mind, AF488 and PE were combined for dual-color fluorescent labeling experiments

with antibodies. Between 2×10^8–2×10^9 particles were incubated with CD9-AF488 and CD81-PE at optimal working dilutions indicated in the section above, for 1 h at 37 °C under shaking, covered from light. Antibody in excess was eliminated by 3 to 4 rounds of UF or SEC and labeled sEVs directly analyzed on nFCM. To avoid interference of dyes in the specific binding of antibodies when combining both for sEV double staining, 5×10^8 to 2×10^9 particles were firstly labeled with CD9-AF488 for 1 h at 37 °C under shaking, followed by incubation with CTR (15 µM) for 1 h 30 min at 37 °C under shaking. The volume of double staining reactions was brought to 500 µL with filtered PBS, unbound antibodies and dyes were eliminated by SEC, and samples were examined right after. Since our F-NTA instrument is equipped with only one laser, dual-color labeling was omitted on this platform.

4.3. nFCM: Instrument Setup and EV Analysis

Conventional flow cytometers are not designed to characterize small nanoparticles such as sEVs and thus may provide dubious information. For this reason, nFCM, a dedicated nanoflow cytometry platform, was employed in this study. Our instrument is equipped with two lasers (488 and 638 nm), three single-photon counting modules (SPCM) and enables simultaneous detection in three independent channels. Light is first detected in the SSC channel (bandpass filter: 488/10) and then directed by two dichroic beam splitters (DicF495; DicF555) towards the green channel (bandpass filter: 525/40) and finally to the orange/red channel (bandpass filter: 580/40 or 670/30). Before each experiment, the NanoAnalyzer was aligned using polystyrene QC beads (nanoFCM Inc.). Size and concentration standard nanospheres (nanoFCM Inc.) were read directly after in order to calibrate the instrument for sEV analysis. Once nFCM was aligned and calibrated, sEV samples were diluted in filtered PBS (blank) to the optimal range for measurement (10^8 particles/mL). Samples and blanks (200–800 events) were measured for 1 min, applying a laser power of 15 mW as excitation source, constant pressure of 1 kPa, and at an event rate between 2500 to 12,000 events/min (as recommended by manufacturers), to avoid particle swarm detection [14,15]. Since SSC was set as the trigger channel, each particle that generated a signal above the SSC threshold was acquired as an event. For each event that also generated a signal above thresholds set in the fluorescent channels, the fluorescence intensity was registered. Thresholds were automatically set for each sample, accounting for background signal throughout the run (thresholds = average background measurements + 2× their standard deviation). Any sample with an SSC threshold 10% higher than the reference (size standard nanospheres) was excluded from the study. Similarly, strict criteria were set for the acceptance of fluorescently labeled samples, relying on unstained sEV controls as a reference for background fluorescence. Empty staining reactions (without sEVs) were performed as a control for all fluorescent reagents and measured under the same conditions as complete reactions (with sEVs).

4.4. F-NTA: Instrument Setup and EV Analysis

Particle Metrix ZetaView PMX-120 (software version 8.05.12 SP1) is a nanoparticle tracking analysis instrument equipped with a 488 nm laser (40 mW of power) and CMOS camera sensor which enables enumeration, physical characterization, and fluorescence measurement of particles in suspension. Measurements can be performed in liquid samples with a minimal volume of 500 µL, containing particles as low as 10^6. PMX-120 was set up according to the manufacturer's instructions. Cell check was performed after each start-up, followed by camera and laser alignment using 100 nm polystyrene size standard beads and optimizing profile auto-symmetry. Upon instrument setup, daily performance was conducted with the same beads in order to assess the accuracy and precision. Biological samples were then diluted in PBS to reach the optimal particle count per frame in scatter mode (50–200 particles) and analyzed throughout 11 positions of the cell, with camera sensitivity 85, shutter speed 100, high video quality (capturing 60 frames) at 30 frames/s (1 cycle), minimal area 10, maximal area 1000 and brightness 25.

For fluorescence measurements, a 500 nm cut-on long-pass filter was used with camera sensitivity adjusted to 95 and video quality to low (capturing 15 frames). "Low Bleach" technology was enabled during acquisition in order to reduce the laser exposure time for the fluorophore and capture fluorescence signal at its maximum intensity. 11-position tables and histograms were used in the data analysis.

4.5. Bulk Fluorescence Measurements

After labeling, 200 µL of fluorescent sEV samples were loaded in black 96-well plates (PerkinElmer, Waltham, MA, USA). Plates were inserted in a fluorometer plate reader (CLARIOstar Plus; BMG Labtech, Ortenberg, Germany) and for each fluorescence measurement, optimal gain and focal height were adjusted to the brightest well. Raw fluorescent signals of samples were normalized to a blank (PBS) and data was presented as signal-to-noise.

4.6. Statistical Analysis

Experiments were performed in triplicate unless stated otherwise. All results are presented as average with SEM. GraphPad Prism 9 (San Diego, CA, USA) and Two-way ANOVA with Tukey test for multiple comparisons were used to examine inter-batch (batch #A and batch #B) and cross-platform (nFCM and F-NTA) variability in tetraspanin expression, as well as the correlation between purified and non-purified samples.

5. Conclusions

This work addresses some of the main benefits and limitations of working with two different single-nanoparticle profiling platforms. We propose protocols for optimal sEV characterization on both instruments, but also raise concerns regarding the value of certain dyes, affinity reagents, or methodologies commonly employed. Additionally, composite sEVs characterization addressed in our study represents an important information feed for downstream applications, such as uptake studies, in which the importance of parameters such as size, aggregation status, maintained integrity of sEVs, as well as surface display of molecules that actively mediate the cell uptake (e.g., tetraspanins), has been proven fundamental for correct experimental design (i.e., EV dosage) and results elaboration. Hereby used analytical protocols consume a very small sample fraction, thus leaving a majority of well characterized sEV isolates intact for further testing and use. Throughout this report, we aimed to highlight the aspects and considerations that are often understated but highly important, where a balance between obtaining trustworthy data and pushing instruments to operate at the edges of current technological limits must exist. It is fundamental to underline that a critical attitude must drive experimental works and reports aimed at accurately dissecting the EV field, where irrefutable evidence over major topics is still lacking.

Supplementary Materials: The following are available online at https://www.mdpi.com/article/10.3390/ijms221910510/s1.

Author Contributions: Shared first authorship, authors D.F., D.M. and M.C. contributed equally to this manuscript; Conceptualization, D.F., D.M., M.C. and N.Z.; Methodology, D.F., D.M. and M.C.; Validation, D.F., D.M., M.C. and N.Z.; Formal Analysis, D.F., D.M., M.C., F.L. and K.-L.V.; Investigation, D.F., D.M., M.C., F.L. and K.-L.V.; Data Curation, D.F., D.M., M.C., F.L. and K.-L.V.; Writing—Original Draft Preparation, D.F., D.M. and M.C.; Writing—Review and Editing, N.Z., D.Z. and K.K.; Visualization, D.F., D.M., M.C. and F.L.; Supervision, N.Z. and K.K.; Project Administration, N.Z.; Funding Acquisition, N.Z. All authors have read and agreed to the published version of the manuscript.

Funding: This research has received funding from the European Union's Horizon 2020 research and innovation programme under the Marie Skłodowska-Curie grant agreements No. 765492 and 722148, and FET Proactive grant agreement No. 952183.

Conflicts of Interest: The authors declare no conflict of interest. Funders had no role in the design of the study; in the collection, analyses, or interpretation of data; in the writing of the manuscript, or in the decision to publish the results.

References

1. Yáñez-Mó, M.; Siljander, P.R.M.; Andreu, Z.; Zavec, A.B.; Borràs, F.E.; Buzas, E.I.; Buzas, K.; Casal, E.; Cappello, F.; Carvalho, J.; et al. Biological Properties of Extracellular Vesicles and Their Physiological Functions. *J. Extracell. Vesicles* **2015**, *4*, 27066. [CrossRef] [PubMed]
2. Skotland, T.; Sandvig, K.; Llorente, A. Lipids in Exosomes: Current Knowledge and the Way Forward. *Prog. Lipid Res.* **2017**, *66*, 30–41. [CrossRef] [PubMed]
3. Zebrowska, A.; Skowronek, A.; Wojakowska, A.; Widlak, P.; Pietrowska, M. Metabolome of Exosomes: Focus on Vesicles Released by Cancer Cells and Present in Human Body Fluids. *Int. J. Mol. Sci.* **2019**, *20*, 3461. [CrossRef] [PubMed]
4. Thane, K.E.; Davis, A.M.; Hoffman, A.M. Improved Methods for Fluorescent Labeling and Detection of Single Extracellular Vesicles Using Nanoparticle Tracking Analysis. *Sci. Rep.* **2019**, *9*, 12295. [CrossRef] [PubMed]
5. Filipe, V.; Hawe, A.; Jiskoot, W. Critical Evaluation of Nanoparticle Tracking Analysis (NTA) by NanoSight for the Measurement of Nanoparticles and Protein Aggregates. *Pharm. Res.* **2010**, *27*, 796–810. [CrossRef] [PubMed]
6. Gardiner, C.; Ferreira, Y.J.; Dragovic, R.A.; Redman, C.W.G.; Sargent, I.L. Extracellular Vesicle Sizing and Enumeration by Nanoparticle Tracking Analysis. *J. Extracell. Vesicles* **2013**, *2*, 19671. [CrossRef]
7. Vestad, B.; Llorente, A.; Neurauter, A.; Phuyal, S.; Kierulf, B.; Kierulf, P.; Skotland, T.; Sandvig, K.; Haug, K.B.F.; Øvstebø, R. Size and Concentration Analyses of Extracellular Vesicles by Nanoparticle Tracking Analysis: A Variation Study. *J. Extracell. Vesicles* **2017**, *6*, 1344087. [CrossRef] [PubMed]
8. Dragovic, R.A.; Gardiner, C.; Brooks, A.S.; Tannetta, D.S.; Ferguson, D.J.P.; Hole, P.; Carr, B.; Redman, C.W.G.; Harris, A.L.; Dobson, P.J.; et al. Sizing and Phenotyping of Cellular Vesicles Using Nanoparticle Tracking Analysis. *Nanomed. Nanotechnol. Biol. Med.* **2011**, *7*, 780–788. [CrossRef]
9. Lane, R.E.; Korbie, D.; Anderson, W.; Vaidyanathan, R.; Trau, M. Analysis of Exosome Purification Methods Using a Model Liposome System and Tunable-Resistive Pulse Sensing. *Sci. Rep.* **2015**, *5*, 7639. [CrossRef]
10. Vogel, R.; Willmott, G.; Kozak, D.; Roberts, G.S.; Anderson, W.; Groenewegen, L.; Glossop, B.; Barnett, A.; Turner, A.; Trau, M. Quantitative Sizing of Nano/Microparticles with a Tunable Elastomeric Pore Sensor. Available online: https://pubs.acs.org/doi/pdf/10.1021/ac200195n (accessed on 22 September 2021).
11. Park, J.; Hwang, M.; Choi, B.; Jeong, H.; Jung, J.; Kim, H.K.; Hong, S.; Park, J.; Choi, Y. Exosome Classification by Pattern Analysis of Surface-Enhanced Raman Spectroscopy Data for Lung Cancer Diagnosis. *Anal. Chem.* **2017**, *89*, 6695–6701. [CrossRef]
12. Gualerzi, A.; Niada, S.; Giannasi, C.; Picciolini, S.; Morasso, C.; Vanna, R.; Rossella, V.; Masserini, M.; Bedoni, M.; Ciceri, F.; et al. Raman Spectroscopy Uncovers Biochemical Tissue-Related Features of Extracellular Vesicles from Mesenchymal Stromal Cells. *Sci. Rep.* **2017**, *7*, 9820. [CrossRef] [PubMed]
13. Enciso-Martinez, A.; Van Der Pol, E.; Hau, C.M.; Nieuwland, R.; Van Leeuwen, T.G.; Terstappen, L.W.M.M.; Otto, C. Label-Free Identification and Chemical Characterisation of Single Extracellular Vesicles and Lipoproteins by Synchronous Rayleigh and Raman Scattering. *J. Extracell. Vesicles* **2020**, *9*, 1730134. [CrossRef] [PubMed]
14. Yuana, Y.; Oosterkamp, T.H.; Bahatyrova, S.; Ashcroft, B.; Garcia Rodriguez, P.; Bertina, R.M.; Osanto, S. Atomic Force Microscopy: A Novel Approach to the Detection of Nanosized Blood Microparticles. *J. Thromb. Haemost.* **2010**, *8*, 315–323. [CrossRef] [PubMed]
15. Ashcroft, B.A.; de Sonneville, J.; Yuana, Y.; Osanto, S.; Bertina, R.; Kuil, M.E.; Oosterkamp, T.H. Determination of the Size Distribution of Blood Microparticles Directly in Plasma Using Atomic Force Microscopy and Microfluidics. *Biomed. Microdevices* **2012**, *14*, 641–649. [CrossRef]
16. Chen, C.; Zong, S.; Wang, Z.; Lu, J.; Zhu, D.; Zhang, Y.; Cui, Y. Imaging and Intracellular Tracking of Cancer-Derived Exosomes Using Single-Molecule Localization-Based Super-Resolution Microscope. Available online: https://pubs.acs.org/doi/pdf/10.1021/acsami.6b09442 (accessed on 22 September 2021).
17. Nizamudeen, Z.; Markus, R.; Lodge, R.; Parmenter, C.; Platt, M.; Chakrabarti, L.; Sottile, V. Rapid and Accurate Analysis of Stem Cell-Derived Extracellular Vesicles with Super Resolution Microscopy and Live Imaging. *Biochim. Biophys. Acta Mol. Cell Res.* **2018**, *1865*, 1891–1900. [CrossRef]
18. van der Zwaag, D.; Vanparijs, N.; Wijnands, S.; De Rycke, R.; De Geest, B.G.; Albertazzi, L. Super Resolution Imaging of Nanoparticles Cellular Uptake and Trafficking. *ACS Appl. Mater. Interfaces* **2016**, *8*, 6391–6399. [CrossRef]
19. Lennon, K.M.; Wakefield, D.L.; Maddox, A.L.; Brehove, M.S.; Willner, A.N.; Garcia-Mansfield, K.; Meechoovet, B.; Reiman, R.; Hutchins, E.; Miller, M.M.; et al. Single Molecule Characterization of Individual Extracellular Vesicles from Pancreatic Cancer. *J. Extracell. Vesicles* **2019**, *8*, 1685634. [CrossRef]
20. Morales-Kastresana, A.; Telford, B.; Musich, T.A.; McKinnon, K.; Clayborne, C.; Braig, Z.; Rosner, A.; Demberg, T.; Watson, D.C.; Karpova, T.S.; et al. Labeling Extracellular Vesicles for Nanoscale Flow Cytometry. *Sci. Rep.* **2017**, *7*, 1878. [CrossRef]
21. Pospichalova, V.; Svoboda, J.; Dave, Z.; Kotrbova, A.; Kaiser, K.; Klemova, D.; Ilkovics, L.; Hampl, A.; Crha, I.; Jandakova, E.; et al. Simplified Protocol for Flow Cytometry Analysis of Fluorescently Labeled Exosomes and Microvesicles Using Dedicated Flow Cytometer. *J. Extracell. Vesicles* **2015**, *4*, 25530. [CrossRef]

22. Maia, J.; Batista, S.; Couto, N.; Gregório, A.C.; Bodo, C.; Elzanowska, J.; Strano Moraes, M.C.; Costa-Silva, B. Employing Flow Cytometry to Extracellular Vesicles Sample Microvolume Analysis and Quality Control. *Front. Cell Dev. Biol.* **2020**, *8*, 593750. [CrossRef]
23. Choi, D.; Montermini, L.; Jeong, H.; Sharma, S.; Meehan, B.; Rak, J. Mapping Subpopulations of Cancer Cell-Derived Extracellular Vesicles and Particles by Nano-Flow Cytometry. *ACS Nano* **2019**, *13*, 10499–10511. [CrossRef]
24. Mastoridis, S.; Bertolino, G.M.; Whitehouse, G.; Dazzi, F.; Sanchez-Fueyo, A.; Martinez-Llordella, M. Multiparametric Analysis of Circulating Exosomes and Other Small Extracellular Vesicles by Advanced Imaging Flow Cytometry. *Front. Immunol.* **2018**, *9*, 1583. [CrossRef]
25. Hill, A.F. *Exosomes and Microvesicles: Methods and Protocols*; Methods in Molecular Biology; Springer: New York, NY, USA, 2017; Volume 1545, ISBN 978-1-4939-6726-1.
26. Coumans, F.A.W.; Brisson, A.R.; Buzas, E.I.; Dignat-George, F.; Drees, E.E.E.; El-Andaloussi, S.; Emanueli, C.; Gasecka, A.; Hendrix, A.; Hill, A.F.; et al. Methodological Guidelines to Study Extracellular Vesicles. *Circ. Res.* **2017**, *120*, 1632–1648. [CrossRef]
27. Van der Pol, E.; Coumans, F.A.W.; Grootemaat, A.E.; Gardiner, C.; Sargent, I.L.; Harrison, P.; Sturk, A.; van Leeuwen, T.G.; Nieuwland, R. Particle Size Distribution of Exosomes and Microvesicles Determined by Transmission Electron Microscopy, Flow Cytometry, Nanoparticle Tracking Analysis, and Resistive Pulse Sensing. *J. Thromb. Haemost.* **2014**, *12*, 1182–1192. [CrossRef]
28. Zhu, S.; Ma, L.; Wang, S.; Chen, C.; Zhang, W.; Yang, L.; Hang, W.; Nolan, J.P.; Wu, L.; Yan, X. Light-Scattering Detection below the Level of Single Fluorescent Molecules for High-Resolution Characterization of Functional Nanoparticles. *ACS Nano* **2014**, *8*, 10998–11006. [CrossRef] [PubMed]
29. Mitra, A.; Deutsch, B.; Ignatovich, F.; Dykes, C.; Novotny, L. Nano-Optofluidic Detection of Single Viruses and Nanoparticles. *ACS Nano* **2010**, *4*, 1305–1312. [CrossRef] [PubMed]
30. Bachurski, D.; Schuldner, M.; Nguyen, P.-H.; Malz, A.; Reiners, K.S.; Grenzi, P.C.; Babatz, F.; Schauss, A.C.; Hansen, H.P.; Hallek, M.; et al. Extracellular Vesicle Measurements with Nanoparticle Tracking Analysis—An Accuracy and Repeatability Comparison between NanoSight NS300 and ZetaView. *J. Extracell. Vesicles* **2019**, *8*, 1596016. [CrossRef] [PubMed]
31. Desgeorges, A.; Hollerweger, J.; Lassacher, T.; Rohde, E.; Helmbrecht, C.; Gimona, M. Differential Fluorescence Nanoparticle Tracking Analysis for Enumeration of the Extracellular Vesicle Content in Mixed Particulate Solutions. *Methods* **2020**, *177*, 67–73. [CrossRef]
32. Carnell-Morris, P.; Tannetta, D.; Siupa, A.; Hole, P.; Dragovic, R. Analysis of Extracellular Vesicles Using Fluorescence Nanoparticle Tracking Analysis. In *Extracellular Vesicles*; Humana Press: New York, NY, USA, 2017; Volume 1660, pp. 153–173. [CrossRef]
33. Keerthikumar, S.; Chisanga, D.; Ariyaratne, D.; Al Saffar, H.; Anand, S.; Zhao, K.; Samuel, M.; Pathan, M.; Jois, M.; Chilamkurti, N.; et al. ExoCarta: A Web-Based Compendium of Exosomal Cargo. *J. Mol. Biol.* **2016**, *428*, 688–692. [CrossRef] [PubMed]
34. Mathieu, M.; Névo, N.; Jouve, M.; Valenzuela, J.I.; Maurin, M.; Verweij, F.J.; Palmulli, R.; Lankar, D.; Dingli, F.; Loew, D.; et al. Specificities of Exosome versus Small Ectosome Secretion Revealed by Live Intracellular Tracking of CD63 and CD9. *Nat. Commun.* **2021**, *12*, 4389. [CrossRef]
35. Jeppesen, D.K.; Fenix, A.M.; Franklin, J.L.; Higginbotham, J.N.; Zhang, Q.; Zimmerman, L.J.; Liebler, D.C.; Ping, J.; Liu, Q.; Evans, R.; et al. Reassessment of Exosome Composition. *Cell* **2019**, *177*, 428–445.e18. [CrossRef]
36. Yokoi, A.; Villar-Prados, A.; Oliphint, P.A.; Zhang, J.; Song, X.; De Hoff, P.; Morey, R.; Liu, J.; Roszik, J.; Clise-Dwyer, K.; et al. Mechanisms of Nuclear Content Loading to Exosomes. *Sci. Adv.* **2019**, *5*, eaax8849. [CrossRef]
37. Hoshino, A.; Kim, H.S.; Bojmar, L.; Gyan, K.E.; Cioffi, M.; Hernandez, J.; Zambirinis, C.P.; Rodrigues, G.; Molina, H.; Heissel, S.; et al. Extracellular Vesicle and Particle Biomarkers Define Multiple Human Cancers. *Cell* **2020**, *182*, 1044–1061.e18. [CrossRef]
38. Libregts, S.F.W.M.; Arkesteijn, G.J.A.; Németh, A.; Nolte-'t Hoen, E.N.M.; Wauben, M.H.M. Flow Cytometric Analysis of Extracellular Vesicle Subsets in Plasma: Impact of Swarm by Particles of Non-Interest. *J. Thromb. Haemost.* **2018**, *16*, 1423–1436. [CrossRef] [PubMed]
39. Parish, C.R. Fluorescent Dyes for Lymphocyte Migration and Proliferation Studies. *Immunol. Cell Biol.* **1999**, *77*, 499–508. [CrossRef] [PubMed]
40. Welsh, J.A.; Pol, E.; Bettin, B.A.; Carter, D.R.F.; Hendrix, A.; Lenassi, M.; Langlois, M.; Llorente, A.; Nes, A.S.; Nieuwland, R.; et al. Towards Defining Reference Materials for Measuring Extracellular Vesicle Refractive Index, Epitope Abundance, Size and Concentration. *J. Extracell. Vesicles* **2020**, *9*, 1816641. [CrossRef] [PubMed]
41. Welsh, J.A.; Horak, P.; Wilkinson, J.S.; Ford, V.J.; Jones, J.C.; Smith, D.; Holloway, J.A.; Englyst, N.A. FCMPASS Software Aids Extracellular Vesicle Light Scatter Standardization. *Cytom. A* **2020**, *97*, 569–581. [CrossRef]
42. Tian, Y.; Gong, M.; Hu, Y.; Liu, H.; Zhang, W.; Zhang, M.; Hu, X.; Aubert, D.; Zhu, S.; Wu, L.; et al. Quality and Efficiency Assessment of Six Extracellular Vesicle Isolation Methods by Nano-Flow Cytometry. *J. Extracell. Vesicles* **2020**, *9*, 1697028. [CrossRef] [PubMed]
43. Tian, Y.; Ma, L.; Gong, M.; Su, G.; Zhu, S.; Zhang, W.; Wang, S.; Li, Z.; Chen, C.; Li, L.; et al. Protein Profiling and Sizing of Extracellular Vesicles from Colorectal Cancer Patients via Flow Cytometry. *ACS Nano* **2018**, *12*, 671–680. [CrossRef]
44. Zhang, W.; Tian, Y.; Hu, X.; He, S.; Niu, Q.; Chen, C.; Zhu, S.; Yan, X. Light-Scattering Sizing of Single Submicron Particles by High-Sensitivity Flow Cytometry. *Anal. Chem.* **2018**, *90*, 12768–12775. [CrossRef]
45. Malloy, A. Count, Size and Visualize Nanoparticles. *Mater. Today* **2011**, *14*, 170–173. [CrossRef]
46. Skliar, M.; Chernyshev, V.S.; Belnap, D.M.; Sergey, G.V.; Al-Hakami, S.M.; Bernard, P.S.; Stijleman, I.J.; Rachamadugu, R. Membrane Proteins Significantly Restrict Exosome Mobility. *Biochem. Biophys. Res. Commun.* **2018**, *501*, 1055–1059. [CrossRef]

47. Maguire, C.M.; Rösslein, M.; Wick, P.; Prina-Mello, A. Characterisation of Particles in Solution—A Perspective on Light Scattering and Comparative Technologies. *Sci. Technol. Adv. Mater.* **2018**, *19*, 732–745. [CrossRef]
48. Titus, A.H.; Cheung, M.C.-K.; Chodavarapu, V.P. CMOS Photodetectors. In *Photodiodes-World Activities in 2011*; IntechOpen: Rijeka, Croatia, 2011. [CrossRef]
49. Morales-Kastresana, A.; Musich, T.A.; Welsh, J.A.; Telford, W.; Demberg, T.; Wood, J.C.S.; Bigos, M.; Ross, C.D.; Kachynski, A.; Dean, A.; et al. High-Fidelity Detection and Sorting of Nanoscale Vesicles in Viral Disease and Cancer. *J. Extracell. Vesicles* **2019**, *8*, 1597603. [CrossRef] [PubMed]
50. Ender, F.; Zamzow, P.; von Bubnoff, N.; Gieseler, F. Detection and Quantification of Extracellular Vesicles via FACS: Membrane Labeling Matters! *Int. J. Mol. Sci.* **2019**, *21*, 291. [CrossRef] [PubMed]
51. Oliveira, E.; Bértolo, E.; Núñez, C.; Pilla, V.; Santos, H.M.; Fernández-Lodeiro, J.; Fernández-Lodeiro, A.; Djafari, J.; Capelo, J.L.; Lodeiro, C. Green and Red Fluorescent Dyes for Translational Applications in Imaging and Sensing Analytes: A Dual-Color Flag. *ChemistryOpen* **2017**, *7*, 3. [CrossRef]
52. Engering, A.; Kuhn, L.; Fluitsma, D.; Hoefsmit, E.; Pieters, J. Differential Post-Translational Modification of CD63 Molecules during Maturation of Human Dendritic Cells. *Eur. J. Biochem.* **2003**, *270*, 2412–2420. [CrossRef] [PubMed]
53. Wan, Y.; Cheng, G.; Liu, X.; Hao, S.J.; Nisic, M.; Zhu, C.D.; Xia, Y.Q.; Li, W.Q.; Wang, Z.G.; Zhang, W.L.; et al. Rapid Magnetic Isolation of Extracellular Vesicles via Lipid-Based Nanoprobes. *Nat. Biomed. Eng.* **2017**, *1*, 1–11. [CrossRef]
54. Wei, Z.; Batagov, A.O.; Schinelli, S.; Wang, J.; Wang, Y.; El Fatimy, R.; Rabinovsky, R.; Balaj, L.; Chen, C.C.; Hochberg, F.; et al. Coding and Noncoding Landscape of Extracellular RNA Released by Human Glioma Stem Cells. *Nat. Commun.* **2017**, *8*, 1145. [CrossRef]
55. Channavajjhala, S.K.; Rossato, M.; Morandini, F.; Castagna, A.; Pizzolo, F.; Bazzoni, F.; Olivieri, O. Optimizing the Purification and Analysis of MiRNAs from Urinary Exosomes. *Clin. Chem. Lab. Med.* **2014**, *52*, 345–354. [CrossRef]
56. Welsh, J.A.; Van Der Pol, E.; Arkesteijn, G.J.A.; Bremer, M.; Brisson, A.; Coumans, F.; Dignat-George, F.; Duggan, E.; Ghiran, I.; Giebel, B.; et al. MIFlowCyt-EV: A Framework for Standardized Reporting of Extracellular Vesicle Flow Cytometry Experiments. *J. Extracell. Vesicles* **2020**, *9*, 1713526. [CrossRef] [PubMed]
57. Lázaro-Ibáñez, E.; Lässer, C.; Shelke, G.V.; Crescitelli, R.; Jang, S.C.; Cvjetkovic, A.; García-Rodríguez, A.; Lötvall, J. DNA Analysis of Low- and High-Density Fractions Defines Heterogeneous Subpopulations of Small Extracellular Vesicles Based on Their DNA Cargo and Topology. *J. Extracell. Vesicles* **2019**, *8*, 1656993. [CrossRef] [PubMed]
58. Takahashi, A.; Okada, R.; Nagao, K.; Kawamata, Y.; Hanyu, A.; Yoshimoto, S.; Takasugi, M.; Watanabe, S.; Kanemaki, M.T.; Obuse, C.; et al. Exosomes Maintain Cellular Homeostasis by Excreting Harmful DNA from Cells. *Nat. Commun.* **2017**, *8*, 15287. [CrossRef] [PubMed]
59. Hitomi, K.; Okada, R.; Loo, T.M.; Miyata, K.; Nakamura, A.J.; Takahashi, A. DNA Damage Regulates Senescence-Associated Extracellular Vesicle Release via the Ceramide Pathway to Prevent Excessive Inflammatory Responses. *Int. J. Mol. Sci.* **2020**, *21*, 3720. [CrossRef] [PubMed]
60. Arroyo, J.D.; Chevillet, J.R.; Kroh, E.M.; Ruf, I.K.; Pritchard, C.C.; Gibson, D.F.; Mitchell, P.S.; Bennett, C.F.; Pogosova-Agadjanyan, E.L.; Stirewalt, D.L.; et al. Argonaute2 Complexes Carry a Population of Circulating MicroRNAs Independent of Vesicles in Human Plasma. *Proc. Natl. Acad. Sci. USA* **2011**, *108*, 5003–5008. [CrossRef] [PubMed]
61. Van Deun, J.; Mestdagh, P.; Sormunen, R.; Cocquyt, V.; Vermaelen, K.; Vandesompele, J.; Bracke, M.; De Wever, O.; Hendrix, A. The Impact of Disparate Isolation Methods for Extracellular Vesicles on Downstream RNA Profiling. *J. Extracell. Vesicles* **2014**, *3*, 24858. [CrossRef]

Results

Part 2: Enrichment of specific EV subpopulations from simple and complex matrices and their differential clinical value for early-stage NSCLC detection

Fortunato, D *et al.* Selective isolation of extracellular vesicles from minimally processed human plasma as a translational strategy for liquid biopsies

(In submission)

Selective isolation of extracellular vesicles from minimally processed human plasma as a translational strategy for liquid biopsies

Diogo Fortunato[1], Stavros Giannoukakos[2], Ana Giménez-Capitán[3], Michael Hackenberg[2], Miguel A. Molina-Vila[3], Nataša Zarovni[1]

1. Exosomics SpA, 53100 Siena, Italy
2. Department of Genetics, University of Granada, Spain
3. Laboratory of Oncology, Pangaea Oncology, Barcelona, Spain

Abstract

Intercellular communication is mediated by extracellular vesicles (EVs), as they enclose selectively packaged biomolecules that can be horizontally transferred from donor to recipient cells. Because all cells constantly generate and recycle EVs, they provide accurate timed snapshots of individual pathophysiological status. Although EVs can be isolated from any biofluid, blood plasma circulates through the whole body and it potentially transports EVs derived from most organs, making it the biofluid of choice in most studies. Blood collection is easy and minimally invasive, yet reproducible procedures to obtain pure bulk EV samples and specific EV subtypes from blood are still lacking. Here, we addressed central aspects of EV immunoaffinity isolation from simple and complex matrices, such as plasma. Fluorescent EV spiking allowed us to demonstrate that target EV subpopulations can be efficiently retrieved from plasma, and that their enrichment is dependent not only on complex matrix composition, but also on the EV surface phenotype. Additionally, we found that plasma-derived EVs can be captured and detected using a simple protocol, which sequentially combines isolation and staining of specific surface markers. Finally, we conducted mRNA profiling experiments to prove that distinct EV subpopulations can be captured by directly targeting different surface markers. Furthermore, platelet-derived EVs encapsulated mRNA expression patterns that might be associated to early-stage lung cancer, which demonstrated that each EV subset conferred a differential clinical value, highlighting the advantages of selective isolation. In summary, our EV isolation protocol facilitated the extraction of clinically useful information from plasma. Compatible with common downstream analytics, it is a readily implementable tool that was tailored to provide a truly translational solution in routine clinical workflows, fostering the inclusion of EVs in novel liquid biopsy settings.

Keywords

extracellular vesicle; immunoprecipitation; liquid biopsy; enrichment; platelet; plasma; early-stage cancer

Introduction

Studies focused on EVs have flourished in the last 15 years, accompanied with a persistent concern for developing, comparing and evaluating EV isolation or purification methodologies[1–11]. Most popular approaches, such as ultracentrifugation (UC) or size-exclusion chromatography (SEC) rely on physical properties to isolate particles, depending on their density or size[5,12,13]. Despite the major differences between UC and SEC, when purifying simple samples such as serum-free cell conditioned medium (CCM), where the majority of particles are indeed EVs, both methods recover whole EVs equally well and do not enrich for particular surface phenotypes[7,13–15]. Thus, these methodologies are extremely useful to obtain large batches of fairly pure EV samples from cell cultures and enable unbiased characterization of EV subpopulations. However, complex biosamples, particularly plasma, are composed of highly dynamic biomolecule amounts and plenty of non-vesicular particles, which outnumber actual EVs in several orders of magnitude[16,5,17]. Since the features of some non-vesicular particles and EVs greatly intersect (i.e. size, density or charge), UC and

SEC-isolated EVs from complex biosamples contain considerable amounts of contaminants[5,7,18–21]. Moreover, neither isolation approach is readily compatible with routine clinical workflows, which is still an underappreciated aspect in studies attempting to harness the potential of EVs for medical diagnostics. As research narrows down, the more EVs are recognized as essential players in a variety of key biological events, stretching beyond cell communication roles, sometimes even directly promoting disease[22–30]. In addition, EVs circulate in virtually all biofluids[22,26,31,32], hence their isolation or delivery can be done with minimal invasiveness. All this body of evidence opens the door to novel, high-impact scientific and technological developments, which will foster the establishment of precision medicine and next generation disease diagnostics and monitoring through liquid biopsies. Briefly, liquid biopsies are defined as the collection of blood, and other biofluids, for the analysis of disease-specific markers and signatures. They have been widely regarded as a game changer, particularly in oncology and cancer research, holding promise for early disease detection[33–35]. Mainstream liquid biopsy strategies rely on ultra-sensitive analytical techniques to profile circulating nucleic acids, often generating large datasets that require dedicated bioinformatics pipelines to assure high precision and reproducibility. This opens the question of whether such a strategy should be termed 'biopsy' at all, given that the origin of harvested material is not selected. EVs bring to the liquid biopsy field the promise of selective enrichment and traceable origin, as they carry diverse macromolecular markers distinctive of tissue, cell type or condition.

Most cancer-related EV biomarker studies conducted analytical comparisons of EVs isolated in bulk, from the blood of cancer patients and control cohorts. Research has indicated that EV heterogeneity is even more pronounced than what had been previously anticipated[14,36–42], and consequently, the paradigm is shifting as more scientists strive now to enrich for specific subpopulations. Isolation strategies based exclusively on physical properties do not enable such enrichment, evidencing the need for methodologies able to target and retrieve distinctive phenotypical characteristics of specific EV subpopulations, typically membrane proteins or other surface moieties. As such, several affinity-based EV capture approaches have been employed, making use of solid surfaces such as chips[43–47], or beads coated with antibodies[40,48–52], aptamers[53,54] and even peptides[55]. Still, many reports describing affinity-based methods for EV isolation fail to comprehensively address the key factor of an enrichment strategy, which is the capacity of selecting exclusively targeted subpopulations, or simply put – specificity. Besides, research articles seldom include EV spike-in models or concerns about the impact biological matrices can have on IP performance.

In the present study, we report that nano-sized superparamagnetic beads allow for direct, specific and complete immunoprecipitation (IP) of EV subpopulations from simple or complex matrices, phosphate-buffered saline (PBS) and plasma, respectively. Recovered EV subsets could be easily quantified with a fluorescence-based immunoassay directly on beads that did not interfere with downstream processing. Due to their complex composition, inter-donor biological variation and the lack of standardized harvesting and purification methodologies, plasma samples often introduce unknown unwanted variability in downstream analytics[7,16,17,42,56,57], which can be a major roadblock in translational research. Therefore, we also addressed understated aspects of EV IP, namely interactions between different EV phenotypes and complex plasma matrix components, which are likely relevant in other affinity-based EV isolation contexts and can compromise both recovery and specificity. Together with gene expression profiles of distinct EV subpopulations obtained from minimally processed healthy donor plasma, we concluded that IP specificity could be sustained across plasma samples from different donors. Moreover, mRNA profiles validated that different EV subpopulations were recovered according to the targeted surface marker. Finally, we applied this flow to a small clinical cohort of early-stage Non-Small Cell Lung Cancer (NSCLC) patients, providing a proof of principle that emphasizes the differential clinical value extracted from distinct EV subsets. Platelet-derived EVs were identified as potentially important biomarker repositories in early-stage cancer detection.

Our optimized procedures are simple, quick, scalable and automatable, with the endpoint goal of fitting into realistically feasible clinical workflows. Nonetheless, they can also be valuable in research and development

settings, when a robust enrichment of particular EV subpopulations is required, or to improve the performance of downstream assays that could potentially benefit from this pre-analytical step.

Materials and Methods

Biological samples and patient consent

Human plasma samples for assay optimization were obtained from BioIVT (Westbury, NY, US). Whole blood was collected in K2 EDTA tubes and within 60min post-collection, platelet-rich plasma (PRP) was obtained by centrifugation at 500g for 10min. PRP was further centrifuged at 1500g for 10min to retrieve platelet-poor plasma (PPP). A final centrifugation at 1200g for 20min rendered PPP into platelet-free plasma (PFP). All plasma experiments were performed with PFP.

Patient and healthy donor samples (14 vs. 14) included in the nCounter proof of principle liquid biopsy experiments derived from a prospective single-center study conducted at the Quiron Salud hospital group (Barcelona, Spain). The study was carried out in accordance with the principles of the Declaration of Helsinki under an approved protocol of the institutional review board of Quiron Salud hospital group (internal code 2021/10-ONC-DEX act no. 03/2021). Written informed consent was obtained and documented from all patients and healthy controls; samples were de-identified for patient confidentiality. Blood samples (10 mL) were collected in Vacutainer tubes (BD, Plymouth, UK). After a first centrifugation step at 120g for 20 min, supernatants were transferred to new tubes and immediately submitted to a second centrifugation at 120g for 5min. Finally, supernatants were transferred to clean tubes for a third centrifugation at 360g for 20min. The resulting PFP was frozen at -80°C and used for subsequent EV IP.

Cell culture and EV purification from cell conditioned media (CCM)

Human cell lines HT29, A549, 22RV1 (ATCC) and HEK293-pRTS-CA9 (courtesy of prof. Dr. Reinhard Zeidler, Helmholtz Zentrum München, Germany) were grown in complete medium supplemented with 10% FBS (Euroclone) and 1% pen/strep (Sigma). McCoy's 5A medium (Invitrogen) was used for HT29, DMEM (Euroclone) for HEK293 and A549 and RPMI-1640 (Euroclone) for 22RV1. Cells were expanded in T75 and T150 flasks, under a humid atmosphere of 5% CO2 at 37°C. At 70% confluence, cells were washed 2 times with 1x PBS and conditioned in serum-free medium for 48-72h. CCM was harvested and pre-cleared by differential centrifugation at 300g for 10 minutes, 1200g for 20 minutes, and 10000g for 30 minutes at 4°C. Pre-cleared CCM was stored at -80°C.

For EV purification, pre-cleared CCM was concentrated by ultrafiltration (Amicon® Stirred Cell, Ultracel 100kDa Ultrafiltration Discs, Merck Millipore), from a maximum volume of 500mL down to 10mL. Concentrated CCM was purified by SEC (qEV10 35nm, Izon Science), pre-equilibrated with 1x 0.22µm filtered PBS. Briefly, as 10mL of concentrated CCM were loaded in column, the eluate was immediately collected in 1mL fractions. EV-containing fractions were pooled (16 to 40, pool volume ≈24-25mL) and concentrated down to 0,5-1mL by 100kDa ultrafiltration (Amicon® Ultra-15 Centrifugal Filter Unit, Merck Millipore). Purified EVs were aliquoted and stored at -80°C.

EV Staining protocols

To generate traceable and easily quantifiable EV spikes for IP recovery experiments, purified EVs were stained with CellTrace™ CFSE (Thermo Fisher Scientific). EV concentration was determined by nano flow cytometry (nFCM). Each staining reaction contained $2x10^9$ EVs (10^8 particles/µL) and was incubated with 10µM CFSE for

1h30’ at 37°C. After pooling up to 6 staining reactions, excess CFSE was eliminated by SEC. The volume of pooled staining reactions was adjusted with filtered PBS up to 500µL, which were loaded in SEC columns (qEVoriginal 35nm, Izon Science) and the eluate immediately collected. The first 3mL were discarded and the following 1,5mL collected in a clean tube, according to the EV elution profile. Size and concentration of CFSE-labelled EVs was analysed by nFCM. CFSE-stained spikes were freshly prepared and measured before each experiment. Endogenous staining of 22RV1 EVs was carried out using an amphipathic near infra-red (NIR) fluorescent probe (kindly provided by prof. Dr. Donal O'Shea, RCSI, Dublin, Ireland), which is effectively internalized by cells, spreads through the cytoplasm and becomes stably incorporated in secreted EVs[58]. At 70% of confluence, 22RV1 cells were incubated in complete medium, supplemented with NIR (5µM) for 2h at 37°C, under a humid atmosphere of 5% CO2. NIR-supplemented medium was discarded and cells washed three times with PBS to eliminate all traces of unincorporated dye. Cells were conditioned in serum-free medium for 48-72h and CCM was collected for the purification of NIR-labelled EVs, following the procedures described in the section above. EV Surface protein profiling was performed by staining with fluorescently-tagged primary antibodies. Similarly, $2x10^9$ EVs were incubated with antibodies for 1h at 37°C. Excess unbound antibodies were washed off with three rounds of buffer exchange with filtered PBS on 500µL ultrafiltration spin columns (Nanosep® 300kDa Centrifugal Devices, Pall Corporation).

Nano flow cytometry: Instrument setup and EV analysis

We employed a dedicated nFCM platform (Flow NanoAnalyzer, nanoFCM Inc.) that enables single particle analysis in sheathed flow, for the characterization of EVs between 40-200nm. This system featured three independent single-photon counting modules, which recorded side scatter (trigger channel) and fluorescence signals for each particle that crossed the instrument’s interrogation zone and could be excited with a focused 488nm laser beam. The instrument was aligned and calibrated at each run with size and concentration standard beads (nanoFCM Inc.). Samples and blanks (filtered PBS) were read at a constant pressure of 1kPa for 1min and at a maximum event rate of 12k events/min to avoid swarm effects[59,60] in EV detection. Between samples, the instrument was cleaned with 1x cleaning solution (nanoFCM Inc.) and the capillary rinsed with ultrapure water. Fluorescence thresholds were set based on unstained EV samples and blanks. Background fluorescence stemming from the presence of unbound free dyes resulted in elevated thresholds. Such samples were either further washed or excluded from the study, to ensure accurate detection of fluorescent events. Dot plots were generated using the NF Profession 1.0 software (nanoFCM Inc.), required also to operate the system. On the Y axis, fluorescence intensity was plotted as peak area and on the X axis featured the peak height of side scatter (SSC) values.

Bulk fluorescence measurements

For direct IP readouts, 100µL of bead samples were loaded in black opaque 96-well plates (PerkinElmer) and read in a fluorometric plate reader (CLARIOstar Plus, BMG Labtech). Optimal gain and focal height settings were adjusted to the brightest wells. A total of 81 fluorescence measurements were acquired throughout the entire area of each well (9x9 data point matrix scan). The average value of all measurements was considered per well. As beads did not interfere with measurements, nor contribute to background fluorescence, raw sample fluorescent signals were normalized to filtered PBS and data is presented as signal-to-noise (S/N) or as % of input. For indirect IP readouts, 200uL of the IP flow-through were measured in parallel with input controls (IPs lacking beads). As described above, settings were adjusted to the brightest wells, which in this case were always input controls. Indirect data points were presented as percentage of recovered input, determined as:

$$\%\ of\ input\ (flowthrough) = 1 - \frac{IP\ flowthrough}{input}$$

IP reactions and in-column fluorescent staining

IP reactions were conducted in 0,22µm filtered PBS-BSA 0,1% w/v and plasma, hereon appointed as simple and complex matrices, respectively. EV spikes contained between $5x10^6$ and $5x10^8$ particles, to which superparamagnetic antibody-conjugated MACS beads (Miltenyi Biotec) were added in excess (1 to 5µL), since beads could be accurately quantified by nFCM. As methodologies for correct quantification of true plasma EVs are still lacking, we confirmed that the number of beads applied for IPs in complex matrices allowed for maximum recovery.

Streptavidin MACS beads (Miltenyi Biotec) were coated with 2µg of biotinylated antibody per 20µL of beads under agitation, for 30min at RT. Antibody-coated streptavidin beads were loaded in magnetized pre-equilibrated MACS µColumns (Miltenyi Biotec), washed 3x with 200µL of PBS-Tween20 0,1% v/v and 2x with 400µL of PBS. Columns were removed from the magnet, placed on clean collection tubes and beads eluted in 100µL of PBS, with plungers. Concentration was measured by nFCM. For precise comparisons, the number of antibody-coated streptavidin MACS beads applied per IP was matched to the number of covalently-conjugated ones.

Complete IP reactions were incubated for 1h at RT under agitation. Subsequently, IPs were loaded in magnetized pre-equilibrated MACS µColumns, washed 3x with 200µL of PBS-Tween20 0,1% v/v and 2x with 400µL of PBS. Then, columns were de-magnetized and the beads-EV complex eluted in 100µL of PBS in clean collection tubes. Additionally, bead-bound recovered EVs could also be stained with fluorescently-labelled primary antibodies, directly inside µColumns. Firstly, antibody master mixes were prepared in PBS, containing antibodies at optimized concentrations. Then, 40µL of mix were run through magnetized columns containing washed bead samples. Additional 20µL were added to ensure the void volume of columns was flooded in antibody staining mix. At this point, columns could be de-magnetized and incubated for 1h at RT, protected from light. Stained bead samples were placed back on the magnet and washed 3x with 200µL of PBS-Tween20 0,1% v/v and 2x with 400µL of PBS. With de-magnetized columns on top of clean collection tubes, stained bead samples were eluted in 100µL of PBS.

RNA extraction

Bead sample volume was adjusted to 250µL with PBS, to which 750µL of TRIzol™ LS (Thermo Fisher Scientific) were added. Samples were vortexed for 30s and incubated for 10min at RT. 200µL of chloroform were added, tubes shaken for 30s and incubated for 5min at RT. Phases were separated by centrifugation for 15min at 12000g and 4°C, the aqueous phase was transferred to a clean tube and 2.5µL of RNA-grade glycogen (20mg/mL, ThermoFisher Scientific) and 500µL of isopropanol were added. Samples were incubated for 10min at RT and centrifuged for 10 min at 12000g and 4°C. Supernatants were discarded and 1mL of a 75% ethanol solution was added to wash RNA pellets. Tubes were vortexed briefly and centrifuged for 5min at 7500g and 4°C. Supernatants were discarded and RNA pellets air-dried for 5min. RNA pellets were resuspended in 10µL of nuclease-free water. To 10µL of RNA sample, 1µL of DNA digestion buffer and 1µL of DNase I (Zymo Research) were added. Samples were mixed, spun down and incubated for 15min at RT. For DNase inactivation, EDTA was added at 50mM and samples incubated for 10min at 65°C. RNA samples were cooled at RT and stored at -80°C.

Cryogenic transmission electron microscopy (Cryo-TEM)

For cryo-sample preparation, 2.3µL of the sample were applied to Quantifoil holey carbon grids (copper Multi A, Quantifoil Micro Tools GmbH) that were previously glow discharged. Excess fluid was blotted from the grid and plunge frozen in liquid ethane using a FEI Mark IV plunge freezer to achieve sample vitrification. Frozen samples were stored in liquid nitrogen until EM imaging in a Philips CM200FEG microscope equipped with a TVIPS TemCam-F224HD CCD camera and a Gatan 626 Cryo-Holder.

ddPCR

One-step ddPCR reaction master mixes were prepared considering a volume of 20µL per sample. Briefly, master mixes contained 1x Supermix, 20U/µL of reverse transcriptase and 15mM of DDT (One-Step RT-ddPCR Advanced Kit for Probes, BioRad). Gene expression ddPCR reactions were performed in a duplex configuration, using commercially available assays to amplify GAPDH and CA9 (Assay IDs: dHsaCPE5031597; dHsaCPE5055974, Bio-Rad), containing HEX and FAM-conjugated reporter probes, respectively. Both assays were diluted 1:20 in the master mix. For each sample, 5µL of RNA was thoroughly mixed with master mix and 20µL were transferred to DG8™ Cartridges (Bio-Rad). Positive and no template controls were included in each run. Next, 70µL of Droplet Generation Oil (Bio-Rad) were loaded in the cartridge, which was then placed inside the QX200™ Droplet Generator (Bio-Rad). Droplets were generated and transferred to 96-well PCR plates (suppl). Plates were sealed with heat seal foil (Bio-Rad) on a PX1 PCR Plate Sealer (Bio-Rad) at 180°C for 5 sec. Sealed 96-well plates were inserted in a T100 Thermal Cycler (Bio-Rad) and amplification conditions set as follows: Reverse transcription was performed at 42°C for 60min, followed by an enzyme activation step at 95°C for 10min and 39 cycles of denaturation at 95°C for 30sec and extension at 55°C for 1min, with a ramp rate of 3°C/sec. A final step of 98°C for 10min deactivated the enzyme and amplified products were kept at 4°C. Droplets were read in a QX200 Droplet Reader (Bio-Rad) and gene expression data analysed in QuantaSoft™ Version 1.7 (Bio-Rad).

Magnetic beads and antibodies

Table 3. Magnetic beads (Miltenyi Biotec) confronted in the study

Beads	**Product code**
Streptavidin MicroBeads	130-048-101
Exosome Isolation Kit CD9, human	130-110-913
CD61 MicroBeads, human	130-051-101
Anti-PE MicroBeads UltraPure	130-105-639
Exosome Isolation Kit Pan, human	130-110-912

Table 4. Primary antibodies (all from Exbio Praha, a.s.)

Antibody	**Final concentration (µg/mL)**	**Product code**
Anti-Human CD9 Alexa Fluor® 488	5,2	A4-208-T100
Anti-Human CD9 PE	4	1P-208-T100
Anti-Human CD41 PE	2	1P-309-T100
Mouse IgG1 Isotype Control PE	2	1P-632-C100
Anti-Human CD9 Biotin	stock at 1000	1B-208-C100
Mouse IgG1 Isotype Control Biotin	stock at 1000	1B-632-C100

Statistical tests and specificity

Experimental points were obtained in triplicate, unless stated otherwise. Mean values were plotted with standard deviation error bars throughout. Paired t-test comparisons were conducted in Prism 9.1.1 (GraphPad Software), which was also used for the visualization and presentation of data.

Specificity was calculated as: $1 - \frac{negative\ control}{target}$

NanoString nCounter sample processing

DNAse-treated RNA samples were converted to cDNA using the nCounter® Low RNA Input Kit (NanoString Technologies), following instructions provided by the supplier. Briefly, cDNA conversion was followed by a pre-amplification step, which consisted on 14 cycles of target-specific PCR amplification using the Human Immunology V2 Primer Pool (NanoString Technologies), according to the gene expression panel analysed later on. Hybridization reactions were prepared using the Reporter CodeSet and Capture ProbeSet regents from the nCounter Human Immunology v2 Panel (NanoString Technologies) and carried out for 18h at 65°C. This panel includes a total of 594 genes, 579 of them involved in the immune response and 15 commonly used reference control genes. It contains also spikes of synthetic DNA targets at varying concentrations and 8 ERCC RNAs that function as internal positive and negative controls, respectively. Hybridized samples were processed in the nCounter® FLEX Analysis System (NanoString Technologies). Data was exported in RCC files for further analysis.

Data normalisation and Differential Expression analysis

Raw data was exported in RCC-formatted files using the nSolver Analysis Software (version 4.0.70, NanoString Technologies). Pre-processing, normalisation, and downstream exploratory and differential expression (DE) analyses were carried out with R (version 4.0.3). Each single Nanostring run (12 samples per run) was defined as one batch. Essentially, NanoStringQCPro (version 1.22.0) package was utilised to import raw RCC files into the R environment and to perform an initial assessment of data quality and integrity. More precisely, the performance of NanoString standard Imaging, Binding Density, Positive Control Linearity, and Limit of Detection quality control metrics was examined for potential outlier samples. Next, samples were subjected to various exploratory analyses for thorough data examination. Boxplots, correlation heatmaps, PCA plots, and MDS plots (amongst others) were created using the ggplot2 (version 3.3.5), pheatmap (version 1.0.12), and ggpubr (version 0.4.0) packages. Moreover, the interquartile range (1.5 IQR rule) was used to detect, mark and remove potential outlier samples. Pre-processing of the data was then performed gene and sample-wise. In order to remove lowly expressed genes with excess background noise, several filtering steps were used. Firstly, the edgeR (version 3.32.1) function filterByExpr was used to remove lowly expressed genes. One additional function based on the Negative Control (NC) sequences was also used to filter out lowly expressed genes. Specifically, the median value of the 8 NC sequences was calculated for each sample and subtracted from the endogenous genes. After the transformation using NC sequences, genes that fell below 0 in more than 30% of the samples were removed from further analysis. Assessment of the various filtering steps was concluded again by MDS and PCA plots. Normalisation of the raw filtered data and DE analysis was attained using the DESeq2 (version 1.30.1) package with default parameters. Standard relative log expression (RLE) and PCA plots were used to evaluate the performance of the normalisation before proceeding with the differential expression analysis. Finally, fold change and adjusted p-values obtained from DE analyses were log2 and log10 transformed, respectively, and results visualised on a volcano plot. A fold change of 2 and adjusted p-value of 0,05 were set as DE thresholds.

Results

Antibody-conjugated beads outperform antibody-coated streptavidin beads, in simple and complex matrices

Because EVs are small nanoparticles, we reasoned that capture efficiency could be maximized and IP reactions better controlled by utilizing similar-sized nano beads, which may bring advantages over larger ones[61]. To date, EV immunoaffinity isolation has been vastly performed with microbeads, typically sized >1 µm. MACS beads are 50nm superparamagnetic particles that allow for minimal labelling and gentle processing of target structures, whether they are carried on cells or EVs. Initially, we evaluated two different surface chemistries for their specificity and recovery efficacy. Streptavidin-conjugated beads (MACS-STV) can be coated with any biotinylated affinity reagent and thus are a highly versatile system, suitable for direct and indirect IP reactions. On the other hand, the supplier also provides ready-to-use, covalently-conjugated beads (MACS), coated with correctly oriented antibodies, which is known to improve specificity[62]. Streptavidin-biotin systems also allow for correct antibody orientation, though they tend to be more susceptible to non-specific interactions, when compared to covalently-conjugated antibody bead surfaces. We tested the performance of both surface chemistries in the context of EV IP by assessing the recovery of fluorescently-labelled HEK293 EVs in PBS-BSA, with anti-CD9 and isotype control antibody-coated beads. Isotype-coated beads served as negative control to evaluate the specificity of MACS-STV, while anti-CD61-conjugated beads (MACS-CD61) played the same role for MACS. CD61 was absent from our cell lines and their EVs, and since it represents a cluster of differentiation of the platelet lineage, we deemed it an appropriate negative control for cell line-derived EV IPs. To generate traceable EV models, we stained HEK293 EVs with CFSE[15] and obtained 87,9% of fluorescent particles, as detected by nFCM (Sup. Fig. 1A). We also measured bead concentration to assure that the number of beads outnumbered fluorescent EV inputs in this and in the following experiments (Sup. Table 1).

CFSE-stained HEK293 EVs were incubated with beads and fluorescent readouts were acquired for direct (beads) and indirect (IP flow-through) estimations of IP recovery. We obtained 44% of specificity with MACS-STV, regardless of the readout, whereas with MACS, 89% of specificity was observed by direct measurement and 75% by indirect measurement (Fig. 1A). Additionally, the fluorescent signal detected in MACS-CD9 beads evidenced a 48% recovery of CFSE-HEK293 input, which coincides with an average CD9 expression of 42% in these EVs (Sup. Fig. 1B). Considering 5,5% of non-specific pull-down signal by MACS-CD61, we efficiently recovered nearly 100% of the CD9 subpopulation. Instead, direct measurements on MACS-STV revealed that 22,1% and 12,1% of spike was recovered with anti-CD9 and isotype control-coated beads, respectively. This indicates that MACS but not MACS-STV, enabled the IP of the entire CD9-positive subpopulation in PBS-BSA.

Beads, EVs and the IP immune complex formed between them were visually examined by Cryo-TEM. An irregular bead structure could be discerned (Fig. 1B-1), contrasting with the circular shape of EVs and their well-defined membrane (Fig. 1B-2). IP complexes revealed that several beads can decorate the EV surface, which is likely dependent on the number of epitopes available for binding, amongst other factors (Fig. 1B-3).

Next, we evaluated the suitability of covalently-conjugated and streptavidin beads for EV IP in plasma, which is likely the most complex human biofluid. CFSE-labelled HEK293 EVs were spiked in healthy donor plasma (donor 6) and IPs conducted as aforementioned. Only direct bead readouts were plotted, since plasma emitted a great deal of background fluorescence in the CFSE channel, which compromised indirect readouts. Surprisingly, more fluorescent EV spike was recovered by negative control antibodies than with anti-CD9-coated or conjugated beads (Fig. 1C). Such results would imply the lack of specificity of both bead types in the plasma matrix, which was considered true for MACS-STV, where negative control beads were coated with a human isotype control antibody. Nevertheless, the negative control for the covalently-conjugated MACS

beads was anti-CD61. Even though our spiked EVs did not express CD61, due to its abundance in plasma we reasoned that this platelet-related marker could be interacting with fluorescent EV spikes, causing their co-IP.

To confirm that the direct fluorescence readout accurately portrayed spike recovery, we extracted RNA from MACS-pulled down material (from Fig. 1C) and performed ddPCR for GAPDH and CA9, a stably transfected marker expressed in our HEK293 cells, but undetectable in healthy plasma. The expression of both markers faithfully correlated with the previously measured fluorescent signal (Fig. 1C-MACS) and CA9 reads confirmed the recovery of our spike (Fig. 1D), indicating that fluorescence detected on beads stemmed from CFSE-labelled HEK293 EVs rather than from potential plasma-derived contaminants. Thus, ddPCR validated direct fluorescent measurements as reliable readouts of IP recovery.

To have a reliable negative control when assessing IP specificity from plasma, we re-tested the IP of CFSE-labelled HEK293 EVs spiked in plasma with MACS-CD9 against anti-phycoerythrin (PE) coated MACS beads (MACS-PE). PE is a commonly employed fluorophore produced by algae, which makes PE-coated beads an ideal negative control for IPs in human plasma. Spike recovery was now 4.5x higher with MACS-CD9 than with MACS-PE, conferring 78% of specificity to covalently-conjugated MACS beads in this experiment (Fig. 1E) and confirming our suspicion that CD61 was promoting spike co-IP.

Intrigued by this CD61-mediated capture of CD61-negative fluorescent spikes in plasma, we evaluated the recovery of CFSE-HEK293 EVs from the plasma of a different donor (donor 7), using MACS-CD9, CD61 and PE. Remarkably, CD61-mediated co-IP of CFSE spikes was not observed in a different plasma source and both negative controls displayed comparable fluorescence signals (Sup. Fig. 1C), indicating that this effect is dependent on biological variation.

In summary, antibody-coated MACS-STV specifically captured EVs only in a simple matrix, though they were markedly outperformed by antibody-conjugated MACS beads, which captured the totality of the CD9 subset in PBS-BSA and maintained a substantial degree of specificity, even in complex matrices. Therefore, we confirmed that the streptavidin-biotin surface chemistry is more prone to non-specific interactions in affinity-based EV isolation strategies. Importantly, both fluorescence measurement strategies and ddPCR proved to be valuable readouts that complemented and validated each other for precise quantifications of IP recovery.

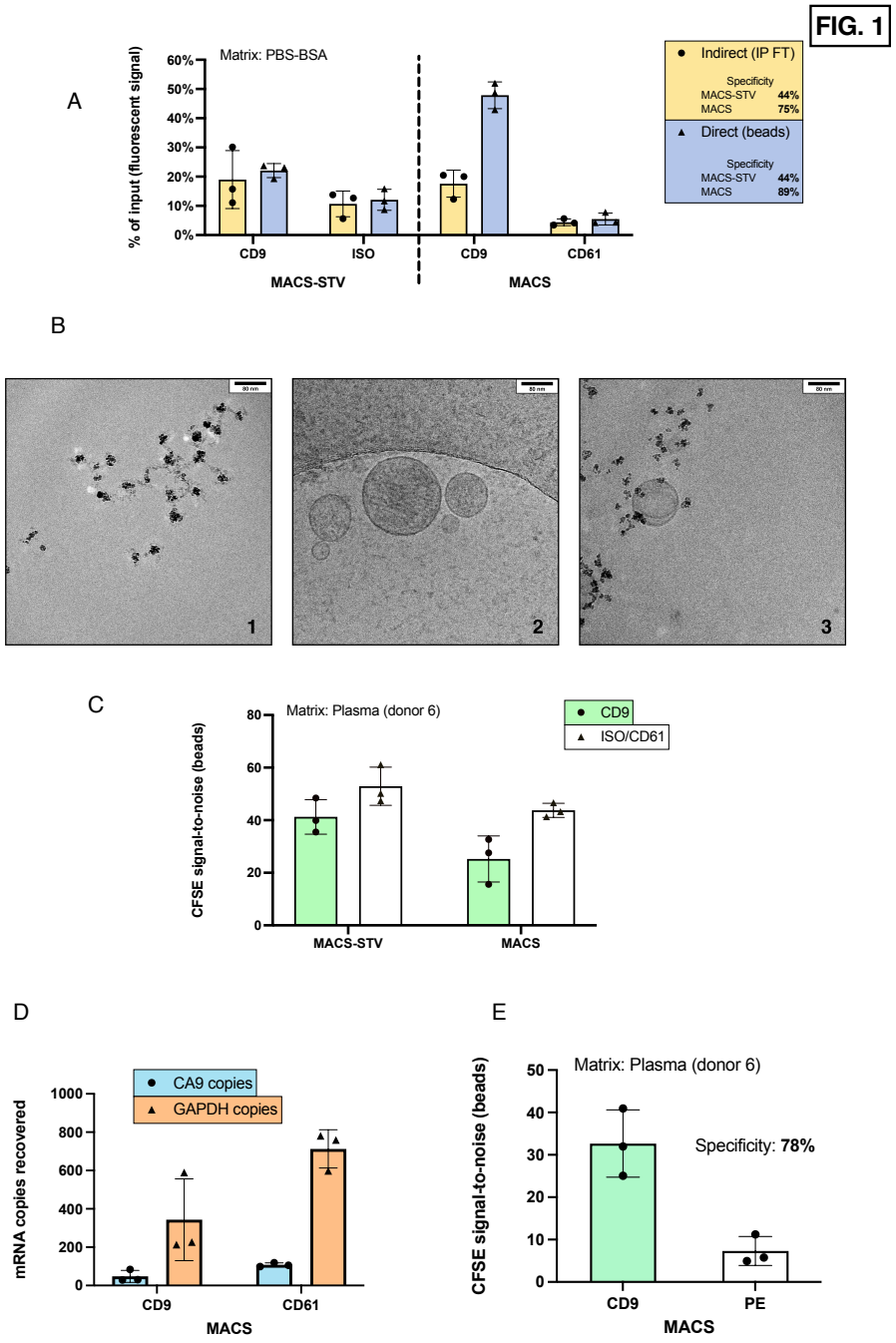

Figure 1. Multiple analytics evidence differential recovery of EV subpopulations in simple and complex matrices, between streptavidin-coated and covalently-conjugated beads.

(A) CFSE-stained HEK293 EVs were captured from PBS-BSA with MACS-STV and MACS. CD9 was the IP target and ISO/CD61 negative controls. Recovery was plotted as % of input, obtained using fluorescent signals of samples and input. Fluorescence of IP flow-throughs (FT) allowed for an indirect calculation of recovery (yellow), whereas fluorescence on beads provided a direct recovery measure (blue). Specificity represents the differences between target and negative controls.

(B) Cryo-TEM images of triple-coated MACS beads (1), HEK293 EVs (2) and the IP complex formed between both in PBS-BSA (3). Respective scale bars are shown on the top right corner of each image.

(C) S/N ratios of CFSE-stained HEK293 EVs recovered from plasma (donor 6) on MACS-STV and MACS. The IP target was CD9 and the negative controls ISO/CD61.

(D) GAPDH and CA9 mRNA copies from MACS CD9 and CD61 used in (C), measured by ddPCR.

(E) S/N ratios of CFSE-stained HEK293 EVs recovered from plasma (donor 6) on MACS beads coated with anti-CD9 and anti-PE antibodies. IP specificity was 78%.

Whole EV subpopulations can be efficiently captured from plasma, while spike recovery is dependent on EV type and biological variation of complex matrices

Having selected covalently-conjugated MACS beads due to their superior performance, we aimed at optimizing and exploring their capability to capture specific EV subsets from plasma. When we attempted to read CFSE-stained spike inputs and IP flow-throughs in plasma, S/N ratios were too low to extract meaningful information. Upon light absorption, plasma emits plenty of blue/green autofluorescence, which ultimately masked CFSE signal. Because biomolecules absorb and emit almost no NIR light, fluorescent NIR probes are a promising tool for *in vivo* and *ex vivo* imaging[63–65]. For this reason, we generated endogenously-labelled NIR EVs by feeding 22RV1 cells with a NIR probe, which is internalized and stably latches on to lipidic membranes, even after EV secretion[58]. After SEC purification of 22RV1-NIR CCM, we detected 92% of NIR-fluorescent particles and observed a CD9 expression of 20% (Fig. 2A). To understand if the entirety of one EV subpopulation could also be retrieved from complex matrices, not only NIR but also CD9-PE-labelled NIR EVs were spiked in plasma, followed by IP with anti-CD9 and anti-PE beads. As expected, NIR spikes delivered better S/N ratios in plasma with respect to CFSE spikes, which allowed us to reliably measure inputs and report both direct and indirect IP readouts. In line with previous plasma experiments, we estimated 87% and 70% of specificity through indirect and direct readouts, respectively, in the IP of NIR spikes (Fig. 2B). Moreover, both readouts indicated a 20% recovery of NIR input, which perfectly matched the proportion of CD9-positive 22RV1-NIR EVs, suggesting that the whole CD9 subpopulation of our spike could be retrieved from plasma (Fig. 2B).

Interestingly, the recovery of CD9-PE-labelled NIR EV spike was comparable between CD9 and PE beads. The direct bead readout even evidenced a slightly higher mean of 18% for PE over 14% for CD9 (Fig. 2C), hinting that CD9 epitopes may be less accessible to MACS-CD9 as anti-CD9-PE had already occupied them. These experiments confirm the high efficacy of this IP approach in recovering distinct EV subsets from plasma, further highlighting its specificity and flexibility also by indirect capture.

IP complexes formed in plasma were monitored by Cryo-TEM, where we could observe an abundance of beads over EVs, while the size of captured EVs spanned over a wide range (Fig. 2D). Whether EVs were recovered from plasma (Fig. 2D-1) or from HEK293-spiked plasma (Fig. 2D-2), IP complexes greatly resembled the ones observed after IP in simple matrices (Fig. 1B), demonstrating that true EVs, with intact structure and function, can be efficiently retrieved from complex matrices.

Still, we reckoned that IP reactions would be more efficient in PBS-BSA than in plasma, due to the richness of the latter in biomolecules that can hinder affinity interactions. To assess that, we spiked 22RV1-NIR and HT29-CFSE in both matrices, performed IP with triple-coated, anti-tetraspanin (CD9, CD63 and CD81) MACS beads and read their recovered fluorescence. As anticipated, higher recovery was always obtained in PBS-BSA. On average, spike recovery was 22% and 52% higher in buffer than in plasma with 22RV1-NIR and HT29-CFSE, respectively (Fig. 3A). This observation suggested that depending on the identity of EV spikes, different interactions between EVs, matrix components and affinity reagents likely occur, affecting IP recovery.

To evaluate the impact of IP conditions on spike recovery, HT29-CFSE EVs were spiked in plasma from donor 6 (the same used in aforementioned experiments) and triple-coated MACS incubated for 10, 25 or 60min. We confirmed a maximum fluorescence signal at 60min, whilst maintaining specificity (Sup. Fig. 2A). Moreover, the same HT29-CFSE spike was equally captured from donor 6 plasma increasingly diluted with PBS (Sup. Fig. 2B), showing that matrix dilution did not improve IP performance.

Having confirmed that IP conditions did not contribute to the variable recovery of different EV spikes, we further addressed this aspect by spiking CFSE-labelled EVs from three different cell lines (HT29, HEK293 and A549) in PBS-BSA and plasma from a different donor (donor 7), applying triple-coated MACS for IP. This time, HT29 EVs were similarly recovered from both matrices, displaying an average fluorescent signal only 4% higher in PBS-BSA. The recovery of A549 EVs was 18% greater also in PBS-BSA while surprisingly, 33% more

HEK293 spike was captured from plasma (Fig. 3B). In conclusion, these results demonstrate that the surface properties of distinct EV subsets can influence on how they are targeted and retrieved by affinity reagents, within a given matrix.

The complexity of plasma samples, exacerbated by consistent inter-individual variation, is one of the major factors limiting the clinical use of affinity-based assays. The disparity observed in HT29 EV recovery between PBS-BSA and plasma from donors 6 and 7 in two independent experiments (Fig. 3A, B), prompted us to estimate the real impact of biological variation on spike IP from complex matrices.

For this purpose, CFSE-labelled HEK293 and HT29 EVs were spiked in three different plasma sources and recovery assessed through direct IP fluorescence readouts. The recovery of HEK293 spike was similar between the plasma of donor 5 and 7, but it doubled in donor 8 plasma. Plasma from donor 5 resulted in the lowest recovery of HT29 EVs, as this signal tripled in donor 7 and reached its maximum in donor 8 plasma (Fig. 3C). Intriguingly, the recovery of HEK293 EVs remained constant in plasma from donors 5 and 7, but it tripled for HT29 EVs, further highlighting the weight of EV surface phenotypes in IP efficiency. Taken together, these results show how the affinity isolation of EV subpopulations depends both on their intrinsic surface characteristics and on the components of the matrix they are carried in.

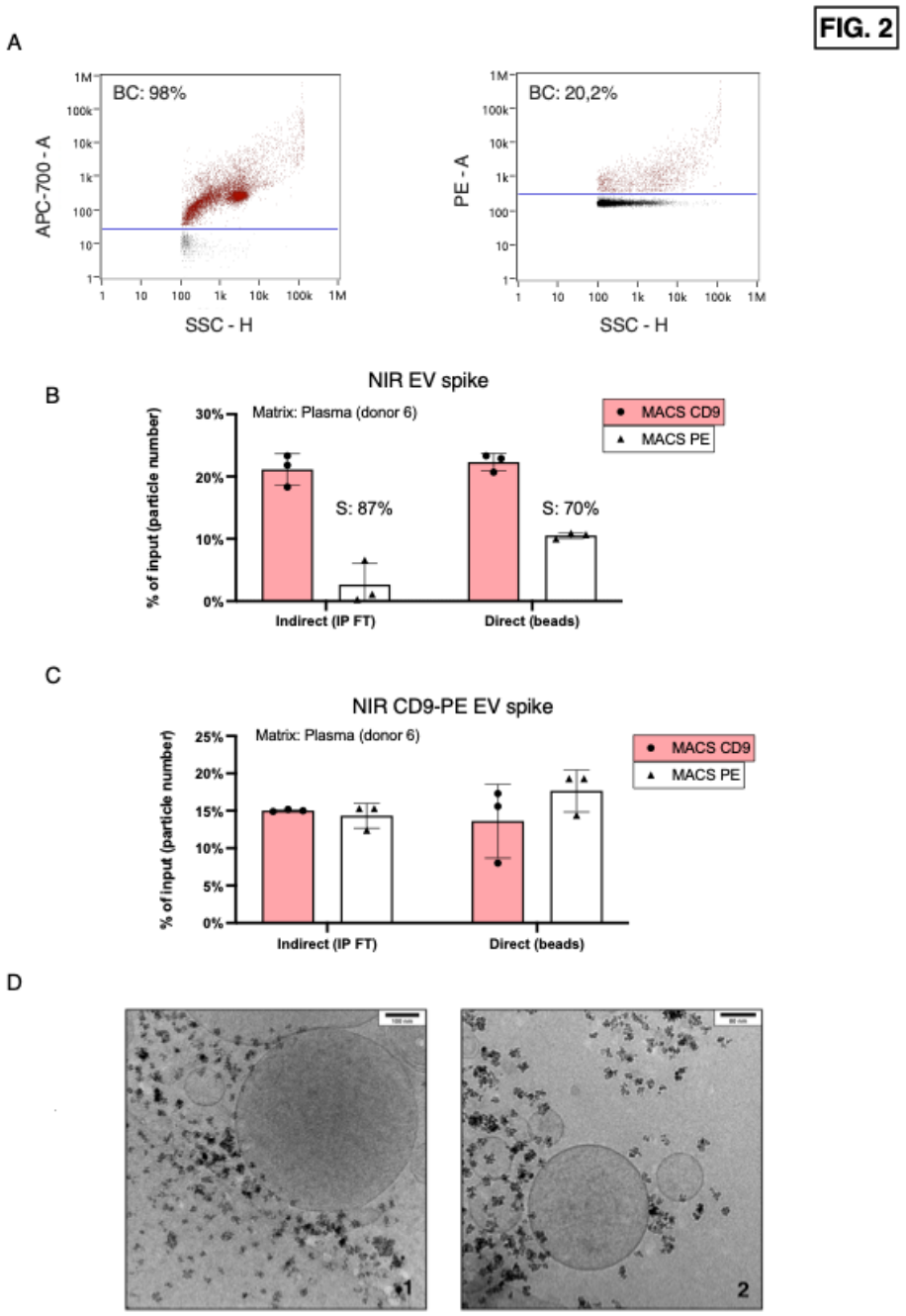

Figure 2. Intact EV subpopulations spiked in plasma can be completely recovered using antibody-conjugated beads.

(A) Single-particle analysis of fluorescent 22RV1-NIR EVs by nFCM. The dot plot on the left shows that the majority of 22RV1 EVs incorporated the NIR fluorophore, whereas the one on the right indicates the CD9-positive subpopulation, determined after staining with CD9-PE. Percentages of fluorescent particles were background-corrected (BC) with buffer (PBS).

(B) IP of 22RV1-NIR EVs spiked in plasma (donor 6). Recovery (% of input) was appreciated indirectly, through the NIR signal of IP flow-throughs (FT) and directly, by measuring the fluorescence of NIR EVs captured on beads. 22RV1-NIR EVs were used to plot a calibration curve correlating particle numbers with their fluorescent signal, which allowed to present percentages of input based on the actual number of particles recovered vs. input particles. Specificity (S) was calculated for both readouts.

(C) IP of 22RV1-NIR-CD9-PE-stained EVs spiked in plasma (donor 6). Recovery, plotted as % of input, was assessed by indirect and direct fluorescence readouts. The NIR signal of 22RV1-NIR-CD9-PE EVs was used to plot a calibration curve, correlating particle numbers with their fluorescent signal, which allowed to present percentages of input based on the actual number of particles recovered vs. input particles.

(D) Cryo-TEM images of EVs captured from plasma (1) and plasma spiked with HEK293 EVs (2), using triple-coated beads.

FIG. 3

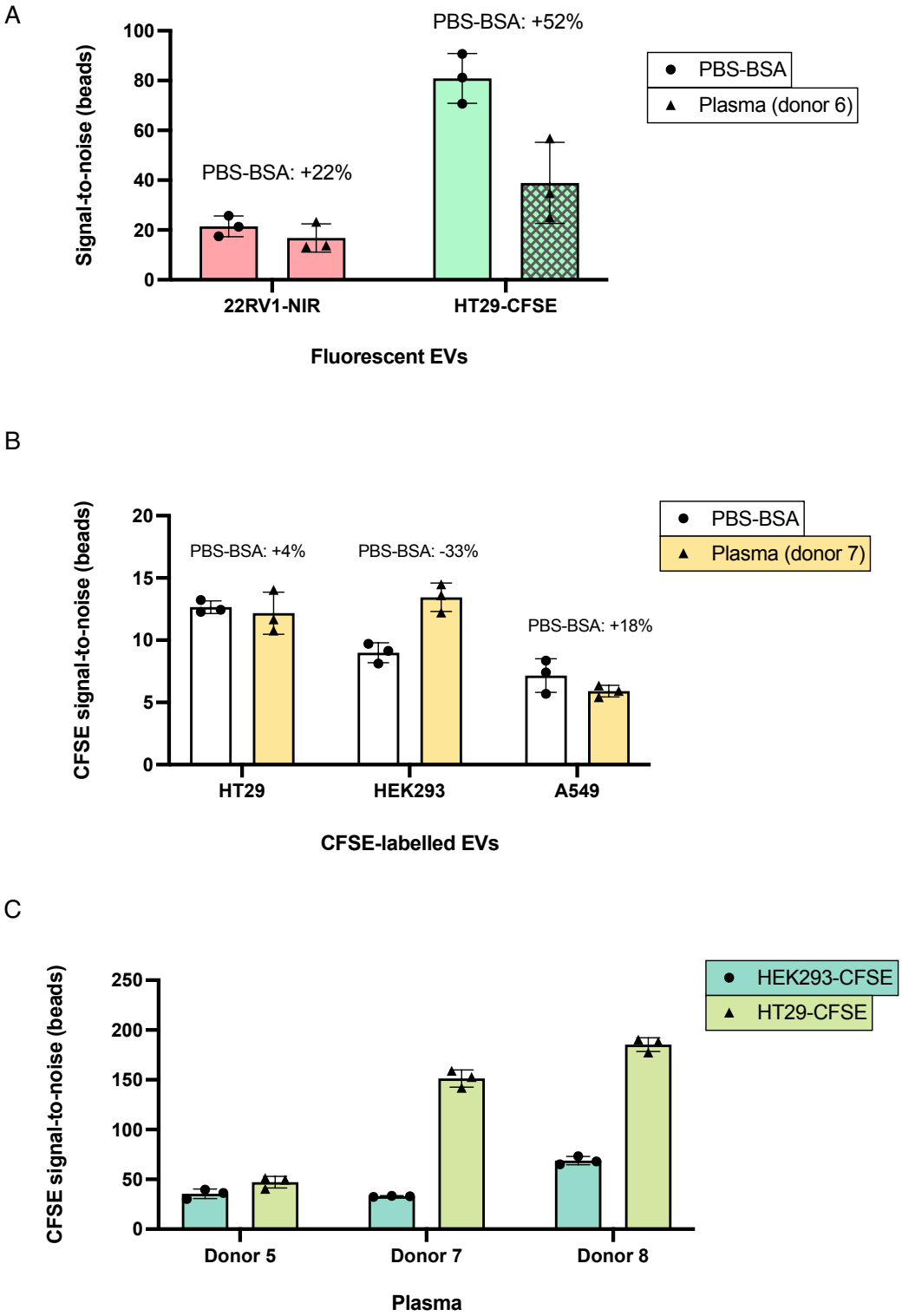

Figure 3. IP efficiency is dependent on EV surface properties, complex matrix components and interactions between both.

(A) Fluorescence S/N ratios were assessed on triple-coated beads upon the IP of 22RV1-NIR and HT29-CFSE spiked in either PBS-BSA or plasma (donor 6). Average recovery (S/N) differences between the two matrices are reported in percentage.

(B) CFSE-labelled EVs were spiked in plasma (donor 7) or in PBS-BSA and recovered using triple-coated beads. Average recovery (S/N) differences between the two matrices are reported in percentage.

(C) CFSE-labelled HEK293 (blue) and HT29 EVs (orange) were spiked in the plasma of 3 different donors and recovered with triple-coated beads. CFSE S/N on beads is directly proportional to the amount of captured spike.

Multiple surface markers can be directly detected to quantify EV subpopulations captured from simple and complex matrices

After optimization and characterization of our IP strategies employing fluorescently-labelled EV spike-in models, we wondered if captured EVs could be stained directly on beads using fluorescently-tagged primary antibodies. With the goal of quantitatively detecting EV subpopulations retrieved from plasma, we firstly set out to gauge the staining of HT29 EVs with CD9-PE, after IP with triple-coated beads in PBS-BSA. S/N ratios obtained on increasing EV numbers could be faithfully represented by simple linear regression (R^2 = 0,9992), from $1x10^8$ down to $5x10^6$ EVs, which corresponded to a S/N of 7 (Fig. 4A). As such, this approach was extremely robust for EV detection and quantification in simple matrices. To understand its applicability in plasma, we initially depleted endogenous plasma EVs with triple-coated beads, then delivered our HT29 spike to this "EV-depleted plasma" and sequentially performed IP using the same beads. Detection with CD9-PE also displayed a linear trend from $1x10^8$ to $1x10^7$ HT29 EVs (R^2 = 0,9783), however at the lowest amount of spike ($5x10^6$), an unexpected sharp increment in S/N ratios was noticed (Fig. 4B). Moreover, CD9-PE S/N ratios were substantially larger in plasma-derived bead samples (Fig. 4A, B), which could suggest that either the pre-IP depletion step was incomplete, or that the majority of signal stemmed from nonspecific antibody binding.

To address the specificity of fluorescently-labelled primary antibody staining of plasma-derived material on beads, we isolated platelet-derived EVs from the plasma of 3 independent donors using anti-CD61-coated beads. Detection was done by targeting CD41, a platelet-specific marker that forms a heterodimer with CD61 known as integrin αIIbβ3[66,67], while an isotype-matched antibody was used as negative control. Specific CD41 signal was measured with different intensity across all three plasma samples, always significantly higher than respective negative controls, confirming that this bead-based sandwich immunoassay assay can specifically detect EV-carried markers retrieved from plasma (Fig. 4C). Through Cryo-TEM we verified that, consistent with aforementioned images, CD61 beads clearly enabled the isolation of EV-like structures, suggesting that platelet-derived EVs could be efficiently captured from plasma (Fig. 4D).

Subsequently, we explored the possibility of simultaneously detecting two markers through the double staining of platelet EVs, isolated from plasma with anti-CD61 beads. S/N ratios obtained after staining with anti-CD41-PE and anti-CD9-AF488 were comparable, regardless of their incubation being conducted in single or in combination (Fig. 5A), meaning that staining efficiency and accuracy is maintained as two markers are concomitantly detected.

Finally, we investigated if double staining could provide meaningful information in the analysis of EV subpopulations derived from complex samples, using a platelet-derived EVs as paradigmatic example. To do so, 1mL of plasma was first heated to 56°C or treated with thrombin (2U) for 8min. Both procedures cause the precipitation of fibrinogen from plasma, noticeable by increased opacity or by the polymerization of an insoluble clot after 56°C or thrombin treatment, respectively[68,69]. Insoluble fibrinogen was eliminated by centrifugation at 5000g for 5min and the resulting supernatant collected in a clean tube, to which either triple-coated MACS or MACS-CD61 were added for EV IP. Since fibrinogen strongly interacts with the CD41/CD61 complex on platelets[70] (also termed the fibrinogen receptor, required for clot formation), we postulated that the effects of such treatments would mostly reflect on the detection of platelet markers, on platelet-derived EVs. To verify this, CD9-AF488 and CD41-PE double staining was performed on recovered beads after incubation in treated and untreated plasma.

Treatments did not majorly impact CD9 detection on triple-coated MACS, however on MACS-CD61, a significant drop of signal could be appreciated upon plasma pre-heating at 56°C (Fig. 5B). On the other hand, a drastic decrease in CD41-PE signal was observed after treatments, on both triple-coated MACS and on MACS-CD61 (Fig. 5C). These results confirmed our hypothesis, as mostly platelet-related markers were indeed lost upon thrombin or 56°C treatment, indicating that not only fluorescent EV tracers but also

endogenous plasma EVs are specifically selected from plasma samples and that multiple EV subpopulations from complex samples can be simultaneously detected using this staining protocol. Of note, neither of the plasma pre-analytic treatments resulted in increased overall EV recovery.

Taken together, we establish that a simple incubation step of fluorescently-labelled antibodies with EV-carrying beads, recovered from simple or complex matrices, enables an accurate detection and quantification of multiple surface markers expressed on EV immunoprecipitates.

FIG. 4

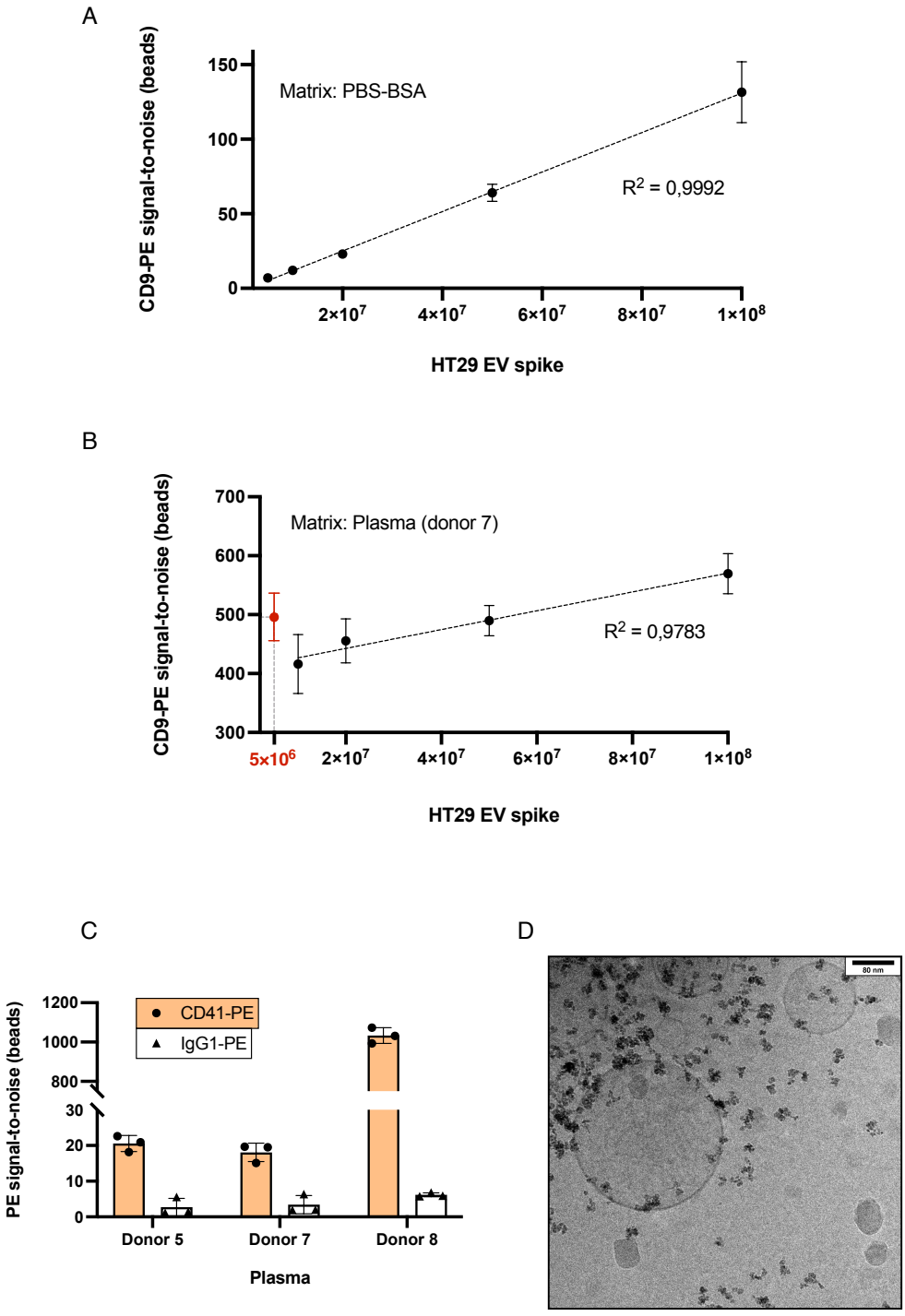

Figure 4. Direct detection and quantification of EV subsets on beads using fluorescently-tagged antibodies.

(A) Increasing numbers of HT29 EVs captured from PBS-BSA with triple-coated beads were detected by staining IP complexes with CD9-PE. PE fluorescence signals highly correlated with the number of spiked and recovered EVs, evidenced by a linear trendline (R2 = 0,9992).

(B) Scalar amounts of HT29 EVs were also spiked in "EV-depleted plasma" (donor 7) and recovered using triple-coated beads, which were stained by CD9-PE. A linear trendline proves the correlation between the amount of spike and the S/N obtained from CD9-PE from 1x108 to 1x107 EVs (R2 = 0,9783). An outlier mean S/N value at 5x106 spiked EVs is presented in red.

(C) Platelet-derived EVs were isolated from the plasma of 3 different donors using anti-CD61 beads. Target subpopulations (CD41-PE) were detected against a negative control antibody (IgG1k-PE).

(D) Cryo-TEM image of platelet-derived EVs recovered from plasma with anti-CD61 beads.

FIG. 5

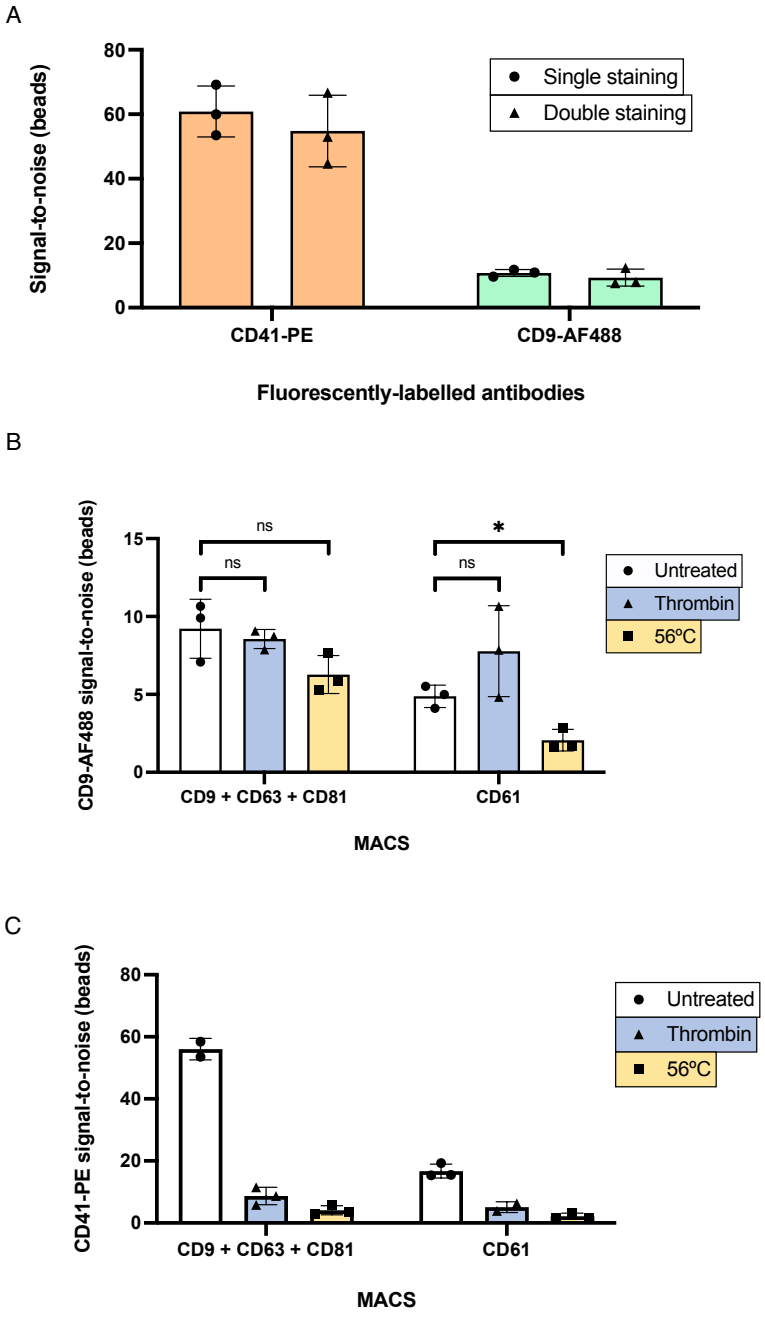

Figure 5. Double antibody staining on IP complexes allow for meaningful quantification of surface markers on plasma-recovered EVs.

(A) Platelet EVs isolated from plasma with anti-CD61 beads were stained with CD41-PE and CD9-AF488 in single or double staining settings. Fluorescence signal for both markers was equivalent, despite the incubation with 1 or 2 antibodies simultaneously.

(B) Triple-coated or anti-CD61 beads were incubated in untreated, thrombin treated or 56°C heated plasma and double stained with CD41-PE and CD9-AF488. Paired t-tests on the S/N ratios obtained with CD9-AF488 revealed a significant drop in CD61 beads (P = 0,036631), when untreated was compared with the 56°C condition. All the other comparisons were deemed non-significant (ns).

(C) Refers to the same experiment described in (B), although reports CD41-PE measurements. A substantial decrease in CD41-PE signal was detected upon staining IP complexes obtained with both beads, across treatments. Untreated and thrombin from triple-coated and CD61 beads, respectively, are shown as duplicates.

Different EV subpopulations carry distinct mRNA biomarkers that can be valuable for liquid biopsy-based early-stage NSCLC detection

As any *bona fide* enrichment strategy depends on its' specificity, we ultimately sought to provide definitive evidence that validated the performance of the IP protocol herein described. To do so, the mRNA content of different plasma EV subpopulations recovered either by triple-coated MACS or MACS-CD61 was profiled using the nCounter platform. Moreover, to inquire about the utility of our IP strategy in a liquid biopsy scenario, these different EV subpopulations were isolated from the plasma of two different cohorts, each composed of 14 donors. We measured the expression of 594 transcripts using the nCounter Human Immunology v2 Panel. To avoid biased conjectures and guarantee the quality of gene expression reads, we developed a dedicated bioinformatics pipeline including the internal standard nCounter QC checks, exploratory data analysis (EDA), low-count gene filtering steps, normalization and differential expression (DE) analysis.

Firstly, we questioned whether different EV subpopulations from the same healthy donor samples contained distinct mRNA profiles. During EDA on the comparison of healthy donor EVs obtained with triple-coated or CD61 beads, PCA revealed that samples seemed to slightly cluster by the number of unnormalized reads and group (Sup. Fig. 3A, B, C), but not by batch (Sup. Fig. 3D). However, after examining the unnormalized counts per group we could conclude that CD61+ EVs displayed a significantly higher number when compared to CD9, CD63 or CD81+ EVs ($p=0.00053$, Wilcoxon; Sup. Fig. 4A), indicating that the apparent clustering by group (defined in this case by IP target) did not actually occur as it was driven by the number of mRNA counts. RLE plots demonstrated that optimal sample normalization could be achieved with DESeq2 (Sup. Fig. 3E, left) and normalized samples were visually inspected on a PCA plot, which evidenced the two most variable samples depicted on RLE plots (Sup. Fig. 3E, right). DESeq2 output four DE genes, one upregulated and three downregulated in the dataset obtained with MACS-CD61 over triple-coated MACS (Fig. 6A). Supervised hierarchical clustering analysis was performed using the four DE genes and presented on a heatmap (Fig. 6B). Altogether, our data supports that depending on the targeted surface markers, we could effectively isolate different EV subsets from healthy donor plasma.

To understand the potential clinical value of each EV subset as biomarker carrier, we confronted our healthy cohort against a prospective early-stage NSCLC cohort using the same bioinformatics pipeline. Surprisingly, no DE genes were found when comparing EV mRNA obtained from healthy and cancer samples with triple-coated beads (Fig. 7A). On the other hand, the platelet-derived EV dataset allowed the comparison of healthy and early-stage cancer cohorts. As previously observed during EDA, samples only seemed to somewhat cluster by the number of unnormalized gene counts, but not by group or batch (Sup Fig. 5A-D). Despite being marginally elevated, the average number of unnormalized counts was not significantly higher in the early-stage NSCLC cohort ($p=0.43$, Wilcoxon; Sup. Fig. 4B). As before, DESeq2 alone optimally normalized all samples (Sup Fig. 5E left). Similarly, on the PCA plots of normalized counts we could appreciate a separation of the most variable samples (RLE plots, Sup Fig. 5E left) from the main sample cluster (Sup Fig. 5E right). DE analysis with DESeq2 found 47 DE genes, which were evidenced on a volcano plot (Fig. 7B). These results suggest that the identified mRNA expression patterns displayed by CD61-positive EVs may effectively allow the distinction between healthy and early-stage cancer samples. In summary, our experimental data demonstrates that different EV subpopulations can indeed be captured by targeting different surface markers, which reflected on their mRNA profiles and disclosed how distinct EVs subsets may confer differential clinical values in a liquid biopsy setting. In this case, the identification of 47 putative biomarkers for blood-based early-stage NSCLC detection demonstrated that platelet-derived EVs represent an appealing biomarker source that warrants extended studies.

FIG. 6

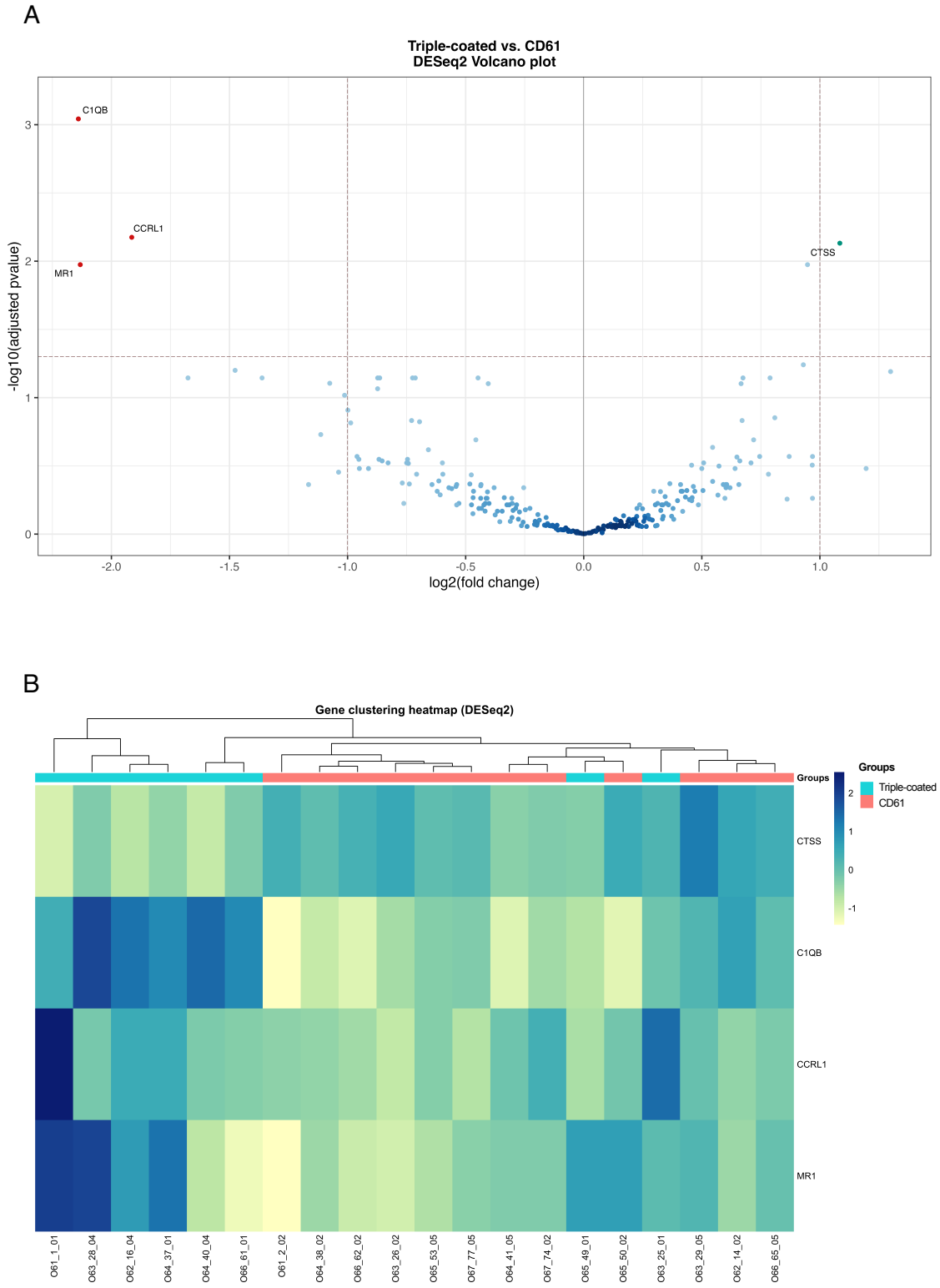

Figure 6. Differential expression (DE) analysis by DESeq2 between CD61+ and CD9, CD63 or CD81+ EV datasets on the healthy cohort.

(A) Volcano plot showing DE genes between the two groups. Cutoffs were defined for adjusted pvalues (0.05, Y axis) and log2 fold change (2, X axis). Upregulated genes and downregulated genes are depicted by green and red circles, respectively.

(B) Supervised hierarchical clustering heatmap analysis based on the four DE genes discovered by DESeq2, samples and their respective group.

FIG. 7

A

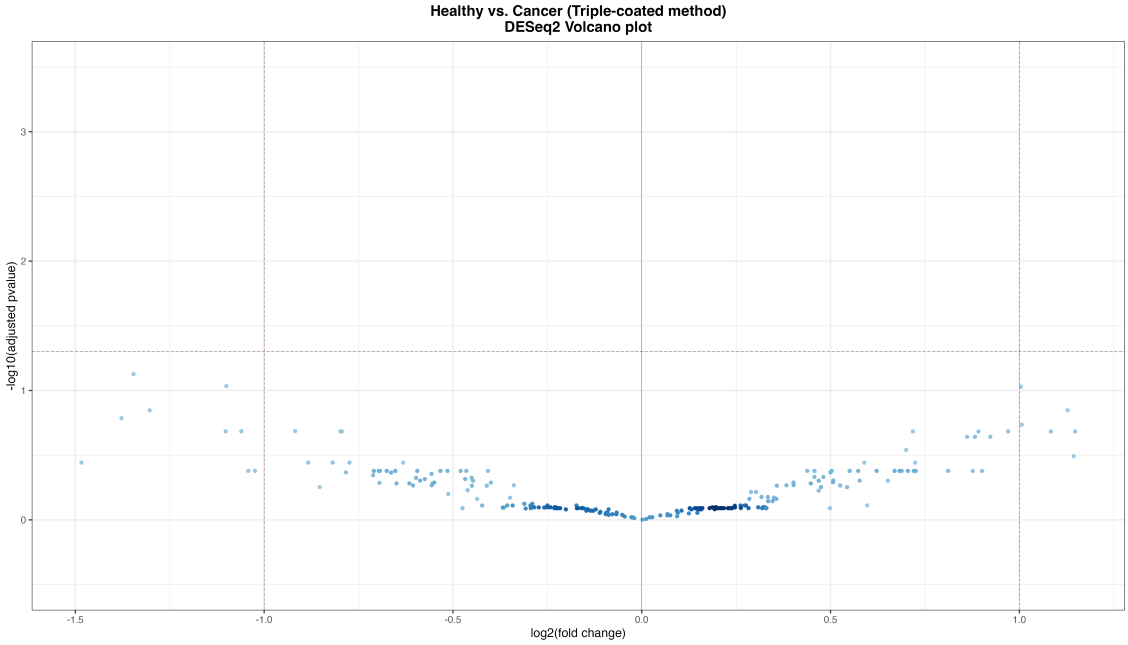

B

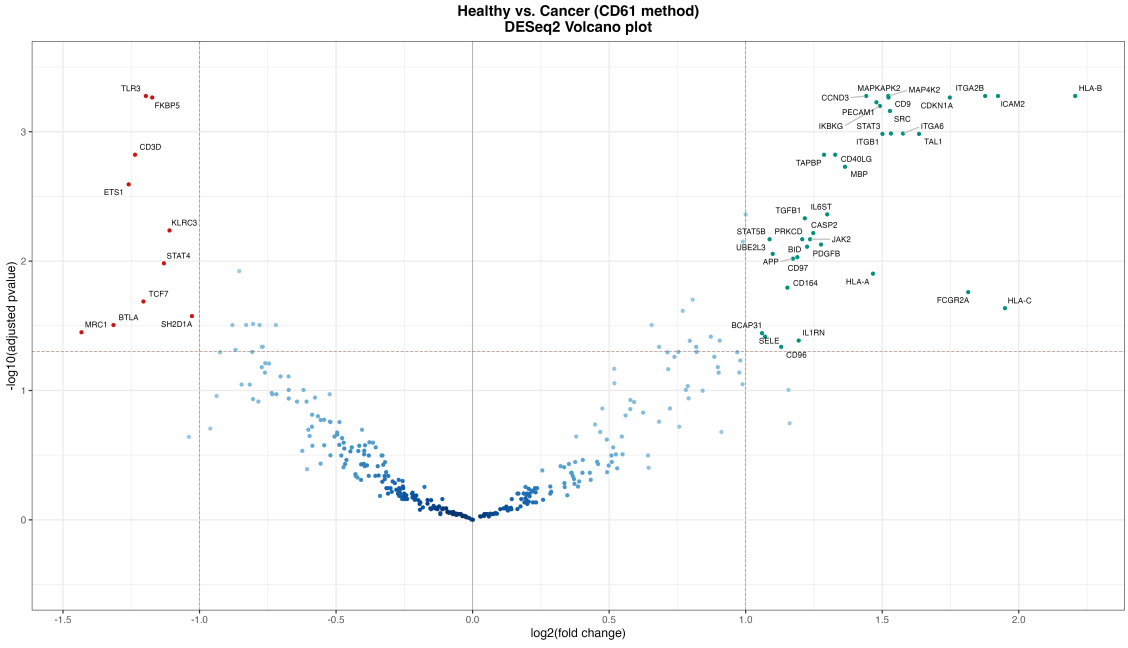

Figure 7. DE analysis by DESeq2 identified 47 DE genes between healthy and early-stage NSCLC cohorts, using platelet-derived EVs as biomarker source.

(A) Volcano plot showing that no DE genes were found between the two cohorts, based on the triple-coated EV dataset. Cutoffs were defined for adjusted pvalues (0.05, Y axis) and log2 fold change (2, X axis).

(B) Volcano plot showing DE genes between the two cohorts, based on the platelet-derived EV dataset. Cutoffs were defined for adjusted pvalues (0.05, Y axis) and log2 fold change (2, X axis). Upregulated genes and downregulated genes are depicted by green and red circles, respectively.

Discussion

In the present study, we thoroughly optimized a nanobead-based EV immunoaffinity capture strategy and demonstrate that distinct subpopulations can be efficiently isolated and selectively enriched, despite the complexity of IP matrices. Antibody-conjugated beads were chosen over streptavidin-coated ones as they allowed for superior EV recovery and purity with a simpler protocol, since bead coating steps were not required. Target EV subsets were also efficiently recovered through indirect IP markers, conferring more flexibility to antibody-conjugated beads, a hallmark characteristic of the streptavidin-biotin system. Routine laboratory fluorescence readouts, validated through ddPCR and nFCM, delivered precise estimations of IP recovery. Cryo-TEM observation of bead-EV complexes formed in various IP matrices evidenced that actual membranous particles were decorated with beads, without noticeable signs of contaminating particles. While measuring fluorescent spike recovery between simple and complex matrices, we realized how the surface properties of different EVs can greatly impact IP efficiency. Moreover, we verified that not only the EV phenotype, but also the composition of biological samples can shape how EVs are retrieved through affinity capture. Altogether, the nano-scale trinity formed between EVs, matrix components and affinity reagents, comprising all their complex interactions, determined the success of our IP experiments. We postulate that the same holds true under many other affinity-based EV enrichment conditions. The recovery of endogenous plasma EVs after pre-analytical treatments could be accurately quantified using fluorescently-tagged primary antibodies, which supported the suitability of this simple detection method. Finally, triple-coated anti-tetraspanin (CD9, CD63 and CD81) beads and anti-CD61 beads were applied for EV IP in merely 500µL of human plasma obtained from 14 healthy donors and 14 early-stage NSCLC patients. Gene expression profiling of CD9, CD63 or CD81+ and CD61+ (platelet-derived) EVs revealed that each subset carried unique mRNA pools, emphasizing the selectivity of our IP approach and the prevalent notion that EV subpopulations are highly heterogeneous. More importantly, we provided proof of principle for selective human EV enrichment strategies as valuable tools in a real-world clinical liquid biopsy context. In this study, platelet-derived EVs better grasped differences between the mRNA pool of healthy and early-stage NSCLC samples, when compared to the tetraspanin-positive EV subpopulation. We identified a relationship between 47 potential biomarkers for early tumour detection in platelet-derived EVs, while strikingly none could be found in the tetraspanin-positive subpopulation.

Platelets have been extensively studied for biomarker discovery and detection, as they quickly respond to inflammation and can engulf numerous biomolecules sustaining pathophysiological states. Due to the uptake of tumour-shed material, platelets transform into tumour-educated platelets (TEPs) and actively start favouring cancer progression through processes extensively reviewed elsewhere[71,72]. Platelet and TEP-derived EVs generate a positive feedback loop that amplifies platelet education and contributes to tumour growth. These EVs may also participate in metastatic processes as platelets do, however irrefutable evidence is still lacking[72–74]. Such ideas support the significance of platelet-derived EVs as valuable biomarker sources, which may actually be more enriched in disease-specific analytes than the actual platelets generating them.

The endpoint goal of our study lied in assembling a selective EV isolation approach, tailored to comply with ideal routine procedures required in clinical liquid biopsy environments. Realistically, it is extremely challenging to introduce new techniques into the clinic, as emphasized by Ignatiadis et al., who elegantly defined a roadmap for the translation of novel liquid biopsy assays into clinical practice[75]. Accordingly, we demonstrated the analytical validity and set off the clinical validation of our method, which simply required 500µL of minimally processed PFP, while IP reactions were completed within 1h. The superparamagnetic properties of beads can be leveraged for scalability and automation. Immunostaining is conducted directly on the bead-EV complex latched inside magnetized columns, which resulted in straightforward and reliable surface protein quantification, merely adding one extra hour to the protocol. It is important to stress that the detachment of immunocomplexes was not required, as MACS beads did not interfere with fluorescence measurements.

A similar bead-based MACS immunostaining protocol to profile EV surface markers has been developed[14]. Despite its convincing performance on the analysis of purified EVs, it cannot be directly applied in plasma samples. Moreover, this methodology relies on flow cytometry, which is not always straightforward, as instruments require precise optimization and frequent maintenance. Additional limitations stem from the size detection limit of conventional cytometers, which dictates that large size beads (4,8µm) must be used for EV immobilization before fluorescence measurements, rendering the assay semi-quantitative. Also, it is likely that the large MACSPlex beads employed in this assay are easily outperformed by their smaller MACS beads (50nm) counterpart[61], which were used in the present study. Our bulk fluorescence measurements obtained with a common plate reader provided the same kind of semi-quantitative information. We opted for direct (bead-EV complex) instead of indirect (IP flowthrough) IP readouts as the former was conceptually more solid and better represented actual EV recovery. Also, it could be applied regardless of the IP matrix or fluorescence of spiked EVs, and enabled in-column staining of the bead-EV complex.

One limitation in our experiments was the calculation of specificity. IP recovery always increased with the amount of spike when using specific antibodies against EV markers, while with negative control antibodies it remained relatively stable. Logically, the ratio between the fluorescent signal measured in negative controls and targets becomes smaller as the number of EV input increases and consequently, specificity will also indirectly increase. In other words, the higher is the EV input, the higher we can expect specificity to be. Moreover, since fluorescence does not vary linearly with quantity, this effect should ideally be accounted for. Therefore, we propose a less biased way to calculate specificity, based on the experiments depicted in Fig. 2, where we performed calibration curves for the fluorescence of NIR spikes. In this way, we could convert NIR S/N ratios in number of NIR EVs and were able to directly compare the number of particles recovered in both target and negative control beads, with respect to the initial particle number. However, this was only possible because the NIR dye was fed to cells, which released a population of 100% endogenously-stained EVs. Since exogenous CFSE labelling was conducted on previously purified EV samples, the protocol required dye removal steps, which may still leave traces of free dye that can skew fluorescence calibration curves. Thus, we avoided this approach when reporting data obtained using CFSE-stained EV spikes.

Instead, antibodies in excess could be efficiently washed off after in-column staining of the bead-EV complex, for which we determined a lowest limit of detection (LOD) in the order of 10^6 HT29 EVs upon anti-CD9-PE staining. Since PE is one of the brightest fluorophores available, it is unlikely that the LOD can be further extended by simply employing fluorescently-tagged primary antibodies. We want to underline that the LOD of this assay is surely influenced by the EV source and amount of target marker displayed, thus it should be experimentally confirmed in each particular setting. Spike detection after IP from plasma was accurate down to 10^7 EVs. Lower spike amounts resulted in unrealistic S/N ratios, indicating that in this scenario, co-precipitated plasma material impeded specific antibody staining. Incomplete upstream depletion of plasma EVs might be responsible for this phenomenon, while EV-associated proteins might also circulate as individual soluble markers in plasma, which could limit the detection of low abundance EV targets through single primary antibody staining. Smaller affinity reagents such as nanobodies could potentially improve detection of nanostructures retrieved from plasma.

Intriguingly, while experimenting with plasma from donor 6, we realized that anti-CD61 beads recovered more HEK293 spike than anti-CD9 beads. Our cell-derived EVs did not express CD61, suggesting that CD61-positive material captured from plasma mediated the co-IP of fluorescent spikes. We confirmed this by ddPCR, however the same effect could not be reproduced across plasma donors, hinting that potential matrix-dependant CD61-mediated EV co-IP interactions can only occur under certain circumstances. Integrins such as CD61 are fundamental regulators of cell communication, forming adhesive complexes that mediate extracellular interactions. They are usually found at the EV surface[23,76], therefore it is conceivable that plasma-derived EVs, together with their associated proteins, can sustain the co-IP of other EV

subpopulations. These events are related with an emerging concept in the EV field, named the EV protein corona, which comprises proteins that interact and associate at the surface of EVs[56,77–79]. The dynamic nature of the EV protein corona and our limited understanding of its implications make it difficult to propose regulators or mediators of these interactions. Still, our observation of spike co-IP through CD61 and the drop in platelet markers after plasma treatments to eliminate insoluble fibrinogen, suggest that integrins together with extracellular matrix proteins, such as CD61/CD41 (or integrin αIIbβ3) and fibrinogen, are surely potential candidates that will help in elucidating the extent of the plasma EV surface interactome. It is important to note that despite being an established cluster of differentiation of the platelet lineage, CD61 contributes to many additional functions and has been extensively implicated in cancer-promoting events, although further investigation is warranted before patients can benefit from CD61-targeted therapies[80].

The data depicted in Fig. 3C revealed to be quite surprising, especially when comparing the signal of both CFSE-stained spikes retrieved from the plasma of donors 5 and 7. The recovery of HT29 EVs from donor 7 plasma was 3-fold higher, however the same was not true for HEK293 EVs. Thus, we can conclude that our HT29 spike selectively interacted with certain matrix components present in the plasma of donors 5 and 7, which either hampered or boosted its recovery (as observed in Fig. 3B for HEK293), respectively, using triple-coated beads. As the recovery of HEK293 spike from both plasma matrices was equal, we can state that the specific HT29 EV surface marker profile was responsible for this effect. It would be crucial to conduct systematic studies aimed at unveiling key surface regulators that mediate interactions between EVs and plasma matrix components, in order to improve and take full advantage of selective affinity-based EV isolation procedures. Notwithstanding, we also demonstrated that plasma from each single individual can differentially impact the success of EV IP. Overall, this can be attributed to the wide variation in biological sample composition. Ultimately, we want to underline that both target EVs and the matrix they are transported in are critical factors to account for.

We conducted plasma pre-analytical treatments with two fundamental goals in mind: Primarily, not only to prove the specificity of the IP technique but also of the bead-based sandwich immunoassay using fluorescently-labelled primary antibodies. Secondarily, to understand if simplification of the plasma matrix would increase endogenous plasma EV recovery, which in this case did not occur. In line with this finding, neither diluting the plasma matrix and its components in PBS result in increased spike recovery (Sup. Fig.2B). However, due to our limited experiments, it is difficult to draw strong conclusions on this frontier and to claim whether or not pre-IP plasma processing would overall improve recovery. It is possible that thoroughly optimized pre-analytical parameters, from blood collection to EV IP, may benefit the affinity capture of at least some specific plasma-derived EVs subpopulations. Nonetheless, biological variability is an extremely difficult factor to control, hence it can be challenging to apply pre-analytical protocols that equally fit all patients. Further research could shed light on the fundamental plasma components hampering EV IP, contributing to minimize or standardize pre-analytical biases. Despite appraising pre-analytical challenges and the impact of complex matrix effects on endpoint biomarker detection, we uphold that our method was still robust enough to extract clinically relevant information from cancer patient EV samples, using as little as 500µL of plasma.

The 47 DE genes identified after profiling platelet-derived EVs from the healthy and early-stage NSCLC pilot cohorts, displayed distinct expression patterns among samples. We found pronounced cancer-indicative profiles in stage II/III patient samples, which were reflected to a certain extent by some stage I NSCLC tumours, confirming that signatures of very early disease onset could be identified (data not shown). It is possible that not all patients might have had a detectable disease burden at early cancer development stages or instead, cancer could have progressed during the time elapsed post-prospective blood collection, until medical diagnosis. It will be critical to exclude the influence of pre-analytical and analytical processes on EV expression profiles to assure that true biological variation is observed. Due to the small size of our clinical cohorts, we took a conservative approach in this proof of principle study by simply interpreting these hints

as remote indications, which will be further addressed in an ongoing, extended clinical prospective cohort study. Prospective studies aiming to pinpoint the time frames at which diseased plasma-derived EV profiles become detectable in different individuals, while closely monitoring tumour development and progression would be extremely valuable. Still, for broad clinical application of this and other novel liquid biopsy strategies it is important to ensure that pre-analytical factors do not hamper early disease onset detection and that cancer-indicating signatures are not extensively shared with other pathologies.

Lastly, we hope to encourage more research aimed at dissecting the complex interactions between EVs, matrix and affinity reagents. EVs are pivotal biomarker vaults that can be found across easily obtainable biofluids. However, identifying and retrieving the most relevant subpopulations remains a central challenge in the field. As established by many exceptional reports during the last two decades, liquid biopsies hold the key for next-generation diagnostics and precision medicine. Ground-breaking work towards clinical implementation will propel the widespread dissemination of liquid biopsy-based tools, which will help to routinely guide medical doctors. Scalable and automatable procedures are essential to devise truly translational solutions, which meet the standards and expectations of clinical units.

Acknowledgements

We would like to thank Dr. Eugenio Paccagnini (Department of Life Sciences, University of Siena, Italy) for all the great support with Cryo-TEM experiments. We also thank C. Pedraz, J. Bracht and A. Küçükosmanoğlu for valuable work discussions and guidance.

Authorship

D.F. and N.Z. designed the study. D.F. conducted the main experimental work and initiated the manuscript. S.G. and M.H. were responsible for all the bioinformatics analysis. A.G.C. and M.A.M.V provided clinical plasma samples, facilities and instruments for the proof of principle study. A.G.C. supported Nanostring experiments. N.Z. supervised the study. All authors contributed to the elaboration of the manuscript, read and approved its final version.

Funding

This research has received funding from the European Union's Horizon 2020 research and innovation programme under the Marie Skłodowska-Curie grant agreements No. 765492 and FET Proactive grant agreement No. 952183.

Declaration of Interest Statement

The authors declare no conflicts of interest.

Authors' information

Researcher IDs (ORCID)

D.F. - 0000-0003-2732-477X

A.G.C. - 0000-0003-2575-1225

M.H. - 0000-0003-2248-3114

M.A.M.V - 0000-0001-8866-9881

References

1. Lobb, R. J. *et al.* Optimized exosome isolation protocol for cell culture supernatant and human plasma. *J. Extracell. Vesicles* **4**, 27031 (2015).
2. Van Deun, J. *et al.* The impact of disparate isolation methods for extracellular vesicles on downstream RNA profiling. *J. Extracell. Vesicles* **3**, 24858 (2014).
3. Mol, E. A., Goumans, M.-J., Doevendans, P. A., Sluijter, J. P. G. & Vader, P. Higher functionality of extracellular vesicles isolated using size-exclusion chromatography compared to ultracentrifugation. *Nanomedicine Nanotechnol. Biol. Med.* **13**, 2061–2065 (2017).
4. Vergauwen, G. *et al.* Confounding factors of ultrafiltration and protein analysis in extracellular vesicle research. *Sci. Rep.* **7**, 2704 (2017).
5. Johnsen, K. B., Gudbergsson, J. M., Andresen, T. L. & Simonsen, J. B. What is the blood concentration of extracellular vesicles? Implications for the use of extracellular vesicles as blood-borne biomarkers of cancer. *Biochim. Biophys. Acta BBA - Rev. Cancer* **1871**, 109–116 (2019).
6. Kırbaş, O. K. *et al.* Optimized Isolation of Extracellular Vesicles From Various Organic Sources Using Aqueous Two-Phase System. *Sci. Rep.* **9**, 19159 (2019).
7. Koster, H. J. *et al.* Surface enhanced Raman scattering of extracellular vesicles for cancer diagnostics despite isolation dependent lipoprotein contamination. *Nanoscale* **13**, 14760–14776 (2021).
8. Maia, J. *et al.* Employing Flow Cytometry to Extracellular Vesicles Sample Microvolume Analysis and Quality Control. *Front. Cell Dev. Biol.* **8**, 1165 (2020).
9. Tian, Y. *et al.* Quality and efficiency assessment of six extracellular vesicle isolation methods by nano-flow cytometry. *J. Extracell. Vesicles* **9**, 1697028 (2020).
10. Takov, K., Yellon, D. M. & Davidson, S. M. Comparison of small extracellular vesicles isolated from plasma by ultracentrifugation or size-exclusion chromatography: yield, purity and functional potential. *J. Extracell. Vesicles* **8**, 1560809 (2019).
11. McNamara, R. P. *et al.* Large-scale, cross-flow based isolation of highly pure and endocytosis-competent extracellular vesicles. *J. Extracell. Vesicles* **7**, 1541396 (2018).
12. Théry, C., Amigorena, S., Raposo, G. & Clayton, A. Isolation and Characterization of Exosomes from Cell Culture Supernatants and Biological Fluids. *Curr. Protoc. Cell Biol.* **30**, 3.22.1-3.22.29 (2006).
13. Böing, A. N. *et al.* Single-step isolation of extracellular vesicles by size-exclusion chromatography. *J. Extracell. Vesicles* **3**, 23430 (2014).
14. Wiklander, O. P. B. *et al.* Systematic Methodological Evaluation of a Multiplex Bead-Based Flow Cytometry Assay for Detection of Extracellular Vesicle Surface Signatures. *Front. Immunol.* **9**, 1326 (2018).
15. Fortunato, D. *et al.* Opportunities and Pitfalls of Fluorescent Labeling Methodologies for Extracellular Vesicle Profiling on High-Resolution Single-Particle Platforms. *Int. J. Mol. Sci.* **22**, 10510 (2021).
16. Anderson, N. L. *et al.* The human plasma proteome: a nonredundant list developed by combination of four separate sources. *Mol. Cell. Proteomics MCP* **3**, 311–326 (2004).
17. Anderson, N. L. & Anderson, N. G. The Human Plasma Proteome: History, Character, and Diagnostic Prospects *. *Mol. Cell. Proteomics* **1**, 845–867 (2002).
18. Muller, L., Hong, C.-S., Stolz, D. B., Watkins, S. C. & Whiteside, T. L. Isolation of biologically-active exosomes from human plasma. *J. Immunol. Methods* **411**, 55–65 (2014).
19. Simonsen, J. B. What Are We Looking At? Extracellular Vesicles, Lipoproteins, or Both? *Circ. Res.* **121**, 920–922 (2017).

20. Zhang, X., Borg, E. G. F., Liaci, A. M., Vos, H. R. & Stoorvogel, W. A novel three step protocol to isolate extracellular vesicles from plasma or cell culture medium with both high yield and purity. *J. Extracell. Vesicles* **9**, 1791450 (2020).

21. Karimi, N. *et al.* Detailed analysis of the plasma extracellular vesicle proteome after separation from lipoproteins. *Cell. Mol. Life Sci.* **75**, 2873–2886 (2018).

22. Peinado, H. *et al.* Melanoma exosomes educate bone marrow progenitor cells toward a pro-metastatic phenotype through MET. *Nat. Med.* **18**, 883–891 (2012).

23. Hoshino, A. *et al.* Tumour exosome integrins determine organotropic metastasis. *Nature* **527**, 329–335 (2015).

24. Han, Y., Ren, J., Bai, Y., Pei, X. & Han, Y. Exosomes from hypoxia-treated human adipose-derived mesenchymal stem cells enhance angiogenesis through VEGF/VEGF-R. *Int. J. Biochem. Cell Biol.* **109**, 59–68 (2019).

25. Chen, G. *et al.* Exosomal PD-L1 contributes to immunosuppression and is associated with anti-PD-1 response. *Nature* **560**, 382–386 (2018).

26. Pucci, F. *et al.* SCS macrophages suppress melanoma by restricting tumor-derived vesicle-B cell interactions. *Science* **352**, 242–246 (2016).

27. Poggio, M. *et al.* Suppression of Exosomal PD-L1 Induces Systemic Anti-tumor Immunity and Memory. *Cell* **177**, 414-427.e13 (2019).

28. Sheehan, C. & D'Souza-Schorey, C. Tumor-derived extracellular vesicles: molecular parcels that enable regulation of the immune response in cancer. *J. Cell Sci.* **132**, jcs235085 (2019).

29. Takahashi, A. *et al.* Exosomes maintain cellular homeostasis by excreting harmful DNA from cells. *Nat. Commun.* **8**, 15287 (2017).

30. Capello, M. *et al.* Exosomes harbor B cell targets in pancreatic adenocarcinoma and exert decoy function against complement-mediated cytotoxicity. *Nat. Commun.* **10**, 254 (2019).

31. Zomer, A. *et al.* In Vivo Imaging Reveals Extracellular Vesicle-Mediated Phenocopying of Metastatic Behavior. *Cell* **161**, 1046–1057 (2015).

32. Skog, J. *et al.* Glioblastoma microvesicles transport RNA and proteins that promote tumour growth and provide diagnostic biomarkers. *Nat. Cell Biol.* **10**, 1470–1476 (2008).

33. Brock, G., Castellanos-Rizaldos, E., Hu, L., Coticchia, C. & Skog, J. Liquid biopsy for cancer screening, patient stratification and monitoring. *Transl. Cancer Res.* **4**, (2015).

34. Heitzer, E., Perakis, S., Geigl, J. B. & Speicher, M. R. The potential of liquid biopsies for the early detection of cancer. *Npj Precis. Oncol.* **1**, 1–9 (2017).

35. Bracht, J. W. P., Mayo-de-las-Casas, C., Berenguer, J., Karachaliou, N. & Rosell, R. The Present and Future of Liquid Biopsies in Non-Small Cell Lung Cancer: Combining Four Biosources for Diagnosis, Prognosis, Prediction, and Disease Monitoring. *Curr. Oncol. Rep.* **20**, 70 (2018).

36. Zhang, H. *et al.* Identification of distinct nanoparticles and subsets of extracellular vesicles by asymmetric flow field-flow fractionation. *Nat. Cell Biol.* **20**, 332–343 (2018).

37. Johansson, S. M., Admyre, C., Scheynius, A. & Gabrielsson, S. Different types of in vitro generated human monocyte-derived dendritic cells release exosomes with distinct phenotypes. *Immunology* **123**, 491–499 (2008).

38. Willms, E. *et al.* Cells release subpopulations of exosomes with distinct molecular and biological properties. *Sci. Rep.* **6**, 22519 (2016).

39. Bobrie, A., Colombo, M., Krumeich, S., Raposo, G. & Théry, C. Diverse subpopulations of vesicles secreted by different intracellular mechanisms are present in exosome preparations obtained by differential ultracentrifugation. *J. Extracell. Vesicles* **1**, 18397 (2012).

40. Kowal, J. *et al.* Proteomic comparison defines novel markers to characterize heterogeneous populations of extracellular vesicle subtypes. *Proc. Natl. Acad. Sci.* **113**, E968–E977 (2016).

41. Willms, E., Cabañas, C., Mäger, I., Wood, M. J. A. & Vader, P. Extracellular Vesicle Heterogeneity: Subpopulations, Isolation Techniques, and Diverse Functions in Cancer Progression. *Front. Immunol.* **9**, 738 (2018).

42. Bastos-Amador, P. *et al.* Proteomic analysis of microvesicles from plasma of healthy donors reveals high individual variability. *J. Proteomics* **75**, 3574–3584 (2012).

43. Kanwar, S. S., Dunlay, C. J., Simeone, D. M. & Nagrath, S. Microfluidic device (ExoChip) for on-chip isolation, quantification and characterization of circulating exosomes. *Lab. Chip* **14**, 1891–1900 (2014).

44. Im, H. *et al.* Label-free detection and molecular profiling of exosomes with a nano-plasmonic sensor. *Nat. Biotechnol.* **32**, 490–495 (2014).

45. Jørgensen, M. *et al.* Extracellular Vesicle (EV) Array: microarray capturing of exosomes and other extracellular vesicles for multiplexed phenotyping. *J. Extracell. Vesicles* **2**, 20920 (2013).

46. Jakobsen, K. R. *et al.* Exosomal proteins as potential diagnostic markers in advanced non-small cell lung carcinoma. *J. Extracell. Vesicles* **4**, 26659 (2015).

47. Zhao, Z., Yang, Y., Zeng, Y. & He, M. A microfluidic ExoSearch chip for multiplexed exosome detection towards blood-based ovarian cancer diagnosis. *Lab. Chip* **16**, 489–496 (2016).

48. Clayton, A. *et al.* Analysis of antigen presenting cell derived exosomes, based on immuno-magnetic isolation and flow cytometry. *J. Immunol. Methods* **247**, 163–174 (2001).

49. Yoshioka, Y. *et al.* Ultra-sensitive liquid biopsy of circulating extracellular vesicles using ExoScreen. *Nat. Commun.* **5**, 3591 (2014).

50. Tauro, B. J. *et al.* Two Distinct Populations of Exosomes Are Released from LIM1863 Colon Carcinoma Cell-derived Organoids*. *Mol. Cell. Proteomics* **12**, 587–598 (2013).

51. Chen, S., Shiesh, S.-C., Lee, G.-B. & Chen, C. Two-step magnetic bead-based (2MBB) techniques for immunocapture of extracellular vesicles and quantification of microRNAs for cardiovascular diseases: A pilot study. *PLOS ONE* **15**, e0229610 (2020).

52. Park, J. *et al.* An integrated magneto-electrochemical device for the rapid profiling of tumour extracellular vesicles from blood plasma. *Nat. Biomed. Eng.* **5**, 678–689 (2021).

53. Wang, S. *et al.* Aptasensor with Expanded Nucleotide Using DNA Nanotetrahedra for Electrochemical Detection of Cancerous Exosomes. *ACS Nano* **11**, 3943–3949 (2017).

54. Wang, Y.-M. *et al.* Enhancement of the Intrinsic Peroxidase-Like Activity of Graphitic Carbon Nitride Nanosheets by ssDNAs and Its Application for Detection of Exosomes. *Anal. Chem.* **89**, 12327–12333 (2017).

55. Bijnsdorp, I. V. *et al.* Feasibility of urinary extracellular vesicle proteome profiling using a robust and simple, clinically applicable isolation method. *J. Extracell. Vesicles* **6**, 1313091 (2017).

56. Buzás, E. I., Tóth, E. Á., Sódar, B. W. & Szabó-Taylor, K. É. Molecular interactions at the surface of extracellular vesicles. *Semin. Immunopathol.* **40**, 453–464 (2018).

57. Ramirez, M. I. *et al.* Technical challenges of working with extracellular vesicles. *Nanoscale* **10**, 881–906 (2018).

58. Monopoli, M. P. *et al.* Endogenous exosome labelling with an amphiphilic NIR-fluorescent probe. *Chem. Commun.* **54**, 7219–7222 (2018).

59. van der Pol, E., van Gemert, M. J. C., Sturk, A., Nieuwland, R. & van Leeuwen, T. G. Single vs. swarm detection of microparticles and exosomes by flow cytometry. *J. Thromb. Haemost. JTH* **10**, 919–930 (2012).

60. Libregts, S. F. W. M., Arkesteijn, G. J. A., Németh, A., Nolte-'t Hoen, E. N. M. & Wauben, M. H. M. Flow cytometric analysis of extracellular vesicle subsets in plasma: impact of swarm by particles of non-interest. *J. Thromb. Haemost.* **16**, 1423–1436 (2018).

61. Miltenyi, S., Müller, W., Weichel, W. & Radbruch, A. High gradient magnetic cell separation with MACS. *Cytometry* **11**, 231–238 (1990).

62. Puertas, S. *et al.* Designing novel nano-immunoassays: antibody orientation versus sensitivity. *J. Phys. D: Appl. Phys.* **43**, 474012 (2010).

63. Frangioni, J. V. In vivo near-infrared fluorescence imaging. *Curr. Opin. Chem. Biol.* **7**, 626–634 (2003).

64. Weissleder, R. A clearer vision for in vivo imaging. *Nat. Biotechnol.* **19**, 316–317 (2001).

65. Smith, A. M., Mancini, M. C. & Nie, S. Second window for in vivo imaging. *Nat. Nanotechnol.* **4**, 710–711 (2009).

66. Jennings, L. K. & Phillips, D. R. Purification of glycoproteins IIb and III from human platelet plasma membranes and characterization of a calcium-dependent glycoprotein IIb-III complex. *J. Biol. Chem.* **257**, 10458–10466 (1982).

67. Phillips, D., Charo, I., Parise, L. & Fitzgerald, L. The platelet membrane glycoprotein IIb-IIIa complex. *Blood* **71**, 831–843 (1988).

68. Millar, H. R., Simpson, J. G. & Stalker, A. L. An evaluation of the heat precipitation method for plasma fibrinogen estimation. *J. Clin. Pathol.* **24**, 827–830 (1971).

69. Houssein, I., Wilcox, H. & Barron, J. Effect of heat treatment on results for biochemical analysis of plasma and serum. *Clin. Chem.* **31**, 2028–2030 (1985).

70. Weisel, J. W., Nagaswami, C., Vilaire, G. & Bennett, J. S. Examination of the platelet membrane glycoprotein IIb-IIIa complex and its interaction with fibrinogen and other ligands by electron microscopy. *J. Biol. Chem.* **267**, 16637–16643 (1992).

71. Best, M. G., Wesseling, P. & Wurdinger, T. Tumor-Educated Platelets as a Noninvasive Biomarker Source for Cancer Detection and Progression Monitoring. *Cancer Res.* **78**, 3407–3412 (2018).

72. Antunes-Ferreira, M., Koppers-Lalic, D. & Würdinger, T. Circulating platelets as liquid biopsy sources for cancer detection. *Mol. Oncol.* **15**, 1727–1743 (2021).

73. Lazar, S. & Goldfinger, L. E. Platelets and extracellular vesicles and their cross talk with cancer. *Blood* **137**, 3192–3200 (2021).

74. Nazari, M., Javandoost, E., Talebi, M., Movassaghpour, A. & Soleimani, M. Platelet Microparticle Controversial Role in Cancer. *Adv. Pharm. Bull.* **11**, 39–55 (2021).

75. Ignatiadis, M., Sledge, G. W. & Jeffrey, S. S. Liquid biopsy enters the clinic — implementation issues and future challenges. *Nat. Rev. Clin. Oncol.* **18**, 297–312 (2021).

76. Fuentes, P. *et al.* ITGB3-mediated uptake of small extracellular vesicles facilitates intercellular communication in breast cancer cells. *Nat. Commun.* **11**, 4261 (2020).

77. Tóth, E. Á. *et al.* Formation of a protein corona on the surface of extracellular vesicles in blood plasma. *J. Extracell. Vesicles* **10**, e12140 (2021).

78. Palviainen, M. *et al.* Extracellular vesicles from human plasma and serum are carriers of extravesicular cargo—Implications for biomarker discovery. *PLOS ONE* **15**, e0236439 (2020).

79. Skliar, M. *et al.* Membrane proteins significantly restrict exosome mobility. *Biochem. Biophys. Res. Commun.* **501**, 1055–1059 (2018).

80. Zhu, C. *et al.* ITGB3/CD61: a hub modulator and target in the tumor microenvironment. *Am. J. Transl. Res.* **11**, 7195–7208 (2019).

Supplementary Material

Supplementary Table 1

Quantification of bead input and EV spikes used across IP experiments. We assured beads always exceeded the number of EVs, but also avoided an overabundance of the former.

Figure	Beads	Target	Input (particle number)
1A	MACS-STV	CD9	1,84E+09
		ISO	1,46E+09
	MACS	CD9	5,50E+09
		CD61	2,46E+09
	Spike: HEK293-CFSE		5,15E+08
1C	MACS-STV	CD9	1,61E+09
		ISO	1,18E+09
	MACS	CD9	5,50E+09
		CD61	2,46E+09
	Spike: HEK293-CFSE		3,76E+08
1E	MACS	CD9	6,05E+09
		PE	6,75E+09
	Spike: HEK293-CFSE		4,91E+08
2B	MACS	CD9	2,12E+10
		PE	3,27E+10
	Spike: 22RV1-NIR		2,82E+08
2C	MACS	CD9	2,12E+10
		PE	3,27E+10
	Spike: 22RV1-NIR + CD9-PE		7,86E+07
3A	MACS CD9 + CD63 + CD81		1,42E+10
	Spike: 22RV1-NIR		1,83E+08
	Spike: HT29-CFSE		5,01E+08
3B	MACS CD9 + CD63 + CD81		1,42E+10
	Spike: HT29-CFSE		2,00E+08
	Spike: HEK293-CFSE		2,00E+08
	Spike: A549-CFSE		2,00E+08
3C	MACS CD9 + CD63 + CD81		1,42E+10
	Spike: HEK293-CFSE		4,00E+08
	Spike: HT29-CFSE		4,00E+08

SUP. FIG. 1

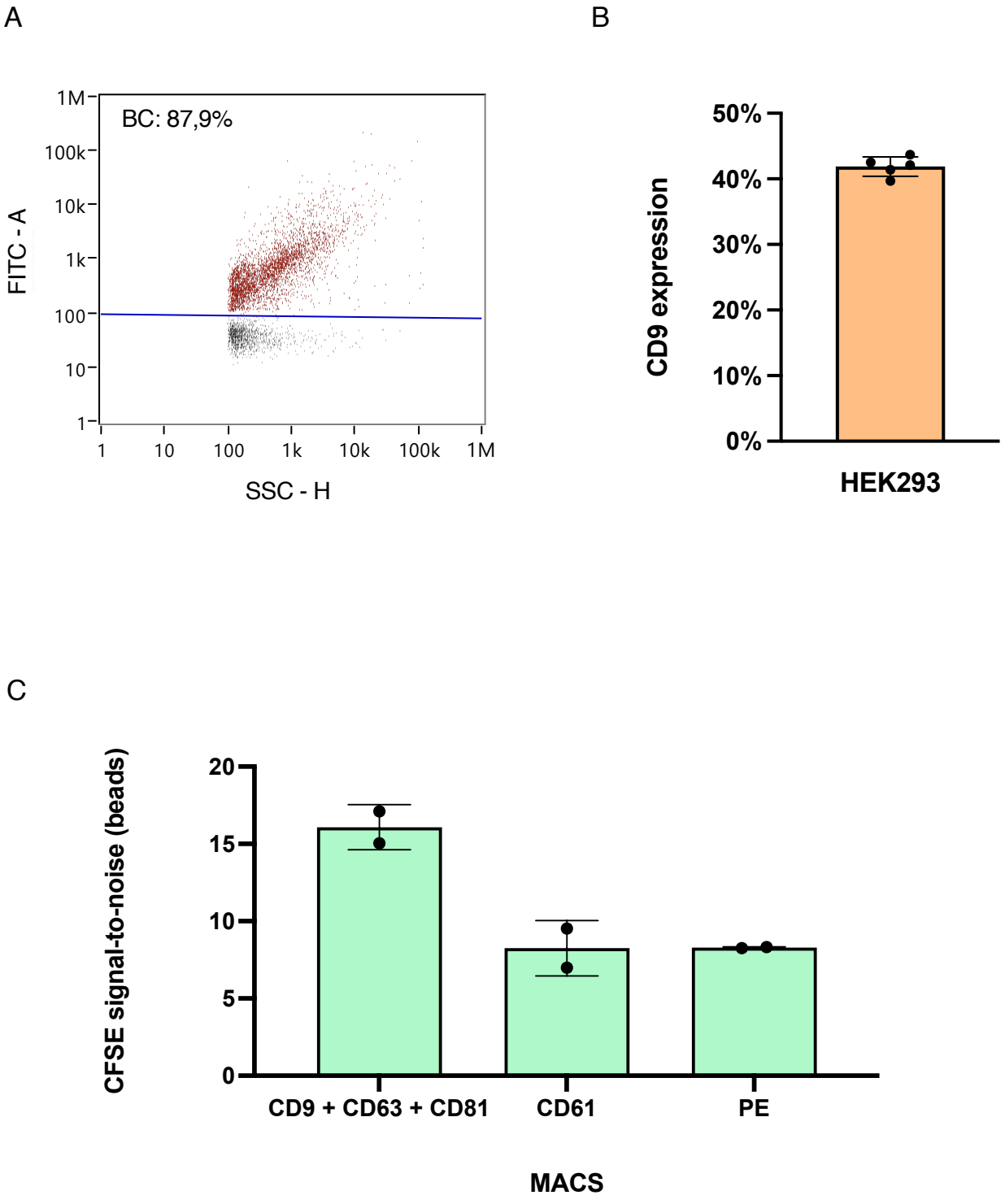

Supplementary Figure 1

(A) Representative nFCM dot plot, showing a single-particle quantification of HEK293 EVs after CFSE staining. After background correction (BC), we determined that nearly 88% of EVs incorporated the dye.

(B) CD9 expression was determined by labelling HEK293 EVs with CD9-PE. Five independent experiments were plotted, resulting in a mean value of 42%.

(C) HEK293-CFSE were spiked in plasma (donor 7) and IP conducted with triple-coated, anti-CD61 and anti-PE beads. Experiment performed in duplicate.

SUP. FIG. 2

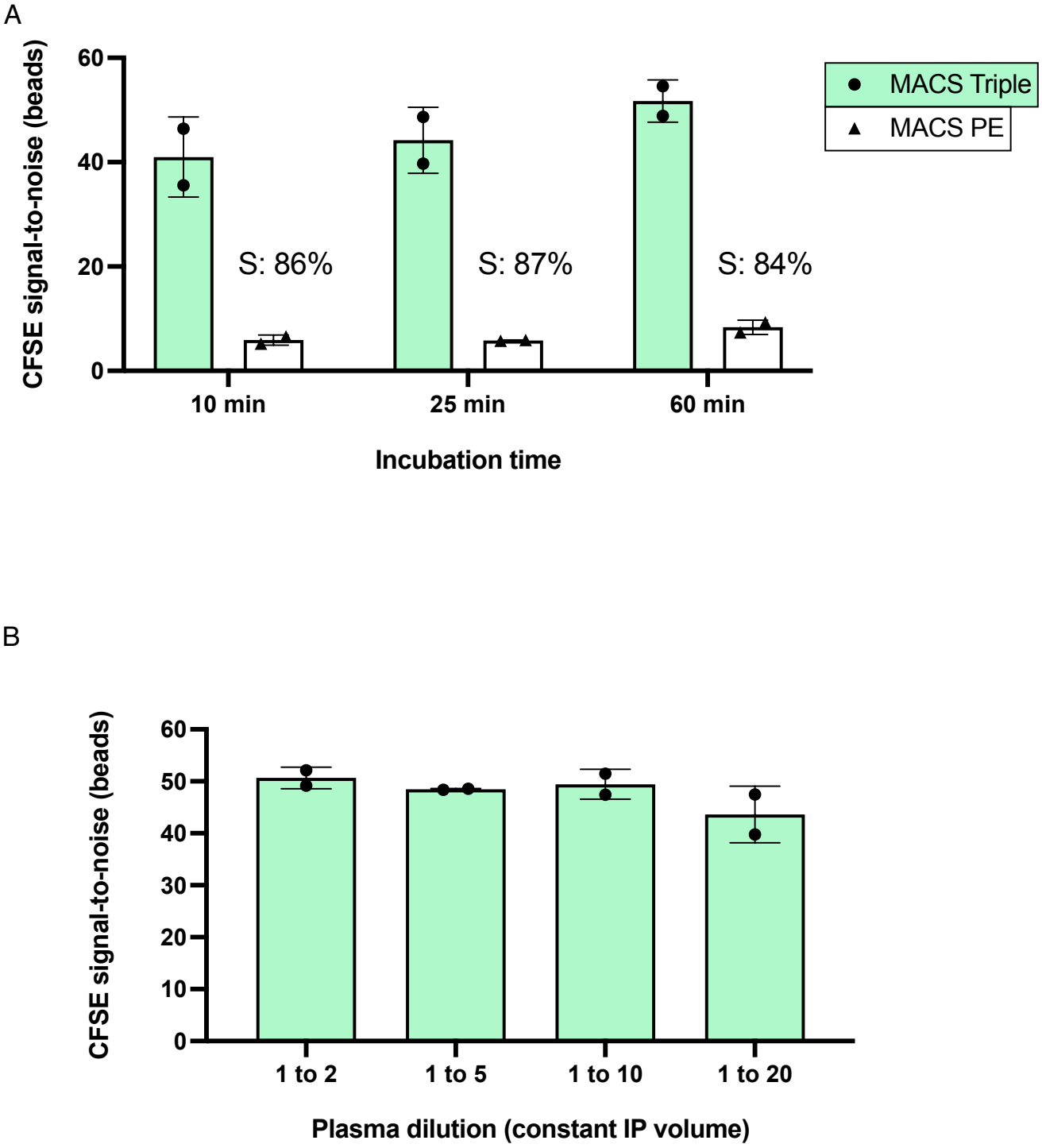

Supplementary Figure 2

(A) Triple-coated or anti-PE beads were incubated for 10, 25 or 60 min in plasma (donor 6) spiked with HT29-CFSE EVs. Fluorescence signals were read on beads and specificity (S) determined. Highest S/N ratios were obtained at 60min. Experiment performed in duplicate.

(B) HT29-CFSE EVs were spiked in plasma (donor 6) diluted 1:2, 1:5, 1:10 or 1:20 with PBS, whilst maintaining a constant volume for IP with triple-coated beads. S/N ratios indicated that a similar recovery was achieved across dilutions. Experiment performed in duplicate.

Sup. Fig 3

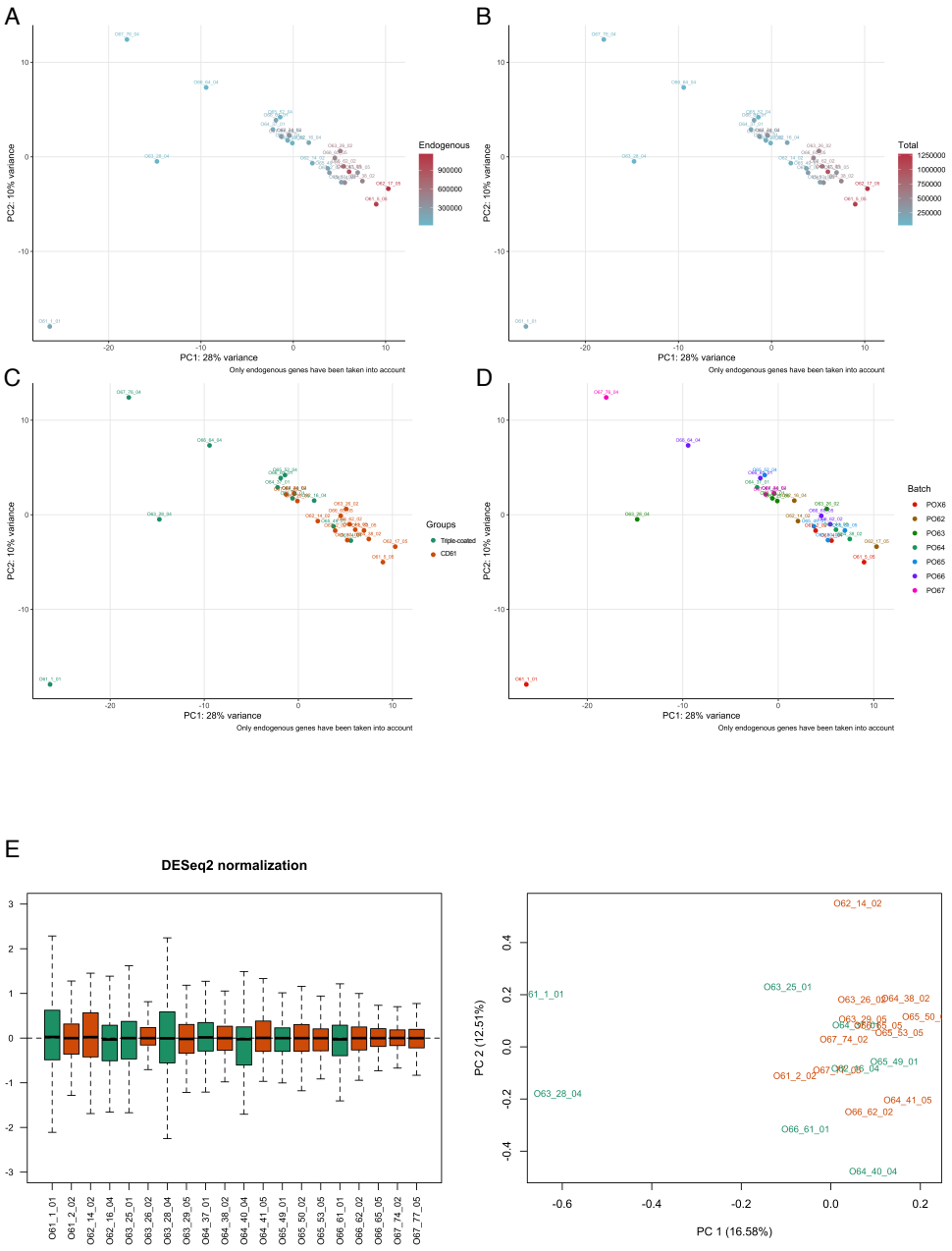

Supplementary Figure 3. mRNA profiles of CD61+ and CD9, CD63 or CD81+ EVs obtained from healthy donor plasma: exploratory data analysis and normalization

(A to D) Principal component analysis (PCA) was performed on unnormalized gene counts for exploratory data analysis. Principal components PC1 and PC2 are plotted on the X and Y axis, respectively. Different variables are evidenced:

(A) Gene counts excluding internally-defined nCounter control genes,

(B) Total read count per sample,

(C) Sample groups, which in this case represented the antibodies immobilized on IP beads. Triple-coated (CD9, CD63 and CD81) or CD61-coated beads,

(D) Due to a maximum number of 12 slots per nCounter experiment, samples were processed in different batches. Each batch represents one individual nCounter run.

(E) Relative log expression (RLE) plots for visualization of the normalization performance with DESeq2 (left). Normalized count data was projected on PC1 and PC2 after PCA (right). Triple-coated and CD61 samples are represented in green and orange, respectively.

SUP. FIG. 4

A

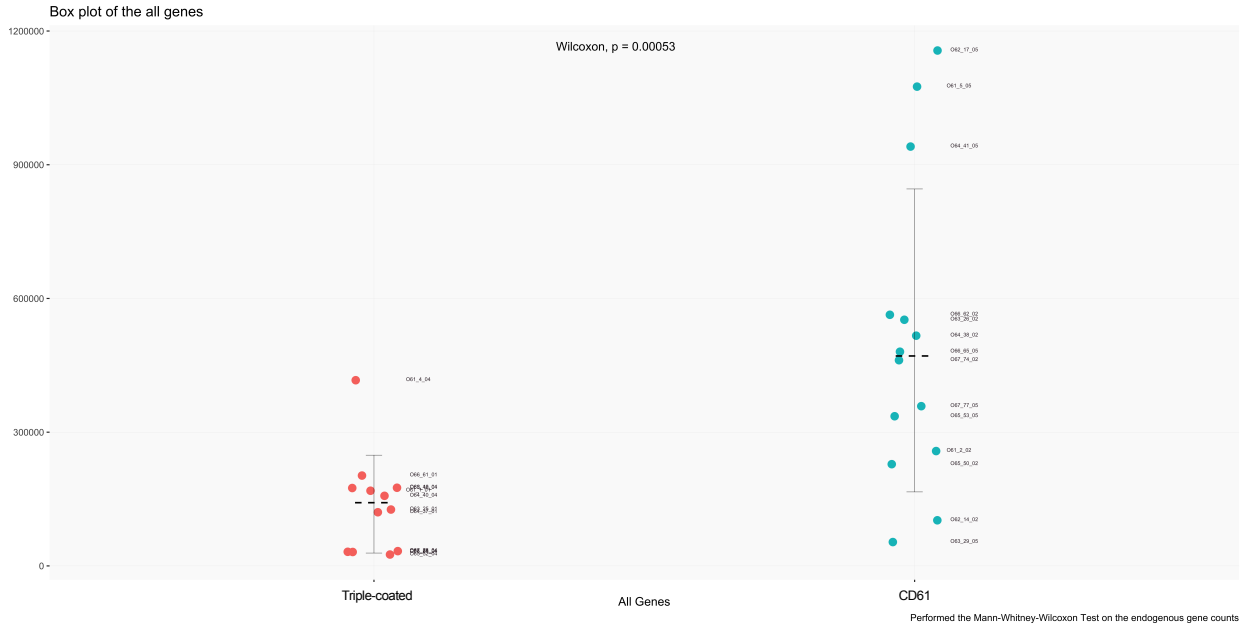

B

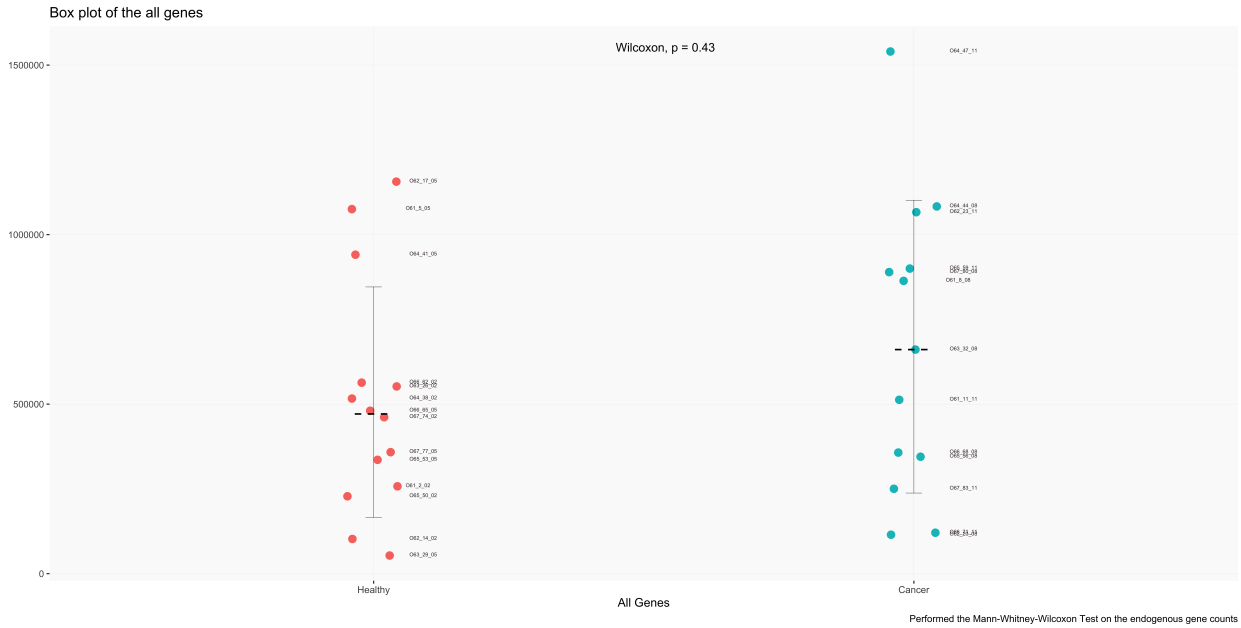

Supplementary Figure 4.

(A) Box plot evidencing raw counts obtained from healthy donor EV samples using both triple-coated or CD61 beads. Statistical analysis demonstrated a statistically significant difference between groups (p = 0.00053)

(B) Box plot evidencing raw counts obtained from healthy donor and patient EV samples using CD61 beads. No statistically significant difference could be found between groups (p = 0.43)

SUP. FIG. 5

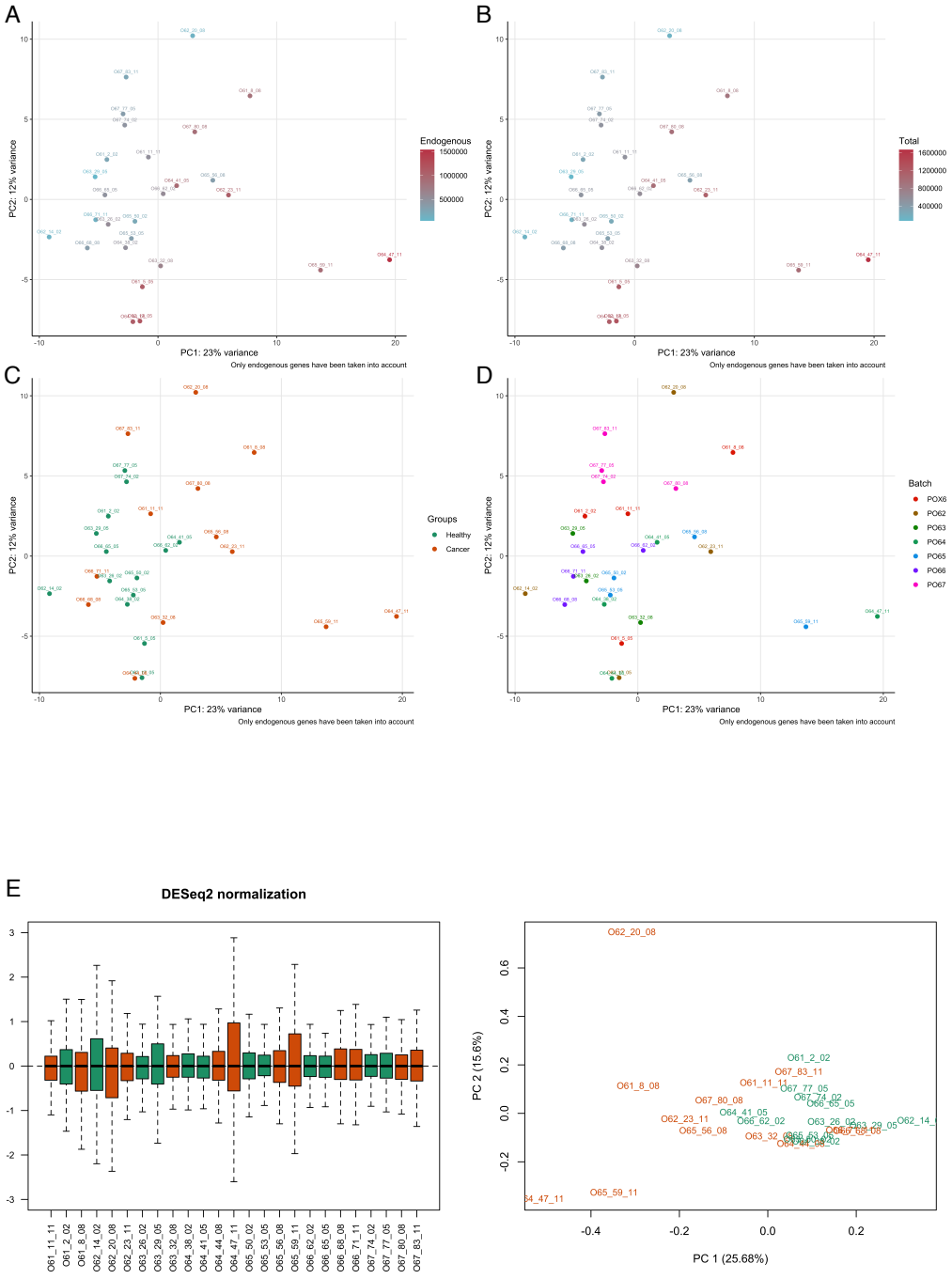

Supplementary Figure 5. EDA and normalization of gene expression data comparing two platelet-derived EV datasets obtained from healthy donors and early-stage NSCLC patients

(A to D) Principal component analysis (PCA) was performed on unnormalized gene counts for exploratory data analysis. Principal components PC1 and PC2 are plotted on the X and Y axis, respectively. Different variables are evidenced:

(A) Gene counts excluding internally-defined nCounter control genes,

(B) Total read count per sample,

(C) Sample groups representing the two cohorts compared, healthy donors vs. early-stage NSCLC,

(D) Due to a maximum number of 12 slots per nCounter experiment, samples were processed in different batches. Each batch represents one individual nCounter run.

(E) Relative log expression (RLE) plots for visualization of the normalization performance with DESeq2 (left). Normalized count data was projected on PC1 and PC2 after PCA (right). Healthy donor and early-stage NSCLC patient samples are represented in green and orange, respectivel

General Discussion

This general discussion aims to provide a broader view of the work herein reported, and to confront the main hurdles encountered throughout. As each manuscript presented in the results section features its own detailed discussion, for the sake of conciseness redundancy will be avoided. Nonetheless, central topics that might have been mentioned before will be further addressed and elaborated upon, in light of the experience acquired during the progression of this PhD project encompassing current perspectives, needs and future directions of the liquid biopsies and EV fields.

Part 1: Single vesicle analysis

The first established premise was: in order to characterize specific EV subsets, there is an absolute need for a technique that profiles each single particle contained within samples, essentially a flow cytometer suited for nanoparticle analysis. Flow cytometers have been around for a while and have become a quite solid and well-established multiparametric technique, both in research and clinical laboratories[156–158]. However, the same is not true for single nanoparticle profiling platforms. In fact, such platforms are quite sought after in the EV field, but it was only in the last decade that some technological solutions rose up to the expectations of attentive researchers[159–165].

Current views in EV research suggest that each single EV produced by one single cell is not entirely equal to another EV produced by the same cell, even though they might have been concomitantly generated or the pathways employed for their formation exactly the same[153]. Furthermore, considering that EV preparations from cell cultures are the product of millions of cells, the extent of EV heterogeneity is conceivably large. Additionally, external factors influence how each cell interacts with their surroundings, which also reflects on alterations at the EV level[166]. Consequently, it becomes clear that characterization of specific EV subsets from whole EV preparations is of utmost importance, not only for the applications herein described, but essentially for any researcher working in the field. Fortunately, EV heterogeneity is ever more acknowledged, together with the notion that bulk, whole EV preparations are not ideal for biomarker discovery or detection, which stimulates the development of increasingly robust approaches to enable targeted EV profiling and isolation[153].

Current state-of-the-art techniques for EV analytics have been previously reviewed[150,154]. Single-particle analysis platforms, such as nano flow cytometers (nFCM), can estimate particle size, concentration or even zeta potential in a label-free manner. However, in order to identify specific phenotypical features, EVs must be labelled with affinity reagents, conjugated to high brightness fluorochromes. Bright dyes are required to push the faint fluorescent signal obtained after staining EV surface markers, which are often present in low abundance. In conclusion, platforms that enable label-free and fluorescence-based measurements can not only discriminate EVs from confounding contaminant particles, but also identify and quantitatively characterize EV subpopulations of interest.

Here, the Flow NanoAnalyzer (nanoFCM INC.) was selected to conduct single-vesicle nFCM. As any cell flow cytometry platform, it can interrogate particles one by one in a multiparametric fashion. Moreover, it performs both label-free and fluorescence measurements, allowing to accurately gauge not only the concentration of total particles, but also of labelled subsets (results section, Part 1, Fig 1 and 2). After careful optimization and validation of staining procedures, even EVs expressing one single copy of the protein of interest at their surface can potentially be detected. Side scatter (SSC) or fluorescence-triggered measurement settings are adjusted for several well-defined size ranges, which enables the generation of narrow particle size histograms to better characterize EVs by size. The entire EV size spectrum (30-1000nm) can be covered using this high-sensitivity platform. In addition to EVs, nanoparticles of other nature can also be detected, however the LOD of the Flow

NanoAnalyzer depends on the refractive index of the materials composing target nanoparticles (i.e. LOD silica = 27nm; LOD gold = 7nm)[162,164,167].

Characterization of EV subpopulations stands as the initial line of research in this PhD project. It was fundamental to proceed with the subsequent testing and development of fluorescently-labelled EV spikes, where staining protocols extensively optimized by nFCM were applied to generate EVs that could controllably function as tracer tools, particularly in IP reactions. In this way, IP efficiency and specificity was accurately evaluated using a simple, quick, widely available, high-throughput, cost-efficient, automatable and precise fluorometric readout. The fluorescently-labelled tracer EV spikes presented here are well suited to diverse research and development needs, commercial pipelines and eventually even clinical diagnostic applications.

One of the major issues dealt with at this stage was background fluorescence, which caused not only the underestimation of fluorescently-labelled events by nFCM, but also an underappreciation of EV spike recovery downstream, after IP reactions. Thus, elimination of background fluorescence, or of its impact, is a critical challenge that rigorous EV labelling strategies must address. Usually, protocols using CFSE or CellTrace dyes to indiscriminately label EVs in a sample, require quite high dye concentrations (10 to 25μM) to achieve complete staining[160,168–173]. Yet, only a small portion is actually incorporated in EVs, resulting in massive amounts of free dye in excess. In addition, other properties of CFSE, such as molecule size, might hamper the performance of EV purification methodologies excess dye elimination. Therefore, CFSE staining reactions reported herein were performed using highly concentrated, CCM-derived EV starting material, in order to reduce reaction volumes and employ the lowest possible absolute amount of dye, while maintaining its optimal concentration (10μM). This approach kept background fluorescence levels at a minimum upon one round of SEC purification, abolishing the need for sequential rounds of purification that can ultimately cause dramatic EV loss. In contrast to CFSE staining, not only lower amounts of fluorescently-labelled antibodies were required for complete EV labelling, but also, they could be easily washed off upon three to four rounds of UF. Ideally, EV subpopulations should not be differentially affected by dye removal techniques. Using an inherently unbiased sample dilution-based approach to bring background fluorescence to undetectable levels before nFCM measurements, we demonstrated that neither SEC nor UF purification alter the composition of EV subpopulations present in simple matrices (results section, Part 1, Fig. 3B).

Furthermore, it is important to stress that cellular dyes generally used to indiscriminately stain EVs, such as CFSE or CellTrace dyes[160,168–173], are actually not EV-specific. It is usually hypothesised that CFSE preferably stains EVs over other biological particles due to the enzymatic activity occurring at the EV lumen. Upon enzymatic cleavage, CFSE reportedly becomes fluorescence and binds to nearby protein epitopes, causing its intraluminal retention and rendering only EVs, but not confounding particles fluorescent[174,175]. However, CFSE fluorescence was detected independently of its required enzymatic cleavage. Also, CFSE even stained large protein complexes and lipoproteins, which are the two main contaminants of EV preps (results section, Part 1, supplementary).

In fact, the prime challenge faced throughout this project is one shared across the field, which has to do with the precise identification and quantitative measurement of EVs in biological samples. The overabundance of contaminating particles is so overwhelming that not even high sensitivity, state-of-the-art techniques like nFCM can find the “needle in the haystack”, even after employing the best currently available methodologies for EV purification from biological samples[145,151]. Since contaminant particles (large proteins and lipoproteins) obscure the detection of EV-specific markers, neither nFCM nor any other state-of-the-art single particle system would allow for reliable and accurate plasma-derived EV characterization. One possible solution to circumvent this limitation

would be to selectively deplete the major contaminant particles (lipoproteins) through IP. Nonetheless, it is highly unlikely that this would completely solve the particle overabundance problem, while it is also unclear how it would impact the representation of EV subpopulations. Therefore, without methodologies that can actually enrich for EVs derived from complex biological samples, it is not feasible to profile the circulating EV subpopulations, which remains a central challenge to basic research and development, translational science and even clinical research.

Part 2: EV immunoaffinity isolation for plasma liquid biopsies

Researchers that might not be entirely familiarized or up to date with the EV field, frequently underappreciate the drastic challenge gap between working with cell culture EVs, derived from simple matrices such as cell conditioned medium (CCM), and EVs obtained from highly rich biological samples (i.e., plasma, serum, urine, saliva, cerebrospinal fluid).

Thorough characterization of CCM-derived EVs was conducted to understand which ones would be better suited as scientific model for each IP experiment. Cultured cell-lines were conditioned in the absence of serum to guarantee that CCM was devoid of bovine vesicles and contaminant serum-derived particles, which co-purify during EV isolation. This aspect deserves some attention during experimental designs, as serum starvation induces cellular stress and can influence EV phenotypes and properties[67,176,177]. Since the project was not intensively focused on fundamental biological questions, but rather on more technical and translational aspects, producing serum-free CCM was critical to assure that the majority of its constituent particles seen by nFCM were truly EVs. Additionally, any indiscriminate EV type would have served as model for IP experiments, as long as it could be stably and effectively stained with fluorescent dyes or antibodies, and captured using affinity reagents.

In this project, a great deal of attention and experimental work has been dedicated to the selection of appropriate affinity reagents. Firstly, it was established that the used methods had to excel in their specificity, which should always be considered the most important factor of any enrichment strategy. Subsequently, it was envisaged that magnetic properties would be extremely valuable to tackle the milestones set beforehand. Hence, the attention was directed towards testing several affinity reagents using magnetic beads as support, which provide a high ratio of surface area to volume, can quickly react with target analytes, allow for gentle isolation of biological structures and have been widely used for biomolecule separation[178,179].

Concretely, due to the nanometric size of EVs, it is conceivable that similar-sized nano beads could potentially outperform larger ones (i.e., ≥ 1μm) in EV IP. Absence of multi-point attachment between targets, quick binding reactions, maintenance of optical sample properties and zero aggregation are important factors enabled by nano-sized beads that can drastically improve IP protocols[180]. Therefore, MACS beads (Miltenyi Biotec), which are approximately 50nm in diameter and do not interfere with downstream assays, were chosen for further testing. This is a particularly useful feature, since detachment of the EV-bead complex, a rather sensitive and unpredictable procedure, is not required. In a recently published study, several affinity-based EV isolation strategies were orthogonally compared based on their specificity, efficiency, and purity in human serum[181]. The authors included MACS beads in their analysis, which delivered the highest IP efficiency out of all magnetic beads tested, evidenced by the recovery of the classical EV markers CD9, CD63 and CD81 on western blot (WB). They also showed by WB and qPCR that MACS beads non-specifically captured the lowest levels of common contamination markers in EV isolates[181]. These observations

were in agreement with the results and experience acquired over the course of this project and contribute to sustain the conclusions drawn.

Despite the immense variety of commercially available affinity reagents (particularly magnetic beads) claiming to enable selective isolation of pure EV subpopulations, perhaps only a few might be well-suited for EV subpopulation enrichment studies. Protocols employing magnetic beads coated with streptavidin or protein A/G (data not shown) for EV IP might be applicable in simple matrices, however, the same does not hold true in complex ones. In fact, covalently-conjugated greatly outperformed antibody-coated streptavidin MACS beads in EV IP, especially in plasma but also in PBS-BSA (results section, Part 2, Fig. 1A, C). This suggests that covalently-conjugated affinity reagents have more potential utility for EV IP, especially from complex matrices, than non-covalent ones. Covalent conjugation of affinity reagents can be better controlled and customized, being less prone to variations in sample matrix composition and properties. Also, they are more frequently used for active epitope targeting than non-covalent-based strategies[182]. However, it was not possible to clearly address the binding capacity and topology of antibody-coated MACS streptavidin, leaving the antibody coating step open to further optimization. Despite that, considering that the biotin tag was located on the Fc domain of antibodies, they should at least be correctly positioned on streptavidin beads, which helps maintaining their functionality. Therefore, it is still up for debate whether streptavidin-based EV IP approaches could mimic the performance of solid surfaces coated with covalently-conjugated, properly oriented and spaced antibodies. Surprisingly, considering the interest of the field in EV-enriching methodologies, systematic studies addressing such technical but critical parameters in the light of EV affinity capture, have yet to be conducted.

Flexibility, a perk which suppliers often claim is enabled by reagents coated with protein A/G or streptavidin, could easily be replicated here using beads coated with covalently-conjugated antibodies. In this case, phycoerythrin (PE)-conjugated antibodies were employed as primary capture reagents binding target EVs. Thus, despite its fluorescence, the PE tag here served then as a molecular beacon to pull down the EV-primary antibody complex using anti-PE conjugated beads (results section, Part 2, Fig. 2B). For this purpose, since PE is a protein produced by algae, it represented the ideal tag as its potential cross reactivity with human biomolecules might be reduced. Additionally, it is a widely established fluorophore, many PE-conjugated reagents are commercially available and it served as reference dye during nFCM optimization experiments due to its properties. As such, PE was also useful to understand EV labelling efficiencies, which directly supported IP protocol development. Furthermore, PE fluorescence could be further leveraged to obtain an indication of how many antibodies are present per bead, allowing to empirically estimate their binding capacity. Therefore, anti-PE and other antibodies targeting commonly employed protein tags, can confer flexibility and possibly other benefits to IP protocols.

Several parameters that must be accounted for proper conjugation of affinity reagents to solid supports include conjugation efficiency, correct antibody orientation and enough spacing between affinity molecules across the coating surface. These and other aspects maintain the performance of affinity reagents after their conjugation to solid surfaces. However, they are usually disregarded, even by established manufacturers, which impairs the affinity of even the most specific antibodies. Linkers and anti-fouling surface chemistries can sustain and improve the functionality of affinity reagents. Altogether, results herein reported showed that even while applying exactly the same bead as solid support, bead surface coating determines the surface properties of particles and dictates the extent of non-specific interactions (results section, Part 2, Fig. 1A), as extensively reported across the literature[183–187].

Nonetheless, co-purified contaminants from plasma and specific EV interactors, located at external outer membrane, might obscure target surface moieties, resulting not only in their impaired recovery

during IP but also in skewed detection. Difficulties in fluorescence detection might have to do with the fluorometric platform, as not all provide the same sensitivity. On several occasions, it was noted that high sensitivity fluorimeters were required for the detection of low abundance protein markers. Here, fluorescently-labelled primary antibodies were directly applied on the EV-bead complex, enabling a straightforward profiling of captured EV subpopulations. However, the LOD of such a staining approach can be further improved by signal amplification, which require for instance secondary antibodies or even enzymatic signal amplification techniques.

One of the main difficulties encountered at this stage was the staining of low abundance markers at the EV surface, especially in limited amounts of plasma-derived EVs (results section, Part 2, Fig. 4B). To simulate a clinical scenario, where patient samples are highly valuable and scarce, EVs were pulled-down from a low plasma volume – only 500μL. The staining of low spike amounts recovered from plasma resulted in unrealistic S/N ratios, which might have been exacerbated by co-precipitated plasma material. Even with the experimental model of CCM-derived EVs, the detection of trace surface markers was extremely challenging, suggesting that in this context, higher input and signal amplification steps, coupled with well optimized staining procedures are necessary. Others have previously shared thoughts on similar phenomena[74,150,165,169,188–190].

As seen before, wide variations in complex matrix composition and EV surface phenotypes greatly affect affinity interactions, rendering the results of affinity-based approaches unexpected to some degree. Thus, finding solutions to specifically capture plasma-derived EVs, with minimal impact from inter-donor biological variation remains a critical challenge. However, overcoming it would be crucial for the implementation of novel EV-based clinical liquid biopsy assays. With that in mind, pre-analytical processing steps were one of main focus points of this project. Neither dilution of the plasma matrix nor the pre-analytical treatments tested throughout seemed to improve specific EV recovery from plasma (results section, Part 2, Sup Fig. 2B, Fig 5B and C). Several failed attempts to tackle this issue on the sample pre-processing angle, led to a shift of focus instead towards the selection and improvement of IP methods, as much as possible. Large volumes of plasma (100 to 200mL per donor) from carefully selected donors were acquired to set up our IP approach. By utilizing exactly the same controlled plasma lots and samples throughout all optimization experiments, potential bias introduced by different complex matrix compositions due to inter-donor sample variation, and other pre-analytical factors were systemized.

Finally, despite all the aforementioned pre-analytical challenges, still it was observed that distinct plasma-derived EV subpopulations conferred differential clinical values for liquid biopsy-based disease detection. mRNA profiles carried within platelet-derived EVs were clearly distinct between healthy and early-stage NSCLC cohorts, representing a proof of principle experiment that output 47 potential biomarkers indicative of early-stage cancer, under a clinically relevant liquid biopsy setting (results section, Part 2, Fig. 7). Platelets are first responders to inflammation and directly contribute to orchestrate immune responses, in support of the immune system. Not only can they engulf pathogens, but also tumour-shed biomolecules, which results in their transformation into tumour-educated platelets (TEPs). Together with other effectors, TEPs actively spread malignant phenotypes and contribute to cancer progression. As platelet and TEP-generated EVs mediate these processes through the horizontal transfer of cancer-promoting biomolecules, they have been increasingly considered valuable biomarker sources for liquid biopsies[191,192].

The small-scale proof of principle study herein described was conducted using the Nanostring nCounter platform. Direct digital quantification of hundreds of transcripts and proteins can be performed in a straightforward, simultaneous and multiplexed fashion, using pre-assembled or custom panels[193,194]. All processes, from EV isolation to data analysis, fit realistically feasible routine clinical workflows as they are automatable, require low sample input (500μL) and the turnaround

time of the whole assay can be as low as 2 days, while the EV isolation step simply lasts 1h. In fact, the nCounter Prosigna assay received FDA approval in 2013 as it could effectively predict then risk of breast cancer recurrence, using the 50-gene signature PAM50[195–198]. Additionally, during the past decade the nCounter platform has been extensively employed in both translational and clinical research, as well as in companion diagnostics due to its robustness, ease-of-use, sensitivity, accuracy and reproducibility[199,200]. Only recently, Nanostring systems have also been explored for its potential use in liquid biopsies[195,197], and therefore, it is still a topic awaiting to be further explored. The work herein reported contributes to this early body of evidence, which is currently still in its infancy.

As of today, clinically implemented liquid biopsy tests mostly focus on the analysis of CTCs and cf/ctDNA[201,202,147]. Nonetheless, recent achievements have progressively raised attention regarding the clinical utility of EVs, which has caused the exponential growth in EV-related publications[203,204]. In 2016 ExosomeDx delivered the world's first commercial EV-based clinical liquid biopsy test, the FDA-approved ExoDx™ Prostate (IntelliScore) (EPI). Using a novel 3-gene signature (ERG, PCA3, and SPDEF) researchers profiled urine-derived EVs and were able to predict and manage the development high-grade prostate cancer, in a cohort of men over 50 years of age with "grey-zone" PSA levels (2 to 10ng/mL), through the assessment of a risk score. EPI accuracy, presented as area under the curve (AUC) during independent validation, revealed that it outperformed standard-of-care (SOC) assays (AUC EPI: 0.77; AUC SOC: 0.66), while preventing tissue biopsies in 27% of cases, which avoided potentially harmful invasive procedures[205,206]. Three independent, multi-center studies including prospective cohorts, further demonstrated that EPI outperformed SOC gold standard clinical tests and that it could be used as a companion diagnostics tool for the early detection of prostate cancer, avoiding unnecessary tissue biopsies[207].

Despite the hype of biomarker research for clinical translation in oncology, it is challenging to deliver commercial, clinical-grade liquid biopsy-based tests. Within this scope, studies that integrate carefully curated clinical data of large groups of individuals, representing populations or relevant clinical cohorts, are fundamental for robust biomarker validation and assay development and implementation. As extensively highlighted throughout this thesis, inter-donor variables and their associated pre-existing conditions, as well as sample pre-analytics, can dramatically determine biomarker strength in liquid biopsy assays[204]. Consequently, elimination or standardization of pre-analytical bias is critical and should be a main focus point when devising liquid biopsy-based approaches. As such, not only researchers and developers committed to deliver novel diagnostic tests, but also hospital staff members involved in sample collection, handling and storage should receive further education and training on relevant topics for liquid biopsies. Consensus, standardization, and widespread application of liquid biopsy-based assays will enable better informed medical decisions and data integration. It is likely that the conventional model of conducting clinical tumour evaluation at each hospital will shift to off-site, centralized units operating at national or even international levels, which will be required to truly implement powerful multiparametric analyses dealing with large, high dimensional datasets[147].

Ongoing work and future perspectives

Further experimental work has been conducted, in addition to what could be reported in this thesis. Unfortunately, since some studies and data analysis are not yet complete, it can simply be mentioned what has been accomplished so far, as result of ongoing collaborations.

The Nanostring proof of principle data is currently being further explored to perform sample clustering analysis, which will reveal additional expression patterns and molecular signatures of the different early stage (stage III to I) samples included in the study. Due to the success of the small-scale proof of principle study, this body of work is being further expanded using larger clinical cohorts, as to increase the robustness of mRNA profiling and to compare more healthy donors against a prospective NSCLC cohort (n = 50 x 2). This time, to understand if the combination of different EV-carried analytes improves cohort separation, surface protein markers of plasma-derived EVs were also measured, immediately after IP and before RNA extraction. Moreover, other biomarker sources, such as cfDNA and circular RNA (circRNA), were obtained from the same clinical cohorts to understand the unique and/or complementary value of combining multiple liquid biopsy substrates. This extended clinical study will elaborate on detection accuracy using machine learning classification algorithms, which may reveal additional challenges but still support the inclusion of this IP strategy and complementary biomarker sources in future liquid biopsy workflows. Finally, other interesting contents of selected EV subpopulations obtained from healthy donor and NSCLC patient plasma, such as the small RNA repertoire, are currently being analysed by RNA sequencing (n = 20 x 2).

Lastly, robust EV subpopulation isolation and direct multiparametric characterization remains a central challenge in the field[153]. The experimental work herein reported addresses this need by enabling specific and efficient enrichment of target EV subpopulations from simple and complex matrices, which could be initially profiled directly on solid supports, and further analysed in downstream platforms. In addition, this EV IP methodology is compatible with most analytical platforms, enabling multiplexed characterization of the several different biomarker sources carried within EVs. Upstream interferences introduced by the fluctuating pre-analytical factors, represent the main obstacle limiting commercialization and clinical implementation of this and other affinity-based EV IP solutions. Within this scope, in depth studies focused on unveiling specific and non-specific interactions between complex matrix components and different EV surface phenotypes are highly warranted. They will define the real value of circulating EVs and associated proteins as indicators of individual (patho)physiological states, and decide whether such analytes can truly propel the precision medicine revolution.

Conclusions

Overall, the milestones defined for this PhD project were thoroughly assessed.

Recapitulating the broad objectives of this project, described under the 'motivations and structure of the PhD project' section, achieved milestones can be highlighted:

- Obtain comprehensive, clinically relevant information out of individual standardised blood-based biomarker sources → **Platelet-derived EVs isolated from human plasma revealed specific mRNA profiles distinctive of early-stage NSCLC.**
- Pinpoint diagnostic synergy between biomarker sources or multiple analytes carried within them → **EV surface protein markers and respective mRNA profiles are being tested for their combinatorial performance for early-stage NSCLC detection, in our extended cohort study. Small RNAs contained in platelets and respective platelet-derived EVs are being compared by deep RNA sequencing.**
- Identify and validate biomarkers for the detection of stage I-IV NSCLC → **So far, mRNA profiles of 47 DE genes were identified upon comparison of healthy and early-stage NSCLC cohorts.**
- Identify and validate biomarkers for selection of NSCLC patients for treatment → **Not directly addressed, however, this work paves the way for ever more selective EV isolation strategies, which will be useful for the identification of biomarkers also for patient stratification.**
- Establish novel bioinformatics tools and protocols for the integrative analysis of multi-source liquid biopsy data → **Dedicated bioinformatics pipelines, tailored to the data originally generated herein, have been developed in collaboration with project partners.**
- Develop blood-based assays and delivering scalable prototypes capable of obtaining regulatory approval → **IP and detection strategies employed in this work were devised to be readily implementable in minimally processed biological samples, tailored to facilitate compliance with regulatory and clinical requisites.**

… and reviewing our more concrete deliverables:

5. Testing sample stabilisation and preclearing protocols for maximum recovery of different EV subpopulations from blood → **After testing several sample pre-analytical protocols, improvement of IP methods was prioritized, which allowed to demonstrate that fluorescently labelled EV spikes can be efficiently recovered from plasma.**
6. Development of protocols, devices and immunoaffinity reagents for the selection and capture of target EV subpopulations containing NSCLC markers, from complex matrices such as plasma → **Capture of specific EV subpopulations from simple and complex matrices was verified using EV spikes. 47 potential mRNA biomarkers of early-stage NSCLC in platelet-derived EVs could be identified.**
7. Identification of relevant EV marker profiles holding potential for early-stage cancer detection → **Yes, as stated above.**

8. Compilation of analytical solutions for the analysis of multiple co-expressed EV markers → **Yes, as stated above.**

Knowledge on the frontiers of liquid biopsies and EVs has drastically increased over the last 20 years. This phenomenon has also been evident for the past almost 4 years, since the start of this PhD project. Central challenges currently faced by EV researchers were tackled throughout, without compromising on the quality of the research output, while attempting to deliver solid evidence to support our claims. This work might hopefully encourage more scientists to delve into EV research, keeping in mind that critical awareness and thorough EV characterization are essential to accurately dissect the field, as well as to elaborate high-impact and long-lasting scientific ideas. The mutable and ever-growing knowledge on EVs will potentially shape future perspectives on biomedicine and on the next-generation of widespread clinical care practices.

List of Publications

Fortunato D, Giannoukakos S, Giménez-Capitán A, Hackenberg M, Molina-Vila M, Zarovni, N. Selective isolation of extracellular vesicles from minimally processed human plasma as a translational strategy for liquid biopsies. In submission.

Fortunato D, Mladenović D, Criscuoli M, Loria F, Veiman KL, Zocco D, et al. Opportunities and Pitfalls of Fluorescent Labeling Methodologies for Extracellular Vesicle Profiling on High-Resolution Single-Particle Platforms. Int J Mol Sci. 2021 Sep 29;22(19):10510.

Bianciardi L, Corallo C, Criscuoli M, **Fortunato D**, Zarovni N, Zocco D. Emerging Technologies in Markets for the Early Detection of Head and Neck Cancer. In: El Assal R, Gaudilliere D, Connelly ST, editors. Early Detection and Treatment of Head & Neck Cancers: Practical Applications and Techniques for Detection, Diagnosis, and Treatment. Cham: Springer International Publishing; 2021 p. 17–42. Available from: https://doi.org/10.1007/978-3-030-69859-1_2

Brambilla D, Sola L, Ferretti AM, Chiodi E, Zarovni N, **Fortunato D**, et al. EV Separation: Release of Intact Extracellular Vesicles Immunocaptured on Magnetic Particles. Anal Chem. 2021 Apr 6;93(13):5476–83.

Simonetta M, de Krijger I, Serrat J, Moatti N, **Fortunato D**, Hoekman L, et al. H4K20me2 distinguishes pre-replicative from post-replicative chromatin to appropriately direct DNA repair pathway choice by 53BP1-RIF1-MAD2L2. Cell Cycle Georget Tex. 2018;17(1):124–36.

References

1. Chargaff, E. CELL STRUCTURE AND THE PROBLEM OF BLOOD COAGULATION. *Journal of Biological Chemistry* **160**, 351–359 (1945).
2. Chargaff, E. & West, R. The biological significance of the thromboplastic protein of blood. *J Biol Chem* **166**, 189–197 (1946).
3. Anderson, H. C. Electron microscopic studies of induced cartilage development and calcification. *J Cell Biol* **35**, 81–101 (1967).
4. Anderson, H. C. Vesicles associated with calcification in the matrix of epiphyseal cartilage. *J Cell Biol* **41**, 59–72 (1969).
5. Peress, N. S., Anderson, H. C. & Sajdera, S. W. The lipids of matrix vesicles from bovine fetal epiphyseal cartilage. *Calcif Tissue Res* **14**, 275–281 (1974).
6. Wolf, P. The nature and significance of platelet products in human plasma. *Br J Haematol* **13**, 269–288 (1967).
7. Trams, E. G., Lauter, C. J., Salem, N. & Heine, U. Exfoliation of membrane ecto-enzymes in the form of micro-vesicles. *Biochim Biophys Acta* **645**, 63–70 (1981).
8. Harding, C., Heuser, J. & Stahl, P. Receptor-mediated endocytosis of transferrin and recycling of the transferrin receptor in rat reticulocytes. *Journal of Cell Biology* **97**, 329–339 (1983).
9. Pan, B. T. & Johnstone, R. M. Fate of the transferrin receptor during maturation of sheep reticulocytes in vitro: selective externalization of the receptor. *Cell* **33**, 967–978 (1983).
10. Harding, C., Heuser, J. & Stahl, P. Endocytosis and intracellular processing of transferrin and colloidal gold-transferrin in rat reticulocytes: demonstration of a pathway for receptor shedding. *Eur J Cell Biol* **35**, 256–263 (1984).
11. Pan, B. T., Teng, K., Wu, C., Adam, M. & Johnstone, R. M. Electron microscopic evidence for externalization of the transferrin receptor in vesicular form in sheep reticulocytes. *Journal of Cell Biology* **101**, 942–948 (1985).
12. Bobrie, A., Colombo, M., Raposo, G. & Théry, C. Exosome Secretion: Molecular Mechanisms and Roles in Immune Responses. *Traffic* **12**, 1659–1668 (2011).
13. Harding, C. V., Collins, D. S., Slot, J. W., Geuze, H. J. & Unanue, E. R. Liposome-encapsulated antigens are processed in lysosomes, recycled, and presented to T cells. *Cell* **64**, 393–401 (1991).
14. Raposo, G. *et al.* B lymphocytes secrete antigen-presenting vesicles. *Journal of Experimental Medicine* **183**, 1161–1172 (1996).
15. Emerson, S. G. & Cone, R. E. Turnover and shedding of Ia antigens by murine spleen cells in culture. *J Immunol* **122**, 892–899 (1979).
16. Sachs, D. H., Kiszkiss, P. & Kim, K. J. Release of Ia antigens by a cultured B cell line. *The Journal of Immunology* **124**, 2130–2136 (1980).
17. Emerson, S. G. & Cone, R. E. I-Kk and H-2Kk antigens are shed as supramolecular particles in association with membrane lipids. *J Immunol* **127**, 482–486 (1981).
18. Rubinstein, E. *et al.* CD9, CD63, CD81, and CD82 are components of a surface tetraspan network connected to HLA-DR and VLA integrins. *European Journal of Immunology* **26**, 2657–2665 (1996).
19. Bess, J. W., Gorelick, R. J., Bosche, W. J., Henderson, L. E. & Arthur, L. O. Microvesicles Are a Source of Contaminating Cellular Proteins Found in Purified HIV-1 Preparations. *Virology* **230**, 134–144 (1997).
20. Zitvogel, L. *et al.* Eradication of established murine tumors using a novel cell-free vaccine: dendritic cell derived exosomes. *Nat Med* **4**, 594–600 (1998).
21. Escola, J.-M. *et al.* Selective Enrichment of Tetraspan Proteins on the Internal Vesicles of Multivesicular Endosomes and on Exosomes Secreted by Human B-lymphocytes *. *Journal of Biological Chemistry* **273**, 20121–20127 (1998).

22. Abrams, C., Ellison, N., Budzynski, A. & Shattil, S. Direct detection of activated platelets and platelet-derived microparticles in humans. *Blood* **75**, 128–138 (1990).

23. Sims, P. J. & Wiedmer, T. Repolarization of the membrane potential of blood platelets after complement damage: evidence for a Ca++ -dependent exocytotic elimination of C5b-9 pores. *Blood* **68**, 556–561 (1986).

24. Holme, P. A., Solum, N. O., Brosstad, F., Røger, M. & Abdelnoor, M. Demonstration of platelet-derived microvesicles in blood from patients with activated coagulation and fibrinolysis using a filtration technique and western blotting. *Thromb Haemost* **72**, 666–671 (1994).

25. Heijnen, H. F. G. *et al.* Multivesicular Bodies Are an Intermediate Stage in the Formation of Platelet α-Granules. *Blood* **91**, 2313–2325 (1998).

26. Heijnen, H. F. G., Schiel, A. E., Fijnheer, R., Geuze, H. J. & Sixma, J. J. Activated Platelets Release Two Types of Membrane Vesicles: Microvesicles by Surface Shedding and Exosomes Derived From Exocytosis of Multivesicular Bodies and □-Granules. *Blood* **94**, 3791–3799 (1999).

27. Hess, C., Sadallah, S., Hefti, A., Landmann, R. & Schifferli, J.-A. Ectosomes Released by Human Neutrophils Are Specialized Functional Units. *The Journal of Immunology* **163**, 4564–4573 (1999).

28. Morgan, B. P., Dankert, J. R. & Esser, A. F. Recovery of human neutrophils from complement attack: removal of the membrane attack complex by endocytosis and exocytosis. *J Immunol* **138**, 246–253 (1987).

29. Scolding, N. J. *et al.* Vesicular removal by oligodendrocytes of membrane attack complexes formed by activated complement. *Nature* **339**, 620–622 (1989).

30. Stein, J. M. & Luzio, J. P. Ectocytosis caused by sublytic autologous complement attack on human neutrophils. The sorting of endogenous plasma-membrane proteins and lipids into shed vesicles. *Biochemical Journal* **274**, 381–386 (1991).

31. Sengeløv, H., Kjeldsen, L., Kroeze, W., Berger, M. & Borregaard, N. Secretory vesicles are the intracellular reservoir of complement receptor 1 in human neutrophils. *J Immunol* **153**, 804–810 (1994).

32. Felder, S. *et al.* Kinase activity controls the sorting of the epidermal growth factor receptor within the multivesicular body. *Cell* **61**, 623–634 (1990).

33. Futter, C. E., Felder, S., Schlessinger, J., Ullrich, A. & Hopkins, C. R. Annexin I is phosphorylated in the multivesicular body during the processing of the epidermal growth factor receptor. *Journal of Cell Biology* **120**, 77–83 (1993).

34. Pascual, M., Lutz, H. U., Steiger, G., Stammler, P. & Schifferli, J. A. Release of vesicles enriched in complement receptor 1 from human erythrocytes. *J Immunol* **151**, 397–404 (1993).

35. Théry, C. *et al.* Molecular Characterization of Dendritic Cell-Derived Exosomes: Selective Accumulation of the Heat Shock Protein Hsc73. *Journal of Cell Biology* **147**, 599–610 (1999).

36. Buschow, S. I. *et al.* MHC II in Dendritic Cells is Targeted to Lysosomes or T Cell-Induced Exosomes Via Distinct Multivesicular Body Pathways. *Traffic* **10**, 1528–1542 (2009).

37. Théry, C. *et al.* Proteomic Analysis of Dendritic Cell-Derived Exosomes: A Secreted Subcellular Compartment Distinct from Apoptotic Vesicles. *The Journal of Immunology* **166**, 7309–7318 (2001).

38. Wolfers, J. *et al.* Tumor-derived exosomes are a source of shared tumor rejection antigens for CTL cross-priming. *Nat Med* **7**, 297–303 (2001).

39. Andre, F. *et al.* Malignant effusions and immunogenic tumour-derived exosomes. *The Lancet* **360**, 295–305 (2002).

40. Théry, C. *et al.* Indirect activation of naïve CD4+ T cells by dendritic cell–derived exosomes. *Nat Immunol* **3**, 1156–1162 (2002).

41. Pisitkun, T., Shen, R.-F. & Knepper, M. A. Identification and proteomic profiling of exosomes in human urine. *PNAS* **101**, 13368–13373 (2004).

42. Caby, M.-P., Lankar, D., Vincendeau-Scherrer, C., Raposo, G. & Bonnerot, C. Exosomal-like vesicles are present in human blood plasma. *International Immunology* **17**, 879–887 (2005).

43. Ratajczak, J. *et al.* Embryonic stem cell-derived microvesicles reprogram hematopoietic progenitors: evidence for horizontal transfer of mRNA and protein delivery. *Leukemia* **20**, 847–856 (2006).

44. Valadi, H. *et al.* Exosome-mediated transfer of mRNAs and microRNAs is a novel mechanism of genetic exchange between cells. *Nat Cell Biol* **9**, 654–659 (2007).

45. Hunter, M. P. *et al.* Detection of microRNA Expression in Human Peripheral Blood Microvesicles. *PLOS ONE* **3**, e3694 (2008).

46. van Niel, G., Porto-Carreiro, I., Simoes, S. & Raposo, G. Exosomes: A Common Pathway for a Specialized Function. *The Journal of Biochemistry* **140**, 13–21 (2006).

47. Skog, J. *et al.* Glioblastoma microvesicles transport RNA and proteins that promote tumour growth and provide diagnostic biomarkers. *Nat Cell Biol* **10**, 1470–1476 (2008).

48. Chaput, N. & Théry, C. Exosomes: immune properties and potential clinical implementations. *Semin Immunopathol* **33**, 419–440 (2011).

49. Lakkaraju, A. & Rodriguez-Boulan, E. Itinerant exosomes: emerging roles in cell and tissue polarity. *Trends in Cell Biology* **18**, 199–209 (2008).

50. Nolte-'t Hoen, E. N. M. *et al.* Deep sequencing of RNA from immune cell-derived vesicles uncovers the selective incorporation of small non-coding RNA biotypes with potential regulatory functions. *Nucleic Acids Research* **40**, 9272–9285 (2012).

51. Bellingham, S. A., Coleman, B. M. & Hill, A. F. Small RNA deep sequencing reveals a distinct miRNA signature released in exosomes from prion-infected neuronal cells. *Nucleic Acids Research* **40**, 10937–10949 (2012).

52. Batagov, A. O. & Kurochkin, I. V. Exosomes secreted by human cells transport largely mRNA fragments that are enriched in the 3′-untranslated regions. *Biol Direct* **8**, 1–8 (2013).

53. Wei, Z. *et al.* Coding and noncoding landscape of extracellular RNA released by human glioma stem cells. *Nat Commun* **8**, 1145 (2017).

54. Lázaro-Ibáñez, E. *et al.* Different gDNA content in the subpopulations of prostate cancer extracellular vesicles: Apoptotic bodies, microvesicles, and exosomes. *The Prostate* **74**, 1379–1390 (2014).

55. Jeppesen, D. K. *et al.* Reassessment of Exosome Composition. *Cell* **177**, 428-445.e18 (2019).

56. Cai, J. *et al.* Extracellular vesicle-mediated transfer of donor genomic DNA to recipient cells is a novel mechanism for genetic influence between cells. *Journal of Molecular Cell Biology* **5**, 227–238 (2013).

57. Kahlert, C. *et al.* Identification of Double-stranded Genomic DNA Spanning All Chromosomes with Mutated KRAS and p53 DNA in the Serum Exosomes of Patients with Pancreatic Cancer *. *Journal of Biological Chemistry* **289**, 3869–3875 (2014).

58. Lee, T. H. *et al.* Oncogenic ras-driven cancer cell vesiculation leads to emission of double-stranded DNA capable of interacting with target cells. *Biochemical and Biophysical Research Communications* **451**, 295–301 (2014).

59. Shurtleff, M. J., Temoche-Diaz, M. M. & Schekman, R. Extracellular Vesicles and Cancer: Caveat Lector. *Annu. Rev. Cancer Biol.* **2**, 395–411 (2018).

60. Takahashi, A. *et al.* Exosomes maintain cellular homeostasis by excreting harmful DNA from cells. *Nat Commun* **8**, 15287 (2017).

61. Hitomi, K. *et al.* DNA Damage Regulates Senescence-Associated Extracellular Vesicle Release via the Ceramide Pathway to Prevent Excessive Inflammatory Responses. *International Journal of Molecular Sciences* **21**, 3720 (2020).

62. Yokoi, A. *et al.* Mechanisms of nuclear content loading to exosomes. *Science Advances* (2019) doi:10.1126/sciadv.aax8849.

63. Németh, A. *et al.* Antibiotic-induced release of small extracellular vesicles (exosomes) with surface-associated DNA. *Sci Rep* **7**, 8202 (2017).

64. Thakur, B. K. *et al.* Double-stranded DNA in exosomes: a novel biomarker in cancer detection. *Cell Res* **24**, 766–769 (2014).

65. Lázaro-Ibáñez, E. *et al.* DNA analysis of low- and high-density fractions defines heterogeneous subpopulations of small extracellular vesicles based on their DNA cargo and topology. *Journal of Extracellular Vesicles* **8**, 1656993 (2019).

66. van Niel, G., D'Angelo, G. & Raposo, G. Shedding light on the cell biology of extracellular vesicles. *Nat Rev Mol Cell Biol* **19**, 213–228 (2018).

67. Kowal, J. *et al.* Proteomic comparison defines novel markers to characterize heterogeneous populations of extracellular vesicle subtypes. *PNAS* **113**, E968–E977 (2016).

68. Zhang, H. *et al.* Identification of distinct nanoparticles and subsets of extracellular vesicles by asymmetric flow field-flow fractionation. *Nat Cell Biol* **20**, 332–343 (2018).

69. Johansson, S. M., Admyre, C., Scheynius, A. & Gabrielsson, S. Different types of in vitro generated human monocyte-derived dendritic cells release exosomes with distinct phenotypes. *Immunology* **123**, 491–499 (2008).

70. Willms, E. *et al.* Cells release subpopulations of exosomes with distinct molecular and biological properties. *Sci Rep* **6**, 22519 (2016).

71. Bobrie, A., Colombo, M., Krumeich, S., Raposo, G. & Théry, C. Diverse subpopulations of vesicles secreted by different intracellular mechanisms are present in exosome preparations obtained by differential ultracentrifugation. *Journal of Extracellular Vesicles* **1**, 18397 (2012).

72. Willms, E., Cabañas, C., Mäger, I., Wood, M. J. A. & Vader, P. Extracellular Vesicle Heterogeneity: Subpopulations, Isolation Techniques, and Diverse Functions in Cancer Progression. *Frontiers in Immunology* **9**, 738 (2018).

73. Fortunato, D. *et al.* Opportunities and Pitfalls of Fluorescent Labeling Methodologies for Extracellular Vesicle Profiling on High-Resolution Single-Particle Platforms. *International Journal of Molecular Sciences* **22**, 10510 (2021).

74. Wiklander, O. P. B. *et al.* Systematic Methodological Evaluation of a Multiplex Bead-Based Flow Cytometry Assay for Detection of Extracellular Vesicle Surface Signatures. *Frontiers in Immunology* **9**, 1326 (2018).

75. Alibhai, F. J. *et al.* Cellular senescence contributes to age-dependent changes in circulating extracellular vesicle cargo and function. *Aging Cell* **19**, e13103 (2020).

76. Fafián-Labora, J. A., Rodríguez-Navarro, J. A. & O'Loghlen, A. Small Extracellular Vesicles Have GST Activity and Ameliorate Senescence-Related Tissue Damage. *Cell Metabolism* **32**, 71-86.e5 (2020).

77. Lötvall, J. *et al.* Minimal experimental requirements for definition of extracellular vesicles and their functions: a position statement from the International Society for Extracellular Vesicles. *J Extracell Vesicles* **3**, 10.3402/jev.v3.26913 (2014).

78. Théry, C. *et al.* Minimal information for studies of extracellular vesicles 2018 (MISEV2018): a position statement of the International Society for Extracellular Vesicles and update of the MISEV2014 guidelines. *Journal of Extracellular Vesicles* **7**, 1535750 (2018).

79. Zheng, H. *et al.* The roles of tumor-derived exosomes in non-small cell lung cancer and their clinical implications. *J Exp Clin Cancer Res* **37**, 1–11 (2018).

80. Hanahan, D. & Weinberg, R. A. The Hallmarks of Cancer. *Cell* **100**, 57–70 (2000).

81. Hanahan, D. & Weinberg, R. A. Hallmarks of Cancer: The Next Generation. *Cell* **144**, 646–674 (2011).

82. Kanada, M., Bachmann, M. H. & Contag, C. H. Signaling by Extracellular Vesicles Advances Cancer Hallmarks. *Trends in Cancer* **2**, 84–94 (2016).

83. Xavier, C. P. R. *et al.* The Role of Extracellular Vesicles in the Hallmarks of Cancer and Drug Resistance. *Cells* **9**, 1141 (2020).

84. Antonyak, M. A. *et al.* Cancer cell-derived microvesicles induce transformation by transferring tissue transglutaminase and fibronectin to recipient cells. *PNAS* **108**, 4852–4857 (2011).

85. Yang, L., Wu, X.-H., Wang, D., Luo, C.-L. & Chen, L.-X. Bladder cancer cell-derived exosomes inhibit tumor cell apoptosis and induce cell proliferation in vitro. *Molecular Medicine Reports* **8**, 1272–1278 (2013).

86. Dong, H. *et al.* Exosome-mediated transfer of lncRNA-SNHG14 promotes trastuzumab chemoresistance in breast cancer. *Int J Oncol* **53**, 1013–1026 (2018).

87. Shedden, K., Xie, X. T., Chandaroy, P., Chang, Y. T. & Rosania, G. R. Expulsion of Small Molecules in Vesicles Shed by Cancer Cells: Association with Gene Expression and Chemosensitivity Profiles. *Cancer Res* **63**, 4331–4337 (2003).

88. Safaei, R. *et al.* Abnormal lysosomal trafficking and enhanced exosomal export of cisplatin in drug-resistant human ovarian carcinoma cells. *Mol Cancer Ther* **4**, 1595–1604 (2005).

89. Goler-Baron, V., Sladkevich, I. & Assaraf, Y. G. Inhibition of the PI3K-Akt signaling pathway disrupts ABCG2-rich extracellular vesicles and overcomes multidrug resistance in breast cancer cells. *Biochemical Pharmacology* **83**, 1340–1348 (2012).

90. Lu, J. F. *et al.* Microparticles mediate MRP1 intercellular transfer and the re-templating of intrinsic resistance pathways. *Pharmacological Research* **76**, 77–83 (2013).

91. Samuel, P., Fabbri, M. & Carter, D. R. F. Mechanisms of Drug Resistance in Cancer: The Role of Extracellular Vesicles. *PROTEOMICS* **17**, 1600375 (2017).

92. Maacha, S. *et al.* Extracellular vesicles-mediated intercellular communication: roles in the tumor microenvironment and anti-cancer drug resistance. *Mol Cancer* **18**, 1–16 (2019).

93. Blasco, M. A. Telomeres and human disease: ageing, cancer and beyond. *Nat Rev Genet* **6**, 611–622 (2005).

94. Zomer, A. *et al.* In Vivo Imaging Reveals Extracellular Vesicle-Mediated Phenocopying of Metastatic Behavior. *Cell* **161**, 1046–1057 (2015).

95. Al-Nedawi, K., Meehan, B., Kerbel, R. S., Allison, A. C. & Rak, J. Endothelial expression of autocrine VEGF upon the uptake of tumor-derived microvesicles containing oncogenic EGFR. *PNAS* **106**, 3794–3799 (2009).

96. Hood, J. L., Pan, H., Lanza, G. M. & Wickline, S. A. Paracrine Induction of Endothelium by Tumor Exosomes. *Lab Invest* **89**, 1317–1328 (2009).

97. Kim, C. W. *et al.* Extracellular membrane vesicles from tumor cells promote angiogenesis via sphingomyelin. *Cancer Res* **62**, 6312–6317 (2002).

98. Al-Nedawi, K. *et al.* Intercellular transfer of the oncogenic receptor EGFRvIII by microvesicles derived from tumour cells. *Nat Cell Biol* **10**, 619–624 (2008).

99. Han, K.-Y., Chang, J.-H. & Azar, D. T. MMP14-Containing Exosomes Cleave VEGFR1 and Promote VEGFA-Induced Migration and Proliferation of Vascular Endothelial Cells. *Invest Ophthalmol Vis Sci* **60**, 2321–2329 (2019).

100. Yu, J. L. *et al.* Oncogenic events regulate tissue factor expression in colorectal cancer cells: implications for tumor progression and angiogenesis. *Blood* **105**, 1734–1741 (2005).

101. Giusti, I. *et al.* From glioblastoma to endothelial cells through extracellular vesicles: messages for angiogenesis. *Tumor Biol.* **37**, 12743–12753 (2016).

102. Sun, X. *et al.* Glioma stem cells-derived exosomes promote the angiogenic ability of endothelial cells through miR-21/VEGF signal. *Oncotarget* **8**, 36137–36148 (2017).

103. Pavlyukov, M. S. *et al.* Apoptotic Cell-Derived Extracellular Vesicles Promote Malignancy of Glioblastoma Via Intercellular Transfer of Splicing Factors. *Cancer Cell* **34**, 119-135.e10 (2018).

104. Luga, V. *et al.* Exosomes Mediate Stromal Mobilization of Autocrine Wnt-PCP Signaling in Breast Cancer Cell Migration. *Cell* **151**, 1542–1556 (2012).

105. Clancy, J. W. *et al.* Regulated delivery of molecular cargo to invasive tumour-derived microvesicles. *Nat Commun* **6**, 6919 (2015).

106. Peinado, H. *et al.* Melanoma exosomes educate bone marrow progenitor cells toward a pro-metastatic phenotype through MET. *Nat Med* **18**, 883–891 (2012).

107. Balaj, L. *et al.* Tumour microvesicles contain retrotransposon elements and amplified oncogene sequences. *Nat Commun* **2**, 180 (2011).

108. Poste, G. & Fidler, I. J. The pathogenesis of cancer metastasis. *Nature* **283**, 139–146 (1980).

109. Fidler, I. J. Seed and soil revisited: contribution of the organ microenvironment to cancer metastasis. *Surg Oncol Clin N Am* **10**, 257–269, vii–viiii (2001).

110. Peinado, H., Lavotshkin, S. & Lyden, D. The secreted factors responsible for pre-metastatic niche formation: Old sayings and new thoughts. *Seminars in Cancer Biology* **21**, 139–146 (2011).

111. Hood, J. L., San, R. S. & Wickline, S. A. Exosomes Released by Melanoma Cells Prepare Sentinel Lymph Nodes for Tumor Metastasis. *Cancer Res* **71**, 3792–3801 (2011).

112. Costa-Silva, B. *et al.* Pancreatic cancer exosomes initiate pre-metastatic niche formation in the liver. *Nat Cell Biol* **17**, 816–826 (2015).

113. Moreno-Sánchez, R., Rodríguez-Enríquez, S., Marín-Hernández, A. & Saavedra, E. Energy metabolism in tumor cells. *The FEBS Journal* **274**, 1393–1418 (2007).

114. Lopes-Rodrigues, V. *et al.* Identification of the metabolic alterations associated with the multidrug resistant phenotype in cancer and their intercellular transfer mediated by extracellular vesicles. *Sci Rep* **7**, 44541 (2017).

115. Parolini, I. *et al.* Microenvironmental pH Is a Key Factor for Exosome Traffic in Tumor Cells *. *Journal of Biological Chemistry* **284**, 34211–34222 (2009).

116. Wang, T. *et al.* Hypoxia-inducible factors and RAB22A mediate formation of microvesicles that stimulate breast cancer invasion and metastasis. *PNAS* **111**, E3234–E3242 (2014).

117. Zhao, H. *et al.* Tumor microenvironment derived exosomes pleiotropically modulate cancer cell metabolism. *Elife* **5**, e10250 (2016).

118. Fridman, E. S., Ginini, L. & Gil, Z. The Role of Extracellular Vesicles in Metabolic Reprogramming of the Tumor Microenvironment. *Cells* **11**, 1433 (2022).

119. Taylor, D. D., Gerçel-Taylor, C., Lyons, K. S., Stanson, J. & Whiteside, T. L. T-cell apoptosis and suppression of T-cell receptor/CD3-zeta by Fas ligand-containing membrane vesicles shed from ovarian tumors. *Clin Cancer Res* **9**, 5113–5119 (2003).

120. Huber, V. *et al.* Human colorectal cancer cells induce T-cell death through release of proapoptotic microvesicles: role in immune escape. *Gastroenterology* **128**, 1796–1804 (2005).

121. Andreola, G. *et al.* Induction of lymphocyte apoptosis by tumor cell secretion of FasL-bearing microvesicles. *J Exp Med* **195**, 1303–1316 (2002).

122. Clayton, A., Mitchell, J. P., Court, J., Mason, M. D. & Tabi, Z. Human tumor-derived exosomes selectively impair lymphocyte responses to interleukin-2. *Cancer Res* **67**, 7458–7466 (2007).

123. Liu, C. *et al.* Murine Mammary Carcinoma Exosomes Promote Tumor Growth by Suppression of NK Cell Function. *The Journal of Immunology* **176**, 1375–1385 (2006).

124. Clayton, A. *et al.* Human tumor-derived exosomes down-modulate NKG2D expression. *J Immunol* **180**, 7249–7258 (2008).

125. Szajnik, M., Czystowska, M., Szczepanski, M. J., Mandapathil, M. & Whiteside, T. L. Tumor-derived microvesicles induce, expand and up-regulate biological activities of human regulatory T cells (Treg). *PLoS One* **5**, e11469 (2010).

126. Valenti, R. *et al.* Human tumor-released microvesicles promote the differentiation of myeloid cells with transforming growth factor-beta-mediated suppressive activity on T lymphocytes. *Cancer Res* **66**, 9290–9298 (2006).

127. Wang, G.-J. *et al.* Thymus exosomes-like particles induce regulatory T cells. *J Immunol* **181**, 5242–5248 (2008).

128. Chen, G. *et al.* Exosomal PD-L1 contributes to immunosuppression and is associated with anti-PD-1 response. *Nature* **560**, 382–386 (2018).

129. Poggio, M. *et al.* Suppression of Exosomal PD-L1 Induces Systemic Anti-tumor Immunity and Memory. *Cell* **177**, 414-427.e13 (2019).

130. Ricklefs, F. L. *et al.* Immune evasion mediated by PD-L1 on glioblastoma-derived extracellular vesicles. *Sci Adv* **4**, eaar2766 (2018).

131. Hanahan, D. Hallmarks of Cancer: New Dimensions. *Cancer Discovery* **12**, 31–46 (2022).

132. López-Otín, C., Blasco, M. A., Partridge, L., Serrano, M. & Kroemer, G. The Hallmarks of Aging. *Cell* **153**, 1194–1217 (2013).

133. Brock, G., Castellanos-Rizaldos, E., Hu, L., Coticchia, C. & Skog, J. Liquid biopsy for cancer screening, patient stratification and monitoring. *Translational Cancer Research* **4**, (2015).

134. Cohen, J. D. *et al.* Detection and localization of surgically resectable cancers with a multi-analyte blood test. *Science* (2018) doi:10.1126/science.aar3247.

135. Lennon, A. M. *et al.* Feasibility of blood testing combined with PET-CT to screen for cancer and guide intervention. *Science* **369**, eabb9601 (2020).

136. Liu, M. C. *et al.* Sensitive and specific multi-cancer detection and localization using methylation signatures in cell-free DNA. *Annals of Oncology* **31**, 745–759 (2020).

137. Klein, E. A. *et al.* Clinical validation of a targeted methylation-based multi-cancer early detection test using an independent validation set. *Annals of Oncology* **32**, 1167–1177 (2021).

138. Braunstein, G. D. & Ofman, J. J. Criteria for Evaluating Multi-cancer Early Detection Tests. (2021).

139. Hoshino, A. *et al.* Extracellular Vesicle and Particle Biomarkers Define Multiple Human Cancers. *Cell* **182**, 1044-1061.e18 (2020).

140. Rabinowits, G., Gerçel-Taylor, C., Day, J. M., Taylor, D. D. & Kloecker, G. H. Exosomal microRNA: a diagnostic marker for lung cancer. *Clin Lung Cancer* **10**, 42–46 (2009).

141. Sozzi, G. *et al.* Clinical Utility of a Plasma-Based miRNA Signature Classifier Within Computed Tomography Lung Cancer Screening: A Correlative MILD Trial Study. *JCO* **32**, 768–773 (2014).

142. Levy, B. *et al.* Clinical Utility of Liquid Diagnostic Platforms in Non-Small Cell Lung Cancer. *The Oncologist* **21**, 1121–1130 (2016).

143. Geeurickx, E. & Hendrix, A. Targets, pitfalls and reference materials for liquid biopsy tests in cancer diagnostics. *Molecular Aspects of Medicine* **72**, 100828 (2020).

144. Salvianti, F. *et al.* The pre-analytical phase of the liquid biopsy. *New Biotechnology* **55**, 19–29 (2020).

145. Simonsen, J. B. What Are We Looking At? Extracellular Vesicles, Lipoproteins, or Both? *Circulation Research* **121**, 920–922 (2017).

146. Anderson, N. L. & Anderson, N. G. The human plasma proteome: history, character, and diagnostic prospects. *Mol Cell Proteomics* **1**, 845–867 (2002).

147. Ignatiadis, M., Sledge, G. W. & Jeffrey, S. S. Liquid biopsy enters the clinic — implementation issues and future challenges. *Nat Rev Clin Oncol* **18**, 297–312 (2021).

148. Coumans, F. A. W. *et al.* Methodological Guidelines to Study Extracellular Vesicles. *Circulation Research* **120**, 1632–1648 (2017).

149. Buzás, E. I., Tóth, E. Á., Sódar, B. W. & Szabó-Taylor, K. É. Molecular interactions at the surface of extracellular vesicles. *Semin Immunopathol* **40**, 453–464 (2018).

150. Ramirez, M. I. *et al.* Technical challenges of working with extracellular vesicles. *Nanoscale* **10**, 881–906 (2018).

151. Johnsen, K. B., Gudbergsson, J. M., Andresen, T. L. & Simonsen, J. B. What is the blood concentration of extracellular vesicles? Implications for the use of extracellular vesicles as blood-borne biomarkers of cancer. *Biochimica et Biophysica Acta (BBA) - Reviews on Cancer* **1871**, 109–116 (2019).

152. Aravanis, A. M., Lee, M. & Klausner, R. D. Next-Generation Sequencing of Circulating Tumor DNA for Early Cancer Detection. *Cell* **168**, 571–574 (2017).

153. van Niel, G. *et al.* Challenges and directions in studying cell–cell communication by extracellular vesicles. *Nat Rev Mol Cell Biol* 1–14 (2022) doi:10.1038/s41580-022-00460-3.

154. Wang, W., Luo, J. & Wang, S. Recent Progress in Isolation and Detection of Extracellular Vesicles for Cancer Diagnostics. *Advanced Healthcare Materials* **7**, 1800484 (2018).

155. Akbar, A., Malekian, F., Baghban, N., Kodam, S. P. & Ullah, M. Methodologies to Isolate and Purify Clinical Grade Extracellular Vesicles for Medical Applications. *Cells* **11**, 186 (2022).

156. Bakke, A. C. Clinical Applications of Flow Cytometry. *Laboratory Medicine* **31**, 97–104 (2000).

157. Doan, M. *et al.* Diagnostic Potential of Imaging Flow Cytometry. *Trends in Biotechnology* **36**, 649–652 (2018).

158. Herzenberg, L. A. *et al.* The history and future of the fluorescence activated cell sorter and flow cytometry: a view from Stanford. *Clin Chem* **48**, 1819–1827 (2002).

159. Ricklefs, F. L. *et al.* Imaging flow cytometry facilitates multiparametric characterization of extracellular vesicles in malignant brain tumours. *Journal of Extracellular Vesicles* **8**, 1588555 (2019).

160. Choi, D. *et al.* Mapping Subpopulations of Cancer Cell-Derived Extracellular Vesicles and Particles by Nano-Flow Cytometry. *ACS Nano* **13**, 10499–10511 (2019).

161. Welsh, J. A. *et al.* MIFlowCyt-EV: a framework for standardized reporting of extracellular vesicle flow cytometry experiments. *Journal of Extracellular Vesicles* **9**, 1713526 (2020).

162. Tian, Y. *et al.* Protein Profiling and Sizing of Extracellular Vesicles from Colorectal Cancer Patients via Flow Cytometry. *ACS Nano* **12**, 671–680 (2018).

163. Tertel, T. *et al.* High-Resolution Imaging Flow Cytometry Reveals Impact of Incubation Temperature on Labeling of Extracellular Vesicles with Antibodies. *Cytometry Part A* **97**, 602–609 (2020).

164. Zhu, S. *et al.* Light-Scattering Detection below the Level of Single Fluorescent Molecules for High-Resolution Characterization of Functional Nanoparticles. *ACS Nano* **8**, 10998–11006 (2014).

165. Kuiper, M., van de Nes, A., Nieuwland, R., Varga, Z. & van der Pol, E. Reliable measurements of extracellular vesicles by clinical flow cytometry. *American Journal of Reproductive Immunology* **85**, e13350 (2021).

166. Neven, K. Y., Nawrot, T. S. & Bollati, V. Extracellular Vesicles: How the External and Internal Environment Can Shape Cell-To-Cell Communication. *Curr Environ Health Rep* **4**, 30–37 (2017).

167. Tian, Y. *et al.* Quality and efficiency assessment of six extracellular vesicle isolation methods by nano-flow cytometry. *Journal of Extracellular Vesicles* **9**, 1697028 (2020).

168. Morales-Kastresana, A. *et al.* Labeling Extracellular Vesicles for Nanoscale Flow Cytometry. *Sci Rep* **7**, 1878 (2017).

169. Pospichalova, V. *et al.* Simplified protocol for flow cytometry analysis of fluorescently labeled exosomes and microvesicles using dedicated flow cytometer. *Journal of Extracellular Vesicles* **4**, 25530 (2015).

170. Maia, J. *et al.* Employing Flow Cytometry to Extracellular Vesicles Sample Microvolume Analysis and Quality Control. *Frontiers in Cell and Developmental Biology* **8**, 1165 (2020).

171. Mastoridis, S. *et al.* Multiparametric Analysis of Circulating Exosomes and Other Small Extracellular Vesicles by Advanced Imaging Flow Cytometry. *Frontiers in Immunology* **9**, (2018).

172. Morales-Kastresana, A. *et al.* High-fidelity detection and sorting of nanoscale vesicles in viral disease and cancer. *J Extracell Vesicles* **8**, 1597603 (2019).

173. Ender, F., Zamzow, P., Bubnoff, N. von & Gieseler, F. Detection and Quantification of Extracellular Vesicles via FACS: Membrane Labeling Matters! *Int J Mol Sci* **21**, E291 (2019).

174. Libregts, S. F. W. M., Arkesteijn, G. J. A., Németh, A., Nolte-'t Hoen, E. N. M. & Wauben, M. H. M. Flow cytometric analysis of extracellular vesicle subsets in plasma: impact of swarm by particles of non-interest. *Journal of Thrombosis and Haemostasis* **16**, 1423–1436 (2018).

175. Parish, C. R. Fluorescent dyes for lymphocyte migration and proliferation studies. *Immunol Cell Biol* **77**, 499–508 (1999).

176. Li, J. *et al.* Serum-free culture alters the quantity and protein composition of neuroblastoma-derived extracellular vesicles. *J Extracell Vesicles* **4**, 26883 (2015).

177. Haraszti, R. A. *et al.* Serum Deprivation of Mesenchymal Stem Cells Improves Exosome Activity and Alters Lipid and Protein Composition. *iScience* **16**, 230–241 (2019).

178. Cardoso, V. F. *et al.* Advances in Magnetic Nanoparticles for Biomedical Applications. *Advanced Healthcare Materials* **7**, 1700845 (2018).

179. Wu, K., Su, D., Liu, J., Saha, R. & Wang, J.-P. Magnetic nanoparticles in nanomedicine: a review of recent advances. *Nanotechnology* **30**, 502003 (2019).

180. Miltenyi, S., Müller, W., Weichel, W. & Radbruch, A. High gradient magnetic cell separation with MACS. *Cytometry* **11**, 231–238 (1990).

181. Mitchell, M. I. *et al.* Extracellular Vesicle Capture by AnTibody of CHoice and Enzymatic Release (EV-CATCHER): A customizable purification assay designed for small-RNA biomarker identification and evaluation of circulating small-EVs. *J Extracell Vesicles* **10**, e12110 (2021).

182. Sanità, G., Carrese, B. & Lamberti, A. Nanoparticle Surface Functionalization: How to Improve Biocompatibility and Cellular Internalization. *Frontiers in Molecular Biosciences* **7**, (2020).

183. Chen, H., Huang, J., Lee, J., Hwang, S. & Koh, K. Surface plasmon resonance spectroscopic characterization of antibody orientation and activity on the calixarene monolayer. *Sensors & Actuators: B. Chemical* **2**, 548–553 (2010).

184. van Buggenum, J. A. G. L. *et al.* A covalent and cleavable antibody-DNA conjugation strategy for sensitive protein detection via immuno-PCR. *Sci Rep* **6**, 22675 (2016).

185. Puertas, S. *et al.* Designing novel nano-immunoassays: antibody orientation versus sensitivity. *J. Phys. D: Appl. Phys.* **43**, 474012 (2010).

186. Wiener, J., Kokotek, D., Rosowski, S., Lickert, H. & Meier, M. Preparation of single- and double-oligonucleotide antibody conjugates and their application for protein analytics. *Sci Rep* **10**, 1457 (2020).

187. Niemeyer, C. M., Adler, M. & Wacker, R. Detecting antigens by quantitative immuno-PCR. *Nat Protoc* **2**, 1918–1930 (2007).

188. Zwart, S. R. & Lewis, B. J. Optimization of detection and quantification of proteins on membranes in very high and very low abundance using avidin and streptavidin. *Methods Mol Biol* **418**, 25–34 (2008).

189. Welsh, J. A. *et al.* Towards defining reference materials for measuring extracellular vesicle refractive index, epitope abundance, size and concentration. *Journal of Extracellular Vesicles* **9**, 1816641 (2020).

190. Zhang, H., Cheng, X., Richter, M. & Greene, M. I. A sensitive and high-throughput assay to detect low-abundance proteins in serum. *Nat Med* **12**, 473–477 (2006).

191. Best, M. G., Wesseling, P. & Wurdinger, T. Tumor-Educated Platelets as a Noninvasive Biomarker Source for Cancer Detection and Progression Monitoring. *Cancer Res* **78**, 3407–3412 (2018).

192. Antunes-Ferreira, M., Koppers-Lalic, D. & Würdinger, T. Circulating platelets as liquid biopsy sources for cancer detection. *Molecular Oncology* **15**, 1727–1743 (2021).

193. Geiss, G. K. *et al.* Direct multiplexed measurement of gene expression with color-coded probe pairs. *Nat Biotechnol* **26**, 317–325 (2008).

194. Ullal, A. V. *et al.* Cancer cell profiling by barcoding allows multiplexed protein analysis in fine-needle aspirates. *Sci Transl Med* **6**, 219ra9 (2014).

195. Bracht, J. W. P. *et al.* Analysis of extracellular vesicle mRNA derived from plasma using the nCounter platform. *Sci Rep* **11**, 3712 (2021).

196. Geiss, G. K. *et al.* Direct multiplexed measurement of gene expression with color-coded probe pairs. *Nat Biotechnol* **26**, 317–325 (2008).

197. Giménez-Capitán, A. *et al.* Multiplex Detection of Clinically Relevant Mutations in Liquid Biopsies of Cancer Patients Using a Hybridization-Based Platform. *Clin Chem* **67**, 554–563 (2021).

198. Nielsen, T. *et al.* Analytical validation of the PAM50-based Prosigna Breast Cancer Prognostic Gene Signature Assay and nCounter Analysis System using formalin-fixed paraffin-embedded breast tumor specimens. *BMC Cancer* **14**, 177 (2014).

199. Veldman-Jones, M. H. *et al.* Evaluating Robustness and Sensitivity of the NanoString Technologies nCounter Platform to Enable Multiplexed Gene Expression Analysis of Clinical Samples. *Cancer Research* **75**, 2587–2593 (2015).

200. Eastel, J. M. *et al.* Application of NanoString technologies in companion diagnostic development. *Expert Review of Molecular Diagnostics* **19**, 591–598 (2019).

201. Alix-Panabières, C. & Pantel, K. Liquid Biopsy: From Discovery to Clinical Application. *Cancer Discov* **11**, 858–873 (2021).

202. Snow, A., Chen, D. & Lang, J. E. The current status of the clinical utility of liquid biopsies in cancer. *Expert Review of Molecular Diagnostics* **19**, 1031–1041 (2019).

203. Zhou, B. *et al.* Application of exosomes as liquid biopsy in clinical diagnosis. *Sig Transduct Target Ther* **5**, 1–14 (2020).

204. Yu, W. *et al.* Exosome-based liquid biopsies in cancer: opportunities and challenges. *Ann Oncol* **32**, 466–477 (2021).

205. McKiernan, J. *et al.* A Novel Urine Exosome Gene Expression Assay to Predict High-grade Prostate Cancer at Initial Biopsy. *JAMA Oncology* **2**, 882–889 (2016).

206. McKiernan, J. *et al.* A Prospective Adaptive Utility Trial to Validate Performance of a Novel Urine Exosome Gene Expression Assay to Predict High-grade Prostate Cancer in Patients with Prostate-specific Antigen 2–10ng/ml at Initial Biopsy. *European Urology* **74**, 731–738 (2018).

207. Margolis, E. *et al.* Predicting high-grade prostate cancer at initial biopsy: clinical performance of the ExoDx (EPI) Prostate Intelliscore test in three independent prospective studies. *Prostate Cancer Prostatic Dis* **25**, 296–301 (2022).